January 2022

A Novel Numerical Model For Transient Mixed-Flow Analysis In Pipe And Conduit Systems

David B. Khani

A NOVEL NUMERICAL MODEL FOR TRANSIENT MIXED-FLOW ANALYSIS IN PIPE AND CONDUIT SYSTEMS

by

David Benyamin Khani

Bachelor of Science, Shahid Chamran University of Ahvaz, 1992

Master of Science, Urmia University, 1997

A Dissertation

Submitted to the Graduate Faculty

of the

University of North Dakota

in partial fulfillment of the requirements

for the degree of

Doctor of Philosophy

Grand Forks, North Dakota

May

2022

Name: David Khani

Degree: Doctor of Philosophy

This document, submitted in partial fulfillment of the requirements for the degree from the University of North Dakota, has been read by the Faculty Advisory Committee under whom the work has been done and is hereby approved.

DocuSigned by:
Howe Lim
E2D755C3824A4F5...
Yeo Howe Lim

DocuSigned by:
Ahmad Malekpour
03D732826452457...
Ahmad Malekpour

DocuSigned by:
Michael Mann
46F0545EE5FF405...
Michael Mann

DocuSigned by:
kegang ling
AE10F7CCAFC7487...
Kegang Ling

DocuSigned by:
Sattar Dorafshan
60308943EA7B4C7...
Sattar Dorafshan

DocuSigned by:
Anton Bergant
B8F113DE03D24C0...
Anton Bergant

This document is being submitted by the appointed advisory committee as having met all the requirements of the School of Graduate Studies at the University of North Dakota and is hereby approved.

DocuSigned by:
Chris Nelson
2E0AF088C733403...
Chris Nelson
Dean of the School of Graduate Studies

4/22/2022
Date

PERMISSION

Title A Novel Numerical Model for Transient Mixed Flow Analysis in Pipe and Conduit Systems

Department Civil Engineering

Degree Doctor of Philosophy

In presenting this dissertation in partial fulfillment of the requirements for a graduate degree from the University of North Dakota, I agree that the library of this University shall make it freely available for inspection. I further agree that permission for extensive copying for scholarly purposes may be granted by the professor who supervised my dissertation work or, in his absence, by the Chairperson of the department or the dean of the School of Graduate Studies. It is understood that any copying or publication or other use of this dissertation or part thereof for financial gain shall not be allowed without my written permission. It is also understood that due recognition shall be given to me and to the University of North Dakota in any scholarly use which may be made of any material in my dissertation.

David Benyamin Khani

May 02, 2022

TABLE OF CONTENTS

LIST OF FIGURES

LIST OF TABLES

ACKNOWLEDGMENTS

First and foremost, I would like to thank my advisor Dr. Yeo Howe Lim, and my co-advisor Dr. Ahmad Malekpour, for their clear extracurricular and academic support throughout my Ph.D. Program in Civil Engineering. Their encouragement, support, and advice has provided me with the much-needed energy and insight to complete my Ph.D. study.

My profound gratitude goes out to the other dissertation committee members: Dr. Michael Mann, Dr. Kegang Ling, and Dr. Sattar Dorafshan for their invaluable input throughout my Ph.D. study. My heartfelt appreciation also goes out to all my fellows in the College of Engineering and Mines, as well as the staff and colleagues at the School of Graduate Studies. You have made me feel that the University of North Dakota is my permanent home and have provided me with the opportunity to begin a lifelong friendship with you all.

I would also like to thank Dr. Anton Bergant, who generously provided us with the experimental data utilized for the validation of the proposed model in chapter 4 and for the time he allocated for reading my dissertation and evaluating my work. I would also like to thank Engineers Eduardo Rodal and Rene Autrique who generously provided us with the experimental data and the videos utilized for the validation of the model in chapter 5. I would especially thank Dr. Xuefeng Chu for his role in processing the grant application and his efforts in funding the research through NDWRRI.

Last but not least, I would like to express my greatest appreciation to my lovely family, (Marjaneh, Sophia, and Alissa) for their support and companionship throughout my Ph.D.

program. Huge thanks also go out to my colleagues and my managers at National Grid, Joseph Caniano, Michael King, and our director Michael Kern for their endless support, care, and encouragement, and to Panagiotis Sourlis for his assistance in some proof reading.

Above all, I am very thankful to my creator in this universe, The God Almighty, for making today, a dream of yesterday, come to fulfillment.

FUNDING

This research is supported by the US Geological Survey under Grant/Cooperative No. (G16AP00075) and North Dakota State Water Commission (NDSWC) through a fellowship award by North Dakota Water Resources Research Institute (NDWRRI).

To loving memories of my parents!

ABSTRACT

While responding to a wet weather flow event, stormwater pipe systems experience complex transient flow in which both open channel and pressurized flow regimes may coexist. The resulting transient flows may induce significant positive and negative pressure surges that can be intense enough to compromise the integrity of the system such as pipe rupture or flooding the streets and damage to properties. Unfortunately, available off-the-shelf software such as InfoWorks, Mike Urban, etc. are not comprehensive enough to capture all features of the resulting transient flows. When the elastic feature of the flow system becomes of significant importance, these models fail to capture the magnitude and track of the resulting waterhammer pressures as they produce extensive spurious numerical oscillations that compromise the accuracy of the results and in some cases cause the computer simulation to crash. The existing models are also incapable of capturing water column separation that may occur whenever the negative pressure in the conduits falls to the water vapor pressure. Thus far, several models have been proposed to improve transient flow modeling in sewer pipe systems, but none of them succeeded in addressing the aforementioned issues.

This research proposes an innovative one-dimensional numerical model to address part of the shortcomings associated with the existing state-of-the-art models. The model calculates both cavitating and pressurized flow using a single set of equations that governs unsteady flow in open channel flow. The first order Godunov type finite volume method is utilized to numerically solve the equations. A customized Harten, Lax, and van Leer (HLL) Riemann solver is proposed

to calculate the fluxes at the computational cell boundaries and to dissipate potential post-shock oscillations generated when the cavity is collapsed and the open channel flow beneath the cavity is switched back to pressurized flow. The numerical results are then validated using the data obtained from the experiment, other numerical models, CFD analysis, 1D-CFD analysis conducted as part of this thesis, and analytical solutions. The results show that the model can successfully capture water hammer and column separation in the sewer conduit systems with any conduit cross-sectional shapes. A unique feature of the proposed model is that it can concurrently account for waterhammer, cavitating flow, and free surface flow regimes; this makes the proposed model superior to the existing models. It is also found that the results obtained from the proposed 1D are comparable to those obtained from a comprehensive CFD analysis.

1 CHAPTER ONE

1.1 Introduction, Literature Review and Objectives

1.2 Introduction

Pipe, conduit, and sewer network systems are of great importance in modern societies. If not comprehensively designed, they have the potential to compromise the health and safety of the public as well as cause considerable damage to properties. Inadequate sizing of the key elements of a sewer pipe system, for example, may result in significant overflow in the shafts and manholes during a storm event thereby large content of polluted sewer flow is returned to the streets and environment which in turn produce health risks, damage, and inconvenience (Malekpour et al., 2017).

As an example, sewer pipe systems rarely run under steady-state flow conditions as the inflows into such systems change with time. In dry weather conditions, the flow gradually changes with time inside the conduits, and quasi-steady open channel flow is established across the system. However, when a severe storm occurs, complex transient flows may be onset and the system undergo flow regime transition from open channel to pressurized flow (Vasconcelos et al., 2006). The induced pressurization front serves as a moving piston and makes the air expelled out of the system through different components including, drop shafts, manholes, and outfalls. Fortunately,

during pressurization, the available storage in the partially filled conduit can accommodate the transient flow energy and does not allow the energy to be stored in the pipe and liquid as strain and compression energy (Malekpour et al., 2015). In such conditions, the elastic feature of the flow does not play an important role even if the pace of the transient is high, and the inertia and mass oscillation mainly govern the transient flow.

However, there are some situations in which the elastic feature of the flow becomes important. Two pressurization hydraulic bores moving in the opposite direction can easily trap a large air pocket in the conduit. As the entrapped air becomes pressurized, it may absorb a good portion of the transient energy and can significantly affect the hydraulics of the system. If the energized air pocket finds its way to the drop shafts or manholes, it can violently leave the system and produce geysering (Vasconcelos, 2005; Vasconcelos and Wright, 2011). Nevertheless, the presence of an air vent centered at the right position causes the air pocket to leave the system and remove the risk of geysering. On the other hand, when the last air escapes from the system the two adjacent hydraulic bores collide and depending on the velocities of the adjacent water columns significant water hammer pressures can occur (Malekpour and Karney, 2019). The generated water hammer pressure spike will propagate and affect the rest of the pipe located between two adjacent drop shafts reflecting the pressure spike. The reflected wave may produce intense negative pressures followed by column separation in the system.

Unfortunately, the complexity of the transient flow in the sewer systems is far beyond the level of sophistication of the present off-the-shelf 1D models widely used in the industry. In the

following section, the state-of-the-art in modeling mixed-flow analysis in pipe systems is discussed and the knowledge gaps are highlighted.

1.3 Literature Review

While responding to a wet flow event, storm water pipe systems experience complex transient flow in which both open channel and pressurized flow regimes may coexist (Malekpour, 2017). The resulting transient flows may induce significant positive and negative pressure surges which can be intense enough to compromise the integrity of the system. A 3D multiphase CFD model can theoretically replicate the transient flow but it is computationally too expensive and time-consuming to be used in the context of the design of such systems that are iterative in nature. Thus, simplified models are usually employed in practice to calculate the transient response of sewer systems. Since mass, momentum, and energy are mainly transferred in the longitudinal direction of the pipe, one-dimensional models have shown to be a reliable tool for capturing the main features of transient flow in pipe systems.

One of the simplest models employed to calculate transient mixed flow in pipe systems is built upon the rigid water column theory. Wiggert (1972), Liou and Hunt (1996), Razak and Karney (2008), among others employed the rigid column model both in simple and complex pipe systems and obtained reasonable results. Malekpour & Karney (2011) showed that as long as the water column is not locally disturbed, it tends to move along the pipeline as a rigid column. However, more complete dynamic models are required to calculate and trace the waterhammer pressures induced in the system when the flow is locally disturbed in the system.

Two different types of dynamic models that can be used to calculate transient mixed flow in closed conduit systems (Bousso et al., 2013). The first one is the shock fitting based model which has been widely used in treating transient mixed flow in sewer pipe systems (Song et al., 1983; Cardle and Song, 1988; Guo and Song, 1990; Fumba, 2002; Bourdarias, 2007; Politano et al., 2007; Leon et al., 2009; De Marchis et al., 2010). In this method, the interface separating open channel flow from the pressurized flow is tracked explicitly by both enforcing mass and momentum conservation across the interface. Having the interface flow characteristics calculated, the flow on either side of the interface is then calculated with its own theory. A variety of shock fitting models have been proposed and shown to provide promising results (Bourdarias, 2007; Capart et al., 1997; Cardle and Song, 1988; Fumba, 2002; Leon et al., 2009). Nevertheless, interface tracking is the biggest challenge of the shock fitting approach particularly in complex systems maintaining several simultaneous interfaces. Further, replicating the interaction of the interfaces with themselves and with the boundaries of the system are another challenge of the shock fitting approach, making the implementation of this approach even more difficult.

Shock capturing is another method widely used for calculating transient mixed flows in conduit systems (Garcia Navarro et al., 1994; Capart et al., 1997; Ji, 1998; Trajkovic et al., 1999; Vasconcelos et al., 2006; Vasconcelos et al., 2009; Leon et al., 2009; Sanders and Bradford, 2010; Kerger et al., 2011). In this approach, both open channel and pressurized flow are treated using a single set of equations governing unsteady flow in open channels. One of the most popular and earliest methods is the Preissmann's Slot Method (PSM) (Abbott and Minns, 1998), named after its innovator engineer Preissmann (Cunge and Wegner, 1964). In the PSM, a virtual narrow slot

above the crowns of the pipe allows the system remains in open channel flow condition even when the conduit becomes full. The width of the slot is calculated in such a way that the celerity of the wave motion in the slot becomes identical to the pipe acoustic speed, the higher pipe acoustic speed, the narrower slot width. The main drawback of this approach is the spurious numerical oscillation onset when the flow switches from open channel to pressurized flow. Depending on the magnitude of the acoustic speed of the conduit the resulting numerical oscillations could be strong enough to halt the simulation. The second weak point of the PSM is that it cannot maintain negative pressures. As soon as negative pressure is about to occur, the flow switches back to open channel flow.

A few novel methods have been proposed to resolve the negative pressure problem. Kerger et al. (2011) proposed a Negative Slot Method (NSM) approach in which the mass flow released during depressurization is compensated by a negative slot extended below the crowns of the pipe. In this approach, when negative pressure is imminent the conduit cross section is kept full, and the mass release required for depressurization of the conduit is compensated from the negative slot; negative depth in the slot measures the magnitude of the negative pressure head. Vasconcelos et al. (2006a) proposed a two-component pressure approach (TPA) in which the pressure term in the momentum equation is split into two components that measure the flow depth and pressure head in the conduit. Like NSM, when the negative pressure tends to occur, the flow depth component is set to the maximum depth of the conduit and the pressure head component is let to calculate the magnitude of the negative pressure. This method is successfully used for analyzing transient flow in sewer pipe networks (Vasconcelos et al, 2006a).

Although experimental results show that both NSM and TPA can calculate both negative and positive pressures quite accurately during the transient flow, they both suffer from spurious numerical oscillations induced when the flow regime changes from open channel to pressurized flow. The intensity of the numerical oscillations depends on the magnitude of the acoustic wave speed of the conduit and can be high enough to corrupt the solution. Numerical experiments have shown that beyond an acoustic speed of 30-50 m/s the resulting oscillations tend to corrupt the solution and even cause the computer code to crash. Since the acoustic wave speed in pipes may be significantly higher than 100 m/s the occurrence of numerical oscillation is a real challenge in the use of PSM and its alternative approaches (NSM and TPA), particularly when the capture of waterhammer pressures is the primary concern of modeling. That is why the cause and remediation of spurious numerical oscillation have been the focus of interest in the last four decades.

To suppress the numerical oscillations, several methods have been proposed thus far, but most of them have not been entirely satisfactory. Artificially reducing pipe acoustic speed by increasing the slot width is the most popular approach to reduce the numerical oscillation and has been employed by many (Capart et al., 1997; Trajkovic et al., 1999; Rossman, 2004; Leon et al., 2009). In this method, the numerical oscillations are suppressed by preventing drastic change in wave velocity during flow transition. This approach provides reasonable results as long as inertia dominates the flow, and the elastic feature of the flow is not of great importance. Otherwise, the magnitude and track of the resulting waterhammer pressures are significantly distorted. Furthermore, in deep and long CSO tunnels increasing the width of the slot produces large virtual storage which unrealistically slows down the transient flow discharges and significantly

underestimates the filling bore's speed; this is an issue that is crucially important to the real time operation of pipe systems (Malekpour et al., 2015a). An alternative approach is to connect the pipe to the slot by a smooth transition. Sjoberg (1982) proposed a transition that smoothly connects the pipe to the slot and employed an implicit finite difference method to solve the equations. The model was shown to succeed in capturing transient pressures free of numerical oscillations. Leon et al. (2009) proposed a funnel shape slot along with a second-order Godunov-type numerical solution and showed that the model can provide non-oscillatory solutions over a wide range of operational conditions. However, the method is exclusively presented for circular pipes, and it is not applicable for other conduits. Vasconcelos et al. (2009) contented that the numerical oscillations have the same root as in a slowly moving shock in gas dynamics (Jin and Liue, 1996; Karni and Čanić, 1997; Arora and Roe, 1997). They proposed a first-order Roe scheme in which the numerical viscosity of the scheme increases through calculating the numerical fluxes by a so-called Hybrid Flux Method. In the Hybrid Flux Method, the numerical viscosity of the scheme increases by artificially increasing the wave velocities which permit the fluxes to be calculated. The results showed that the Hybrid Flux Method can partially suppress the numerical oscillations, but data smearing becomes significant when the numerical viscosity further increases to completely remove the spurious numerical oscillations. Nonetheless, the test cases presented by Vasconcelos et al. (2009) imply that this method can be effectively used only when the pipe acoustic speed does not exceed 100 to 150 m/s. Vasconcelos et al. (2009) further proposed a digital filter by which the numerical results obtained in each time step are smoothed before the calculations proceed to the new time step. The results showed that the proposed numerical filter

can suppress the numerical oscillations, though like the Hybrid Flux Method this method is effective only if the pipe acoustic speed is less than around 150 m/s.

Malekpour and Karney (2015) proposed a slot-method based model utilizing the Godunov Finite Volume numerical scheme that employs the Harten, Lax and van Leer (HLL) Riemann solution for calculating the numerical fluxes. To suppress the numerical oscillations, they proposed an HLL solver that can automatically add some artificial viscosity to the scheme by increasing the wave velocity in the vicinity of the locations at which the pipe pressurization is imminent. It was shown that this approach can produce oscillation free solutions even at pipe acoustic speeds of over 1000 m/s.

Another shortcoming of the TPA is that it may generate non-physical negative pressures which are significantly lower than the vapor pressure of the liquid. Sudden changes in velocity may expose pressurized liquid pipe systems to intense negative pressures. Pumps power failure, rapid closing of valves, load rejection/acceptance in hydropower plants are a few examples triggering down surges that can establish intense negative pressures in pipelines (Bergant et al., 2006). When pressures at any location of a pipeline drop to the vapor pressure of the liquid, cavitating flow starts and makes the pressure remain constant at the vapor pressure of the liquid at that region. The constant pressure at this location allows the water columns on either side of the cavitating flow to be hydraulically disconnected such that each column can accelerate and decelerate independently. The flow imbalance at the cavitating flow region produces vapor cavities that separate the water column. When the cavities collapse, the adjacent water columns with different flow velocities collide, and waterhammer pressures are generated. The intensity of the

induced waterhammer pressures depends on the velocity difference of the water columns and the acoustic speed of the pipeline. The generated waterhammer pressures can be severe enough to rupture the pipeline (Chaudhry, 1987).

Joukowsky first identified column separation early in the 20th century, and since then this phenomenon is widely experimented (Bergant et al., 2006): a few examples of which are: Simpson and Wylie (1991), Martin (1983), and Bergant and Simpson (1999), Adamkowski and Lewandowski (2012), and Autrique and Rodal (2013). The insight from the experimental studies had made the researchers propose a variety of numerical models for capturing the essential features of column separation in pipe systems (Bergant and Simpson, 2006).

A variety of numerical models have been presented to capture column separation in pressurized pipe systems among which Discrete Vapour Cavity Model (DVCM), Discrete Gas Cavity model (DGCM), and two-phase flow model are the most popular ones (Bergant and Simpson, 2006). In the DVCM, a vapor cavity is inserted in the computational node as soon as the pressure drops to the vapor pressure. In the subsequent time steps, while keeping the pressure constant at the vapor pressure, the size of the cavity is calculated by balancing the liquid masses entering and leaving the cavity. When the cavity size becomes zero or negative, the computational node is treated as if there is no cavity at the node. The main drawback of this model is the production of numerical noises, which can propagate across the computational domain (Bergant and Simpson, 2006).

Provoost and Wylie (1981) proposed the DGCM to improve the performance of DVCM. A tiny gas pocket in each computational node allows this method to calculate both the water

hammer and cavitation flow regions. As long as the pressure is above the vapor pressure, the cavity remains small enough to propagate transient pressures at the pipe acoustic speed. However, when the pressure drops to the vapor cavity, the gas pocket expands and replicates cavitating flows by keeping the pressure constant at the vapor pressure. Experiments show that the DGCM successfully simulates both discrete and distributed cavitating flow (Bergant and Simpson, 1999; Bergant et al., 2006, Malekpour and Karney, 2014a & 2014b; Malekpour, 2014).

Column separation can be accounted for by different types of two-phase flow models proposed in the literature. The most popular model is the Generalized Interface Vapour Cavity Model (GIVCM) proposed by Bergant and Simpson (1999). In this method, the distributed cavitating zone characterized with very low void fraction and constant pressure (vapor pressure) is calculated by its governing equations while the liquid zone is calculated with the waterhammer equations. The interface between these two flow zones is tracked by an analytical approach within each time step.

In both DVCM and DGCM, the maximum length of the cavity must be small compared to the spatial size of the computational cell. As shown by Simpson and Bergant (1994), if the cavity length exceeds 10 % of the length of the computational cell, the results are not valid, and the use of other alternative models appears to be inevitable. In such a case, the GIVCM proposed by Bergant and Simpson (1999) is a good choice as the interface determining the boundaries of the cavity can be shifted from one computational cell to another if needed. Nevertheless, this approach still assumes that the cavity fills the whole cross section of the pipe which is not confirmed by experimental studies. Investigation on physical models reveals that the cavity

forms on the top section of the pipe, and the liquid beneath the cavity flow in an open channel flow regime. Nevertheless, the GIVCM provides good results as long as the cavity size does not exceed a certain limit otherwise the results would be compromised and cannot be trusted. Malekpour and Karney (2014a, and 2014b) showed that during rapid filling, large vapor cavities may form if a pipe system is exposed to the vapor pressure for quite a long time. In such cases, open channel flow-based models are expected to provide more accurate results as they better describe the physics of column separation.

In the conventional open channel flow-based models, the boundaries separating the cavitating and pressurized flows are tracked and the hydraulic variables in these flow zones are calculated by solving the open channel flow and water hammer equations respectively. Baltzer (1967a, and 1967b) proposed a model of this type that utilizes the method of characteristics to solve both the open channel and water hammer equations. The obtained results imply that although the model can describe the column separation more realistically, the amplitude and frequency of the pressure surge spikes captured by the model are not in good agreement with the experiment. A few other models have been also proposed but none of them succeeded in calculating column separation with reasonable accuracy (Siemons, 1967; Kalkwijk et al., 1972; Marsden and Fox, 1967). One of the major challenges with the models is dealing with the transition from the water hammer flow region to the cavitating flow region. This perhaps explains why open channel flow-based models have not received further attention (Bergant et al., 2006). Other reasons, in the authors' point of view, are that the counterpart models provide

promising results in a wide range of applications and are easier to implement, particularly in complex hydraulic systems.

CFD analysis has not been received significant attention in the realm of column separation probably because 1D models can alternatively cover a wide range of applications. Nevertheless, a few researchers tried to investigate the performance of CFD in capturing the key aspects of cavitating flow and column separation in pipe systems. Tang et al. (2020) and Wang et al. (2016) utilized 2D CFD analysis for calculating column separation that occurs following the rapid closing of a valve in a simple reservoir-pipe-valve system and found that not only can CFD accurately capture the time history of the resulting transient pressures, but it also can successfully account for the spread of the vapor cavity across the pipe. Warda et al. (2020) employed a 3D CFD analysis for calculating column separation in a laboratory-scale pipe system and concluded that CFD can capture key features of cavitating flow and column separation quite accurately. However, CFD analysis is quite expensive, at least at present, in terms of computational resources. Wang et al. (2016) demonstrated that it takes a few days for a personal computer to complete 0.6 s of transient analysis in a pipe with an internal diameter and length of 0.02 and 30 m, respectively. This implies that CFD is inefficient in practice due to the scale of pipe systems and the fact that an engineering design is iterative and may need numerous simulations.

Coupling CFD with 1D analysis appears to be an efficient solution to significantly reduce the computational time. This idea is grown based on the fact that mass, momentum, and energy are dominantly transferred in the longitude dimension of the pipe and the information exchanged

in the radial dimension of the pipe is not of insignificant importance. In CFD-1D analysis, the limited part of the system with the significant 3D feature is calculated by the CFD analysis, and the rest of the system is handled by the 1D analysis; the two computational approaches exchange the information at each computational time level through the interface connecting 1D and CFD domains. This method has been successfully employed for calculating transient flow in liquid pipe systems (Mandair, 2020). For example, Zhang and Cheng (2012) applied 1D-3D analysis to different components of hydropower systems. Zhang et al. (2014) successfully utilized 1D-3D analysis in transient analysis of a pumped-storage system. Wu et al. (2015) applied 1D-3D coupling for steady-state and transient flow analysis in a pumped pipeline. Maddahian et al. (2021) employed 1D-3D analysis in rapid pressurization of a pipe system with an entrapped air pocket and showed that the modeling results are in excellent agreement with experiments. To the best of the authors' knowledge, the 1D-3D coupling approach has not been utilized for calculating column separation so far.

1.4 Dissertation Objectives

This main idea of this thesis grew during several years of experience of the author as a hydraulic modeler in the water and wastewater industry and through an extensive literature review. The literature review reveals that the existing models fail to account for three key features of the transient mixed flow including airflow, waterhammer and column separation. To this end, the following investigation aims to develop a model that can account for the two later features, waterhammer, and column separation. Since the TPA has great potential for further

improvement, it is utilized as the based model in this study. The key objectives of this study are highlighted in the following:

- **Proposed a numerical approach to remove spurious numerical oscillation**

  The TPA generates spurious numerical oscillations when the flow is about to change from open channel to pressurized flow regime. The intensity of the numerical oscillations rests on the magnitude of acoustic wave speed considered in the simulation. The TPA is incapable of accounting for pipe acoustic speeds of higher than a certain limit (100 m/s) because beyond which the generated oscillations come to distort the results and eventually halt the simulation. However, in reality, acoustic speed in pipes may exceed 1000 m/s which is far above the limit at which the TPA can perform. Since the intensity of waterhammer pressure rise depends on the magnitude of the pipe acoustic speed, TPA fails to capture the intensity of the waterhammer pressures. The first object of this thesis is to propose a solution for removing the spurious numerical oscillation such that the model can correctly replicate the waterhammer pressures at any given acoustic speed magnitude.

- **Investigating the universality of the proposed numerical approach**

  A sewer system may include a variety of conduit shapes. To ensure that the proposed numerical approach can provide non-oscillatory solutions under different conduit shapes, this study aims to investigate if the proposed numerical approach can perform equality well while dealing with the most common conduit shapes utilized in the industry.

- **Validation of the proposed numerical approach**

  Any measures taken to resolve the spurious numerical oscillation may compromise the consistency of the resulting numerical scheme thereby the equivalent system of equations may mimic the wrong physics. To ensure the consistency of the proposed numerical scheme, it is validated by comparing the numerical results with the experiment and also with the analytical results associated with some hypothetical pipe systems for which analytical solutions exist.

- **Modification of the TPA to account for column separation**

  The TPA fails to capture column separation. In conditions under which the column separation may form in the system, the TPA produces intense negative pressures which do not have a physical basis. Another goal of this thesis is to modify and empower the TPA to account for column separation.

- **Validating the column separation feature of the proposed model**

  To confirm if the proposed model can successfully capture water or liquid column separation, this study compares the numerical results with experiment, analytical solution, and the numerical results obtained from the most popular conventional method (DGCM), presently utilized for calculating column separation. To further investigate the ability of the proposed model in capturing the shape of the vapor cavity, the model results are compared with the CFD analysis results published in the literature and those obtained from a 1D-3D coupling approach conducted as part of this thesis.

1.5 Co-Authorship

The outcome of this study is presented in the four following journal papers which constitute chapters 2 to 5 of this dissertation respectively. Drs. Yeo Howe Lim and Ahmad Malekpour have been made significant contributions in interpreting the model results and commenting on the content of this dissertation.

1. Khani, D., Lim, Y. H., & Malekpour, A. (2020). Hydraulic Transient Analysis of Sewer Pipe Systems Using a Non-Oscillatory Two-Component Pressure Approach. Water, 12(10), 2896.
2. Khani, D., Lim, Y. H., & Malekpour, A. (2021). A Mixed Flow Analysis of Sewer Pipes with Different Shapes Using a Non-Oscillatory Two-Component Pressure Approach (TPA). Modelling, 2(4), 467-481.
3. Khani, D., Lim, Y. H., & Malekpour, A. (2022). Calculating Column Separation in Conduit Systems Using an Innovative Open Channel Based Model. (Submitted to the ASCE Journal of Hydraulic Engineering, it is under review).
4. Khani, D., Lim, Y. H., & Malekpour, A. (2022). Investigating the Performance of the Modified Two-Component Pressure Approach in Capturing Column Separation with Large Vapor Cavities. (Submitted to the IAHR Journal of Hydraulic Research, it is under review).
5. Khani, D., Lim, Y. H., & Malekpour, A. (2022). Calculating Column Separation in Liquid Pipelines Using a 1D-CFD Coupled Model: (It is being submitted to a journal)

1.6 References

Abbott, M. B., & Minns, A. W. (1998). *Computational hydraulics.* Connecticut: Ashgate.

Adamkowski, A., & Lewandowski, M. (2012). Investigation of hydraulic transients in a pipeline with column separation. *Journal of Hydraulic Engineering, 138*(11), 935-944.

Arora, M., & Roe, P. L. (1997). On postshock oscillations due to shock capturing schemes in unsteady flows. *Journal of Computational Physics, 130*(1), 25-40.

Autrique, R., & Rodal, E. (2013). Laboratory studies of water column separation. *In IOP Conference Series: Materials Science and Engineering. 52*, p. 022022. IOP Publishing. doi:doi:10.1088/1757-899X/52/2/022022

Autrique, R., & Rodal, E. (2013). Laboratory studies of water column separation. *IOP Conference Series: Materials Science and Engineering. 52*, p. 022022. IOP Publishing.

Baltzer, R. (1967b). *A study of column separation accompanying transient flow of liquids in pipes.* PhD Thesis. Michigan: University of Michigan.

Baltzer, R. A. (1967a). Column separation accompanying liquid transients in pipes. *Journal of Basic Engineering*, 837-846.

Bergant, A., & Simpson, A. R. (1999). Pipeline column separation flow regimes. *Journal of Hydraulic Engineering, 125*(8), 835–848.

Bergant, A., & Simpson, A. R. (1999a). Cavitation inception in pipeline column separation. *28th IAHR Congress.* Graz, Austria: CD-ROM.

Bergant, A., Simpson, A. R., & Tijsseling, A. S. (2006). Water hammer with column separation: A historical review. *Journal of Fluids and structures, 22*, 135-171.

Bourdarias, C. &. (2007). A finite volume scheme for a model coupling free surface and pressurised flows in pipes. *Journal of Computational and Applied Mathematics, 209*(1), 109-131.

Bousso, S., Daynou, M., & & Fuamba, M. (2013). Numerical modeling of mixed flows in storm water systems: critical review of literature. *Journal of Hydraulic Engineering, 139*(4), 385-396.

Capart, H., Sillen, X., & Zech, Y. (1997). Numerical and experimental water transients in sewer pipes. *Journal of Hydraulic Research, 35*(5), 659-672.

Cardle, J. A., & Song, C. S. (1988). Mathematical modelling of unsteady flow in storm sewers. *International Journal of Engineering Fluid Mechanics, 1*(4), 495–518.

Chaudhry, M. (1987). *Applied Hydraulic Transients.* New York: Van Nostrana Reinhold Co.

Chaudhry, M. H. (1999). *Open channel flow.* Englewood Cliffs, N.J : Prentice-Hall.

Cunge, J. A., & Wegner, M. (1964). Numerical Integration of Bane de Saint-Venant's Flow Equations by Means of an Implicit Scheme of Finite Differences. Applications in the Case of Alternately Free and Pressurized Flow in a Tunnel. *La Houille Blanche, 1*, 33-39.

De Marchis, M., Fontanazza, C. M., Freni, G., La Loggia, G., Napoli, E., & Notaro, V. (2010). A model of the filling process of an intermittent distribution network. *Urban Water Journal, 7*(6), 321 -333.

Fuamba, M. (2002). Contribution on transient flow modelling in storm sewers. *Journal of hydraulic research, 40*(6), 685-693.

Garcia Navarro, P., Priestley, A., & Alcrudo, F. (1994). Implicit method for water flow modelling in channels and pipes. *Journal of Hydraulic Research, 32*(5), 721–742.

Guo, Q., & Song, C. S. (1990). Surging in urban storm drainage systems. *Journal of Hydraulic Engineering, 116*(12), 1523–1537.

Ji, Z. (1998). General hydrodynamic model for sewer/channel network systems. *Journal of Hydraulic Engineering, 124*(3), 307–315.

Jin, S., & Liu, J. G. (1996). The effects of numerical viscosities: I. Slowly moving shocks. *Journal of Computational Physics, 126*(2), 373-389.

Kalkwijk, J., Kranenburg, C., Vreugdenhil, C., & De Vries, A. (1972). *Cavitation caused by water hammer in horizontal.* Delft: Delft Hydraulics Laboratory,Publication No. 97.

Karni, S., & Čanić, S. (1997). Computations of slowly moving shocks. *Journal of Computational Physics, 136*(1), 132-139.

Kerger, F., Archambeau, P., Erpicum, S., Dewals, B. J., & Pirotton, M. (2011). An exact Riemann solver and a Godunov scheme for simulating highly transient mixed flows. *Journal of Computational and Applied Mathematics, 235*, 2030-2040.

Khani, D., Lim, Y. H., & Malekpour, A. (2020). Hydraulic Transient Analysis of Sewer Pipe Systems Using a Non-Oscillatory Two-Component Pressure Approach. *Water, 12*(10), 2896.

Khani, D., Lim, Y. H., & Malekpour, A. (2021). A Mixed Flow Analysis of Sewer Pipes with Different Shapes Using a Non-Oscillatory Two-Component Pressure Approach (TPA). *Modelling, 2*(4), 467-481.

Khani, D., Lim, Y. H., & Malekpour, A. (2022). An Innovative Open Channel Based Model for Calculating Column Separation in Conduit Systems . *Submitted to the Journal of Hydraulic Engineering*.

Khani, D., Lim, Y. H., & Malekpour, A. (2022). Investigating the Performance of the Modified Two-Component Pressure Approach in Capturing Column Separation with Large Vapor Cavities. *Submitted to the Journal of Hydraulic Research*.

León, A. S., Ghidaoui, M. S., Schmidt, A. R., & García, M. H. (2009). Application of Godunov-type schemes to transient mixed flows. *Journal of hydraulic research, 47*(2), 147-156.

Leon, A. S., Ghidaoui, M. S., Schmidt, A. R., & Garcia, M. H. (2010). A robust two equation model for transient mixed flows. *Journal of Hydraulic Research, 48*(1), 44 -56.

LeVeque, R. (2002). *Finite volume methods for hyperbolic problems.* Cambridge, UK: Cambridge Press.

Liou, C. P., & Hunt, W. A. (1996). Filling of pipelines with undulating elevation profiles. *Journal of Hydraulic Engineering, 122*(10), 534-539.

Maddahian, R., Shaygan, F., & Bucur, D. M. (2021). Developing a 1D-3D model to investigate the effect of entrapped air on pressure surge during the rapid filling of a pipe. *IOP Conference Series: Earth and Environmental Science. 774(1)*, p. 012069. IOP Publishing.

Malekpour, A. (2014). *Analysis of Rapid Pipeline Filling Including Column Separation & Entrapped Air Effects (Doctoral dissertation, University of Toronto).*

Malekpour, A., & B., K. W. (2011). Rapid filling analysis of pipelines with undulating profiles by the method of characteristic. *ISRN Applied Mathematics*, Article ID 930460, 16 pages, http://dx.doi.org/10.5402/2011/930460.

Malekpour, A., & Karney, B. (2015). Spurious Numerical Oscillations in the Preissmann Slot Method: Origin and Suppression. *Journal of Hydraulic Engineering, ASCE*.

Malekpour, A., & Karney, B. W. (2014a). Profile-induced column separation and rejoining during rapid pipeline filling. *Journal of Hydraulic Engineering, 140*(11).

Malekpour, A., & Karney, B. W. (2014b). Column separation and rejoinder during rapid pipeline filling induced by a partial flow blockage. *Journal of Hydraulic Research, 52*(5), 693-704.

Malekpour, A., & Karney, B. W. (2019). Complex interactions of water, air and its controlled removal during pipeline filling operations. *Fluid Mechanics Research International Journal, 3*(1), 4-15.

Malekpour, A., Karney, B., & Nault, J. (2015). Physical Understanding of Sudden Pressurization of Pipe Systems with Entrapped Air: Energy Auditing Approach. *Journal of Hyraulic Engineering, 142*(2), 04015044.

Malekpour, A., Papa, F., & and Radulje, D. (2017). Uncertainty Analysis in Strom Sewer Collection Systems Using Monte Carlo Simulation and Parallel Computing. *WEAO 2017 Technical Conference.* Ottawa.

Malekpour, A., Papa, F., Radulj, D., & Karney, B. (2015a). Understanding of Hydraulic Transients in Sewer Systems. *WEAO 2015 Technical Conference.* Toronto.

Mandair, S. (2020). *1D and 3D Water-Hammer Models: The energetics of high friction pipe flow and hydropower load rejection.* PhD diss., University of Toronto (Canada).

Marsden, N., & Fox, J. (1976). An alternative approach to the problem of column separation in an elevated section of pipeline. *Second International Conference on Pressure Surges* (pp. 1–13). London: BHRA.

Martin, C. (1983). Experimental investigation of column separation with rapid closure of downstream valve. *Fourth International Conference on Pressure Surges* (pp. 77–88). Cranfield, UK: BHRA Fluid Engineering.

Politano, M., Odgaard, A. J., & Klecan, W. (2007). Case study: Numerical evaluation of hydraulic transients in a combined sewer overflow tunnel system. *Journal of Hydraulic Engineering, 133*(10), 1103-1110.

Provoost, G. A., & Wylie, E. B. (1981). Discrete gas model to represent distributed free gas in liquids. *5th International Symposium on Water Column Separation*, *1*, pp. 28-30. Obernach, West Germany.

Razak, T., & Karney, B. (2008). Filling of branched pipelines with undulating elevation profiles. *0th International Conference on Pressure Surges* (pp. 473–487). UK: BHR Groupe.

Sanders, B. F., & Bradford, S. F. (2010). Network implementation of the two-component pressure approach for transient flow in storm sewers. *Journal of Hydraulic Engineering, 137*(2), 158-172.

Siemons, J. (1967). The phenomenon of cavitation in a horizontal pipe-line due to a sudden pump-failure. *Journal of Hydraulic research, 5*(2), 135-152.

Simpson, A., & Bergant, A. (1994). Numerical comparison of pipe column-separation models. *Journal of Hydraulic Engineering, 120*(3), 361–377.

Simpson, A., & Wylie, E. (1991). Large water-hammer pressures for column separation in pipelines. *Journal of Hydraulic Engineering, 117*(10), 1310–1316.

Sjöberg, A. (1982). Sewer network models dagvl-a and dagvl-diff. In B. C. Yen (Ed.), *Urban Stormwater Hydraulics and Hydrology* (pp. 127-136). Littleton, Colo.: Water Resource Publications.

Song, C. S., Cardle, J. A., & Leung, K. S. (1983). Transient mixed flow models for storm sewers. *Journal of Hydraulic Engineering, 109*(11), 1487–1504.

Tang, X., Duan, X., Gao, H., Li, X., & Shi, a. X. (2020). CFD investigations of transient cavitation flows in pipeline based on weakly-compressible model. *Water, 12*(2), 448.

Toro, E. F. (2001). *Shock-capturing methods for free-surface shallow flows.* Chichester, New York: John Wiley.

Trajkovic, B., Ivetic, M., Calomino, F., & D'Ippolito, A. (1999). Investigation of transition from free surface to pressurized flow in a circular pipe. *Water Science and Technology, 39*(9), 105–112.

Vasconcelos, G. J., & Marwell, T. B. (2011). Innovative simulation of unsteady low-pressure flows in water mains. *Journal of Hydraulic Engineering, 137*(11), 1490-1499.

Vasconcelos, J. G., & Wright, S. J. (2011). Geysering generated by large air pockets released through water-filled ventilation shafts. *Journal of Hydraulic Engineering, 137*(5), 543-555.

Vasconcelos, J. G., Wright, S. J., & Roe, P. L. (2006). *Current Issues on modeling extreme inflows in stormwater systems in Intelligent Modeling of Urban Water Systems, Monogrph 14.* Guelph, Ontario: CHI.

Vasconcelos, J. G., Wright, S. J., & Roe, P. L. (2006a). Improved simulation of flow regime transition in sewers: two-component pressure approach. *Journal of Hydraulic Engineering, 132*(6), 553-562.

Vasconcelos, J. G., Wright, S. J., & Roe, P. L. (2009). Numerical oscillations in pipe-filling bore predictions by shock-capturing models. *Journal of Hydraulic Engineering, 135*(4), 296-305.

Wang, H., Zhou, L., Liu, D., Karney, B., Wang, P., Xia, L., . . . Xu, C. (2016). CFD Approach for Column Separation in Water Pipelines. *Journal of Hydraulic Engineering, 142*(10), 04016036.

Warda, H. A., Wahba, E. M., & El-Din, a. M. (2020). Computational Fluid Dynamics (CFD) simulation of liquid column separation in pipe transients. *Alexandria Engineering Journal, 59*(5), 3451-3462.

Wiggert, D. C. (1972). Transient flow in free-surface, pressurized systems. *Journal of the Hydraulics division, 98*(1), 11-27.

Wu, D., Yang, S., Wu, P., & Wang, L. (2015). MOC-CFD coupled approach for the analysis of the fluid dynamic interaction between water hammer and pump. *Journal of Hydraulic Engineering, 141*(6), 06015003.

Zhang, X. X., Cheng, Y. G., Xia, L. S., & Yang, J. D. (2014). Dynamic characteristics of a pump-turbine during hydraulic transients of a model pumped-storage system: 3D CFD simulation. *IOP Conference Series: Earth and Environmental Science. 22(3)*, p. 032030. IOP Publishing.

Zhang, X.-x., & Cheng, Y.-g. (2012). Simulation of hydraulic transients in hydropower systems using the 1-D-3-D coupling approach. *Journal of Hydrodynamics, 24*(4), 595-604.

2 CHAPTER TWO

2.1 Hydraulic Transient Analysis of Sewer Pipe Systems Using a Non-Oscillatory Two-Component Pressure Approach

2.2 Abstract

Based on the two-component pressure approach, a numerical model is developed to capture mixed transient flow in close conduit systems. To achieve this, an innovative Godunov finite volume numerical scheme is proposed to suppress the spurious numerical oscillations occurring during pipe pressurization. To dissipate the spurious numerical oscillations, artificial numerical viscosity is admitted to the numerical scheme through applying a proposed HLL Riemann solver for calculating the numerical fluxes at the computational cell interfaces. The proposed HLL solver controls the magnitude of the numerical viscosity through adjusting the left and right wave velocities. A wave velocity calculator is proposed to optimally distribute the numerical viscosity over several computational cells around the computational cell in which the pressurization front is located. The HLL solver admits significant artificial numerical viscosity when the pipe pressurization is imminent and automatically reduces it in other places; in this way the numerical diffusion and data smearing is minimized. The validity of the proposed model is justified by the aid of several test cases in which the numerical results are compared with both experimental data and the results obtained from analytical methods. The results reveal that the proposed model succeeds in completely removing the spurious numerical oscillations even when

the acoustic speed has exceeded 1000 m/s. The numerical results also show that the model can successfully capture occurrences of negative pressures during the course of transient.

2.3 Introduction

While responding to a wet flow event, storm water pipe systems experience complex transient flow in which both open channel and pressurized flow regime may coexist (Malekpour et al., 2017). The resulting transient flow may induce significant positive and negative pressure surges which can be intense enough to compromise the integrity of the system. A 3D multiphase CFD model can theoretically replicate the transient flow, but it is computationally too expensive and time consuming to be used in the context of the design of such systems that are iterative in nature. Thus, simplified models are usually employed in practice to calculate the transient response of sewer systems in practice. Since mass, momentum and energy is mainly transferred in the longitudinal direction of the pipe, one-dimensional models have shown to be a reliable tool for capturing the main features of the transient flow in pipe systems.

One of the simplest models employed to calculate transient mixed flow in pipe systems is built upon the rigid water column theory. Liou and Hunt (1996), Wiggert (1972), Razak and Karney (2008), among others employed the rigid column model both in simple and complex pipe systems and obtained reasonable results. Malekpour & Karney (2011) showed that as long as the water column is not locally disturbed, it tends to move along the pipeline as a rigid column. However, more complete dynamic models are required to calculate and trace the waterhammer pressures induced in the system when the flow is locally disturbed in the system.

There are two different types of dynamic models which can be used to calculate transient mixed flow in closed conduit systems (Bousso et al., 2013). The first one is the *shock fitting based* model which has been widely used in treating transient mixed flow in sewer pipe systems (Leon et al., 2009a; De Marchis et al., 2010; Bourdarias and Gerbi, 2007; Song et al., 1983; Fuamba, 2002; Cardle and Song, 1988; Guo and Song, 1990; Politano et al., 2007). In this method, the interface separating open channel flow from pressurized flow is tracked explicitly by both enforcing mass and momentum conservation across the interface. Having the interface flow characteristics calculated, the flow on either side of the interface is then calculated with its own theory. A variety of shock fitting models have been proposed and shown to provide promising results. Nevertheless, interface tracking is the biggest challenge of the shock fitting approach particularly in complex systems maintaining several simultaneous interfaces. Further, replicating the interaction of the interfaces with themselves and with the boundaries of the system are other challenges of the shock fitting approach making the implementation of this approach even more difficult.

Shock capturing is another method widely used for calculating transient mixed flow in conduit systems (Garcia Navarro et al., 1994; Carpart et al., 1997; Ji, 1998; and Trajkovic et al., 1999; Leon et al., 2009b; Vasconcelos et al., 2006a; Vasconcelos and Wright, 2007; Sanders and Bradford, 2010; Kerger et al., 2011). In this approach both open channel and pressurized flow are treated using a single set of equations governing unsteady flow in open channels. One of the most popular and earliest methods is the Preissmann's Slot Method (generally abbreviated as PSM) (Abbott and Minns, 1998), named after its innovator engineer Preissmann (Cunge and

Wegner, 1964). In the PSM a virtual narrow slot above the crown of the pipe allows the system remains in open channel flow condition even when the conduit becomes completely full. The width of the slot is calculated in such a way that the celerity of the wave motion in the slot becomes identical to the pipe acoustic speed, the higher pipe acoustic speed, the narrower slot width. The main drawback of this approach is the spurious numerical oscillation onset when the flow switches from open channel to pressurized flow. Depending on the magnitude of acoustic speed of the conduit the resulting numerical oscillation can be strong enough to halt the simulation. The second weak point of the Pressman Slot method is that it cannot maintain negative pressures. As soon as negative pressure is about to occur, the flow switches back to open channel flow.

A few novel methods have been proposed to resolve the negative pressure issue. Kerger et al. (2011) suggested a Negative Slot Method (NSM) approach in which the mass flow discharged during pressure reduction is balanced by a negative or reverse slot extended below the crown of the pipe. In this procedure, when negative pressure is about to happen the conduit cross section is kept full, and the mass discharge required to reduce the pressure in the conduit is compensated from the negative slot; negative depth in the slot measures the magnitude of the negative pressure head. Vasconcelos et al. (2006a) proposed two-component pressure approach (TPA) in which the pressure term in the momentum equation is split into two components that measure the flow depth and pressure head in the conduit. Like NSM, when the negative pressure tends to occur, the flow depth component is set to the maximum depth of the conduit and the pressure head component is let to calculate the magnitude of the negative pressure. This method is

successfully used for analyzing transient flow in sewer pipe networks (Sanders and Bradford, 2010).

Although experimental results show that both NSM and TPA can calculate both negative and positive pressure quite accurately during the course of the transient, they both suffer from spurious numerical oscillation induced when the flow regime changes from open channel to pressurized flow. The intensity of the numerical oscillations depends on the magnitude of acoustic wave speed of the conduit and can be high enough to corrupt the solution. Numerical experiments have shown that beyond an acoustic speed of 30-50 m/s the resulting oscillations tend to corrupt the solution and even cause the computer code to crash. Since the acoustic wave speed in pipes may be significantly higher than 100 m/s the occurrence of numerical oscillation is a real challenge in the use of PSM and its alternative approaches (NSM and TPA), particularly when the capture of waterhammer pressures is the primary concern of modeling. That is why the cause and remediation of spurious numerical oscillation have been the focus of interest in the last four decades.

In order to suppress the numerical oscillations, several methods have been proposed thus far, but most of them have not been entirely satisfactory. Artificially reducing pipe acoustic speed by increasing the slot width is the most popular approach to reduce the numerical oscillation and has been employed by many (examples: Trajkovic et al., 1999; Capart et al., 1997; Rossman, 2010). In this method, the numerical oscillation is suppressed through preventing drastic change in wave velocity during flow transition. This approach provides reasonable model result as long as inertia dominates the flow, and the elastic feature of the flow

is not of great importance. Otherwise, the magnitude and track of the resulting waterhammer pressures are significantly distorted. Furthermore, in deep and long CSO tunnels increasing the width of the slot produces large virtual storage which unrealistically slows down the transient flow discharges and significantly underestimates the filling bore's speed; this is an issue which is crucially important to the real time operation of pipe systems (Karney and Malekpour, 2011). An alternative approach is to connect the pipe to the slot by a smooth transition. Sjoberg (1981) proposed a transition that smoothly connect the pipe to the slot and employed an implicit finite difference method to solve the equations. The model was shown to succeed in capturing transient pressures free of numerical oscillations. Leon et al. (2009) proposed a funnel shape slot along with a second-order Godunov-type numerical solution and showed that the model can provide non-oscillatory solutions over a wide range of operational conditions. However, the method is exclusively presented for circular pipes, and it is not applicable for other conduits. Vasconcelos et al. (2009) contented that the numerical oscillations have the same root as in a slowly moving shock in gas dynamics (Karni and Čanić, 1997; Jin and Liu, 1996; Arora and Roe, 1997). They proposed a first-order Roe scheme in which the numerical viscosity of the scheme increases through calculating the numerical fluxes by a so-called Hybrid Flux Method. In the Hybrid Flux Method, the numerical viscosity of the scheme increases by artificially increasing the wave velocities which permit the fluxes to be calculated. The results showed that the Hybrid Flux Method can partially suppress the numerical oscillations, but data smearing becomes significant when the numerical viscosity further increases to completely remove the spurious numerical oscillations. Nonetheless, the test cases presented by Vasconcelos et al. (2009) imply that this

method can be effectively used only when the pipe acoustic speed does not exceed 100 to 150 m/s. Vasconcelos et al. (2009) further proposed a digital filter by which the numerical results obtained in each time step are smoothed before the calculations proceed to the new time step. The results showed that the proposed numerical filter can suppress the numerical oscillations, though like the Hybrid Flux Method this method is effective only if the pipe acoustic speed is less than around 150 m/s.

Malekpour and Karney (2014) proposed a slot-method based model utilizing the Godunov Finite Volume numerical scheme that employs the HLL Riemann solution for calculating the numerical fluxes. To suppress the numerical oscillations, they proposed a HLL solver that can automatically add some artificial viscosity to the scheme by increasing the wave velocity in the vicinity of the locations at which the pipe pressurization is imminent. It was shown that this approach can produce oscillation free solutions even at pipe acoustic speeds of over 1000 m/s.

The dissipative HLL solver proposed by Malekpour and Karney has been successfully employed by other researchers (Hyunuk et al., 2018; Mao et al., 2020). Nevertheless, it is not known if this solver performs well in conjunction with the TPA approach as well because all the research done so far applied the HLL solver in the context of the slot method. Resolving this uncertainty is the main objective of this paper which will be shown decisively if this HLL solver can also suppress the numerical oscillations while used in the context of the TPA.

2.4 Theoretical Background

2.4.1 Governing Equations

The conservative form of one-dimensional continuity and momentum equations in open channels can be written as follows (Chaudhry, 1999):

$$\frac{\partial \boldsymbol{U}}{\partial t} + \frac{\partial \boldsymbol{F}}{\partial x} = \boldsymbol{R} \qquad 2\text{-}1$$

where $\boldsymbol{U}$, $\boldsymbol{F}$, and $\boldsymbol{R}$ are the vectors representing flow variables, fluxes, and source terms respectively and can be represented as follows:

$$\boldsymbol{U} = \begin{bmatrix} A \\ Q \end{bmatrix}; \boldsymbol{F} = \begin{bmatrix} Q \\ \frac{Q^2}{A} + Agh \end{bmatrix}; \boldsymbol{R} = \begin{bmatrix} 0 \\ gA(S_0 - S_f) \end{bmatrix}; \; S_f = \frac{Q^2 n_m^2}{A^2 R^{\frac{4}{3}}} \qquad 2\text{-}1$$

where A = flow cross sectional area, Q = flow discharge, h = distance between the free surface and the centroid of the flow cross-sectional area, S_0 = bottom slope of channel, S_f = slope of energy grade line, g = gravitational acceleration, ρ = flow density, R = flow hydraulic radius, and n_m = Manning coefficient.

As discussed before, regarding PSM, a virtual slot above the crown of the pipe allows pressurized flows to be regulated by the above equation as well. In such a case when the calculated water depth exceeds the pipe diameter, it represents the pressure head in the system and the amount of mass in the slot replicates the mass compressed in the pipe as the result of the pressure head rise. The width of the slot required to replicate the acoustic wave speed of the pipe (a) can be simply calculated as follows:

$$T_S = \frac{gA_f}{a^2} \qquad 2\text{-}3$$

where A_f = pipe cross section, a is pipe acoustic speed and T_S is the slot width.

In using TPA, it is assumed that the pipe is expanded and contracted during pipe pressurization and depressurization respectively. In this method, the cross-sectional area of the pipe can be related to surcharging pressure head (h_s) through the following equation (Sanders and Bradford, 2010):

$$A = A_f \left(1 + \frac{gh_s}{a^2}\right) \quad 2\text{-}4$$

The above equation accounts for pipe expansion and contraction due to pressurization and depressurization. In is worth mentioning that, by multiplying either side of Equation (2-3) by h_s and doing some algebra Equation (2-4) can be easily reached, confirming that both PSM and TPA have identical underlying concept.

In order to include the effect of negative pressure on the momentum equation, fluxes in equation (1) can be rewritten as follows:

$$\boldsymbol{F} = \begin{bmatrix} Q \\ \frac{Q^2}{A} + Ag(h_c + h_s) \end{bmatrix} \quad 2\text{-}5$$

As can be seen the pressure term in Equation (2-1) is split into two terms, h_c and h_s where h_c measures distance between the free surface and the centroid of the flow cross-sectional area and h_s represents surcharging head. In an open channel flow regime, h_s is set to zero and when the pipe is pressurized h_c represents the distance between the crowns of the pipe to the centroid of the pipe cross-sectional area. Note that during pipe depressurization while the system has sufficient ventilation, negative pressures cannot be maintained. This causes the flow to be switched back to an open channel flow with h_s = 0; otherwise h_s measures negative pressure.

2.5 Numerical Solution

In this work the Godunov scheme is utilized to numerically solve the governing equations. The Godunov scheme is an upwind finite volume based numerical scheme and widely used for solving partial differential equations (Toro, 2001). In this method, the spatial domain of the computation is broken down to a number of computational cells with a spatial distance of Δx and the temporal domain is split by a constant time interval of Δt. The order of accuracy of the Godunov scheme depends on the data reconstruction at the computational cells; piecewise constant data reconstruction provides first order accuracy and the piecewise linear data reconstruction results in second order accuracy. First order accuracy is employed in this research because, as will be discussed later, significant amount of artificial viscosity required for dissipating the spurious numerical oscillation associated with mixed flow modelling prevents the numerical scheme to provide second order accuracy even when a linear data reconstruction is utilized.

By discretizing Equation 2-1, unknowns at the current time level can be explicitly calculated based on the data retrieved from the previous timeline using the following equation.

$$\boldsymbol{U}_i^{n+1} = \boldsymbol{U}_i^n - \frac{\Delta t}{\Delta x}\left(\boldsymbol{F}_{i+\frac{1}{2}}^n - \boldsymbol{F}_{i-\frac{1}{2}}^n\right) + \Delta t \times \boldsymbol{R}_i^n \qquad 2\text{-}6$$

where subscripts i = computational cell number, $i+\frac{1}{2}$ and $i-\frac{1}{2}$ = upstream and downstream boundaries of the i^{th} computational cell, n = previous time step and $n+1$ = current time step. Equation (2-6) can be used to calculate the discharge and flow depth provided the flux at the boundaries of the cells are known. In the Godunov scheme, the fluxes at the cell boundaries are

calculated through solving the Riemann problem. A Riemann problem is the solution of a system of hyperbolic equation at a flow discontinuity with initial piecewise constant data (Toro, 2001). Exact Riemann solution can be obtained for the current system of equation but considering the iterative nature of the solution it is quite time consuming which in turn compromises the efficiency of the numerical analysis. To resolve this problem, approximate Riemann solution can be also utilized to speed up the calculations (Toro, 2001). Several approximate Riemann solutions are proposed among which the HLL Riemann solution is one of the efficient ones, so it is utilized in this study. The HLL Riemann solution is originally proposed by Harten, Lax, and Van Leer (HLL) and developed based on the assumption that the generated waves on the either side of the discontinuity are both of shock wave type.

Figure 2.1

Wave structure at the HLL solver

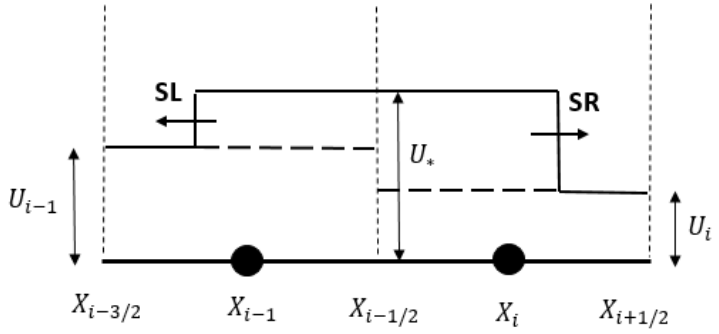

Left and right shock wave velocities can be calculated by the following formula:

$$S = \frac{dF}{dU} \tag{2-7}$$

$$S_L = \frac{F_L - F_*}{U_L - U_*} \tag{2-8}$$

$$S_R = \frac{F_R - F_*}{U_R - U_*} \tag{2-9}$$

In the HLL Riemann solution if the shock waves move in opposite direction flux (i.e., $S_L \leq 0 \; and \; S_R \; \geq 0$) at the cell interface can be calculated by cancelling out U_* in Equations (2-8) and (2-9). Otherwise, data sampling is required for calculating the fluxes. If the left wave velocity (S_L) is greater than zero, the flow would be of supercritical type and the flux at the cell interface becomes equal to F_L. However, if S_R is less than zero the flux at the cell interface would be equal to F_R because the flow is supercritical but moves in the opposite direction. The following equations summarize flux at the cell interface under different flow condition:

$$\begin{cases} F_L & \text{if } S_L > 0 \\ \frac{S_R F_L - S_L F_R + S_L S_R (U_R - U_L)}{S_R - S_L} & \text{if } S_L \leq 0 \; and \; S_R \; \geq 0 \\ F_R & \text{if } S_R < 0 \end{cases} \tag{2-10}$$

Though first order Godunov scheme with the HLL Riemann solver generally provides monotonous and oscillation free solution, it still produces significant spurious oscillation while used in the context of transient mixed flow analysis. Drastic change in wave velocity during the pressurization has been accepted as the key reason of the numerical oscillation. However, under what specific mechanism the change in wave velocity results in numerical oscillation needs more investigation.

Vasconcelos et al. (2009) concluded that the post-shock oscillations associated with the PSM have the same origin as slow-moving shocks in gas dynamics (Arora and Roe 1997; Karni and Čani´c 1997) and proposed two different methods for dissipating the numerical oscillations. In the first method a numerical filter was proposed to smooth the numerical results in each time step. However, this method was shown not to be efficient in higher pipe acoustic speed. In addition, it does not discriminate between spurious numerical oscillation and the numerical oscillations with physical basis. In the second method, a hybrid flux is utilized to gradually add artificial numerical viscosity to the numerical scheme through increasing the wave velocity. This method efficiently supresses spurious numerical oscillation as long as the pipe acoustic speed does not exceed a certain value (100-150 m/s). Nevertheless, in higher pipe acoustic speed too much artificial viscosity is required to dissipate the numerical oscillation but in the expense of significant numerical diffusion that compromises the accuracy of the results.

Malekpour and Karney (Malekpour and Karney, 2014) studied the numerical orbits of a first order Godunov numerical scheme with a HLL Riemann solver on the phase plan and realized that in order to supress the spurious numerical oscillations, artificial numerical viscosity should be admitted only when the flow pressurization is imminent. Also, they found that adding artificial viscosity only at the computational cell in which flow transition occurs may even exacerbate the spurious numerical oscillations. To resolve this problem, they showed that the artificial viscosity should be distributed among several computational cells located around the computational cell receiving flow transition. The numerical results showed that this approach can provide oscillation free results even at as high pipe acoustic speed as over 1000 m/s. The

robustness of the proposed HLL solver by Malekpour and Karney has been confirmed by other researchers (Hyunuk et al., 2018; Mao et al., 2020), so it is adopted in this research.

In order to show how artificial numerical viscosity can be increased in the HLL solver consider Equation (2-10) representing flux at the star zone. Assuming that the absolute value of the left and right wave velocities are equal, flux in the star zone presented in Equation (2-10) can be rewritten as follows:

$$F_* = \frac{F_L + F_R}{2} + \frac{S_W(U_R - U_L)}{2} \qquad 2\text{-}11$$

The first term on the right-hand side of Equation (2-11) provides a flux which is unconditionally unstable (LeVeque, 2002). This concludes that the second term plays an important role to stabilizing the flux through admitting artificial viscosity to the scheme. This implies that the magnitude of the numerical viscosity can be increased by increasing the wave velocity. It is important to note that adding too much numerical viscosity produce significant data smearing and numerical diffusion, which in turn compromises the accuracy of the results. To control data smearing, Malekpour and Karney (2014) proposed a method for calculating the left and right wave velocities that can automatically increase the amount of artificial numerical viscosity in the neighbourhood of the pressurization interface. To calculate the wave velocities, the following formula which is the adjusted version of the Leon et al.'s is adopted in this research.

$$S_L = V_L - \Omega_L \; ; \; S_R = V_R + \Omega_R \qquad 2\text{-}12$$

where $\Omega_{K(K=L,R)}$ is given by

$$\Omega_K = \begin{cases} \sqrt{\frac{g[Y_G A_G - (h_c + h_s)_K A_K] A_G}{A_K (A_G - A_K)}} & \text{if } A_G > A_K \\ C_K & if\ A_G \leq A_K \end{cases} \qquad 2\text{-}13$$

where C = gravity wave velocity and the variables with sub index G are the function of Y_G that need to be estimated.

Malekpour and Karney (2014) shows that if Y_G is greater than the height of the conduit the wave velocity calculated by Equation (2-13) does not differ from the gravity wave velocity except in the vicinity of the conduit roof. In other words, by using Equation (2-13) significant artificial velocity is admitted to the numerical scheme only when the water surface in the conduit becomes very close to the conduit roof and the conduit is about to become pressurized. Extensive numerical experiment by Malekpour and Karney came up with the following formula for calculatingY_G.

$$Y_G = K_a\left[d_{i-NS}, d_{i-NS+1}, .. d_{i,} d_{i+1}, .. d_{NS}\right] \qquad 2\text{-}14$$

where $d = h_c + h_s$.

By using the above equation, the maximum d is calculated within a number of cells (NS) located on either side the i^{th} cell for which the wave velocity is being calculated. Y_G is then calculated by multiplying the maximum d by the factor K_a. In this way, numerical viscosity is distributed within a number of cells rather than being injected just in one cell. If all ds are greater than the conduit height, the system is pressurized and a K_a = 1.001 would provide reasonable

results. When there exists a pressurization, front located within the cells, the numerical viscosity is further intensified by applying K_a = 1.4. The number of cells (NS) considered depend on the resolution of the computational grid and should be selected such that the numerical viscosity is adequately distributed on either side of the computational cell for which the wave velocity is being calculated. Malekpour and Karney (2014) suggested that the number of cells should cover a distance equal to at least three times as large as the conduit height but in any case, it shouldn't be less than 3 cells. If the i^{th} computational cell is found near a boundary, the flow depth at the boundary point should be also incorporated into Equation (2-14).

2.6 Numerical Verification

In this section the performance of the proposed model is investigated using several test cases. These test cases are to verify different aspects of the model including: 1) the ability of the model in suppressing spurious numerical oscillations induced during the pressurization of conduits under different pipe acoustic wave speed; 2) the performance of the model in capturing negative pressures and 3) to justify if the model can capture waterhammer pressures and whether the model adequately discriminates between numerical and physical based numerical oscillation.

2.6.1 Test Case 1

In this test case, it is shown that the proposed model can efficiently suppress the spurious numerical oscillations without producing significant numerical diffusion. To achieve this, rapid filling is simulated in a horizontal and frictionless box shape conduit with a length of 400 m and with the same width and height of 1 m (unit cross sectional area). The conduit initially maintains a stagnant water column with a depth of 0.6 m when the water level in the upstream water tank is

suddenly increased from 0.6 m to 4 m (see Figure 2-1). Due to its simplicity, this problem has an analytical solution and can be employed to verify the model result. By applying momentum and energy equation, it is easy to show that following water level rises in the reservoir; a hydraulic bore is set up in the conduit and moves with the velocity of 10.08 m/s (Malekpour and Karney, 2014). As the bore moves through the conduit, a pressure head of 3.167 m is stabilized in the conduit.

This test case is numerically simulated with a spatial increment of 1 m (400 computational cells) for both the conventional (Leon at al., 2019) and the proposed HLL Riemann solutions. Figure 2.3 presents the pressure head along the conduit calculated by the conventional HLL Riemann solution at 10 s after the water level has risen in the reservoir. The numerical results show that considerable spurious numerical oscillation occurs even when the acoustic speed used is just 50 m/s. The numerical results confirm (not shown here) that by increasing the conduit acoustic speed, the numerical oscillations are violently intensified, and eventual resulting in non-physically sensible solution when the acoustic speed exceed 300 m/s.

Figure 2.2

Schematic of test case 1

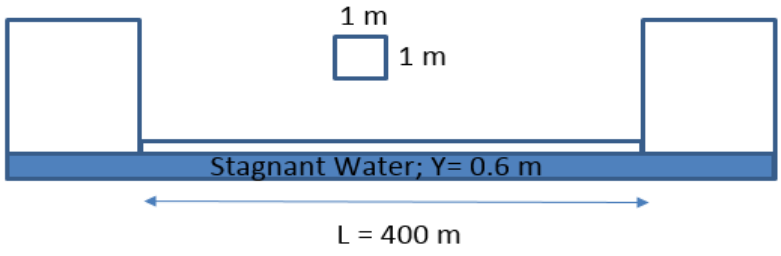

Figure 2.3

The numerical results at 10 s after the water level has risen in a test reservoir with acoustic speed of 50 m/s (conventional HLL solver)

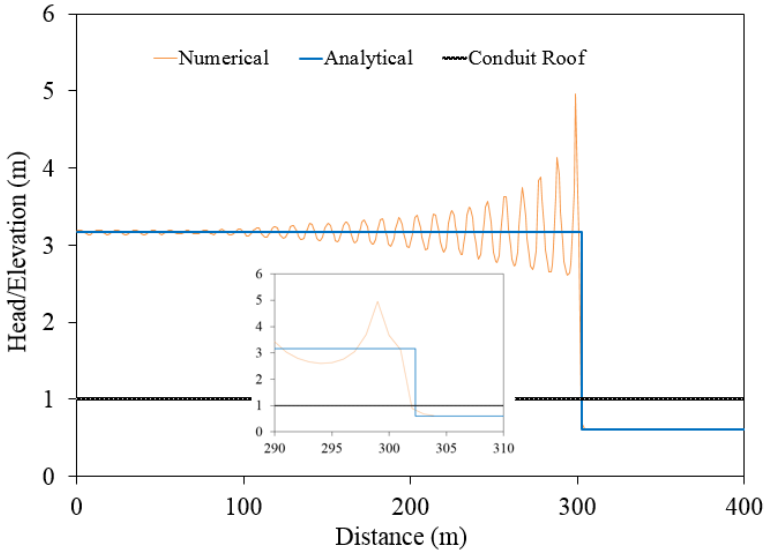

Figure 2.4

The numerical results at 10 s after the water level has risen in a test reservoir with acoustic speed of 1000 m/s (proposed HLL solver)

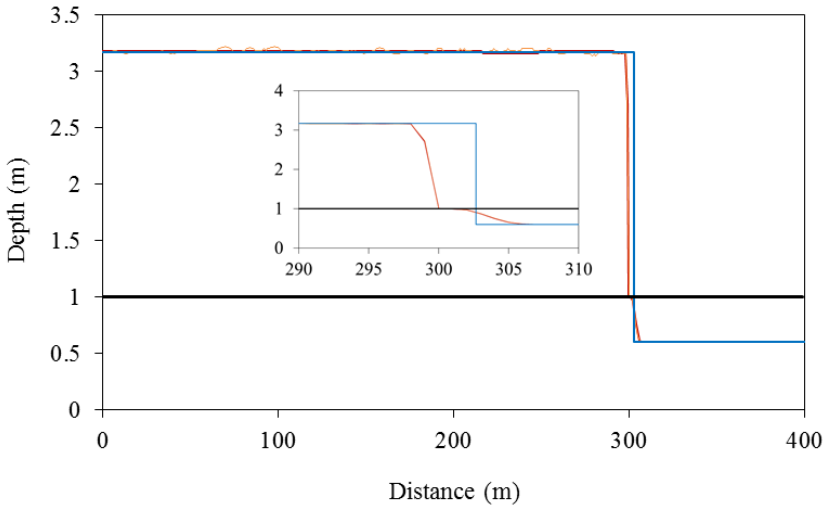

Figure 2.4 shows the numerical results obtained through applying the proposed HLL Riemann solver with NS set at 5. As can be seen, the model provides oscillation free solution even at an acoustic speed of 1000 m/s. Nevertheless, some non-significant numerical wiggles appear in the result at the Courant number of 0.8. The problem is resolved when the Courant number is reduced to 0.5. Comparing Figures 2.3 and 2.4 reveals that the additional numerical viscosity added by the proposed model does not significantly increase data smearing in the open channel flow section right after the hydraulic bore front.

2.6.2 Test Case 2

This test case makes use of the experimental results conducted by Vasconcelos et al. (2006). The performance of the model in capturing both waterhammer pressure and mass oscillation in the system is evaluated. As shown in Figure 2.5, the test apparatus includes a horizontal acrylic pipe with an internal diameter and a length of 9.4 cm and 14.33 m, respectively, that connects two tanks at its upstream and downstream sides. The upstream tank has a square cross section with a side and a height of 25 and 31 cm, respectively. The downstream tank, which is a cylinder shape tank with an internal diameter of 19 cm, is tall enough to prevent overflow during the experiment. A partially open gate valve at the downstream side of the pipe, in conjunction with an air vent, is utilized to remove air during the filling of the pipe and to induce waterhammer pressure when the filling bore impacts the valve. With the pipe initially maintaining a stagnant water column of 7.3 cm, rapid filling is experimented by enforcing a constant flow of 3.1 L/s at the upstream tank. The transient flow in this experiment is dominantly governed by inertia and mass oscillation, but during a short period

of time following the contact of the filling bore with partially open gate valve, the elastic feature of the flow and waterhammer effects becomes of great importance. Since the pipe and valve head loss coefficients as well as the pipe acoustic speed were not reported in the original work, a calibration procedure is undergone to calculate these parameters. Extensive numerical exploration is conducted with N set to 400, NS of 12 and the Courant number of 0.5 to calculate the best values for the unknown parameters. This procedure ends up with 12, 300 m/s and 0.016 $m^{1/6}$ for the valve head loss coefficient, acoustic pipe speed, and pipe's Manning head loss coefficient, respectively.

Figure 2.6 shows the velocity time histories at 9.9 m from the upstream tank obtained from both the proposed model and Vasconcelos et al.'s (2006). Both models replicate the experimental data very well though the proposed model performance is better. Pressure time history obtained from the proposed model is also compared with the experimental data in Figure 2.7. As can be seen, the proposed model results are in a very good agreement with the experimental data, confirming the validity of the proposed model. Figure 2.7 also shows that mass oscillation governs the transient flow except in a very short period of time. Waterhammer pressure spike appeared in both experimental and numerical results are the result of impacting hydraulic filling bore with the partially closed gate. The severity of the waterhammer pressure depends on the magnitude of acoustic wave speed and the results reveal that an acoustic wave speed of 300 m/s makes the numerical results to match the experimental results quite well. The calibrated value of the acoustic speed is within the range typically utilized for the pipe material used in the experiment, another indication confirming the validity of the model results.

It is interesting to see that the numerical results obtained from applying an acoustic wave speed of 500 m/s (Figure 2.8) overestimates the magnitude of the waterhammer pressure but does not affect mass oscillation in the system which is physically feasible. The magnitude of the waterhammer pressure head rise is two times as high as that produced with acoustic wave speed of 300 m/s, showing that the model is correctly capturing the waterhammer effect in the system. Assessing the numerical response in the waterhammer zone reveals that the numerical oscillation remains much longer than what happened in reality. This concludes that the numerical viscosity added by the proposed HLL Riemann solver does not dissipate pressure head oscillation with valid physical basis.

Finally, the gate valve's head loss coefficient calculated through the calibration procedure needs to be justified. Assuming a gate discharge coefficient of 0.6, the gate opening associated with the calibrated head loss coefficient of 12 is estimated by the orifice equation as 48%, which seems to be reasonable.

Figure 2.5

Schematic of test case 2

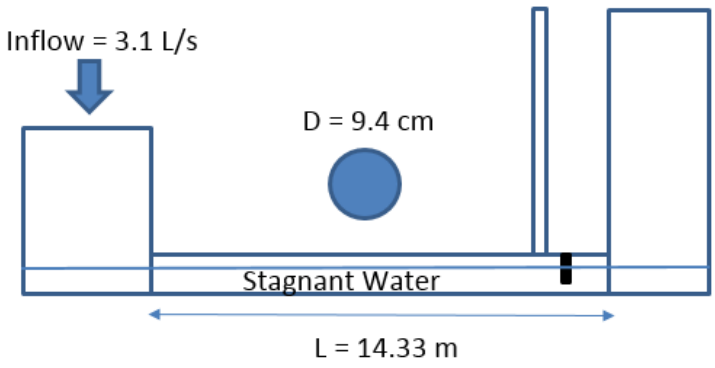

Figure 2.6

Comparing numerical and experimental velocity time histories at 9.9 m from the upstream tank

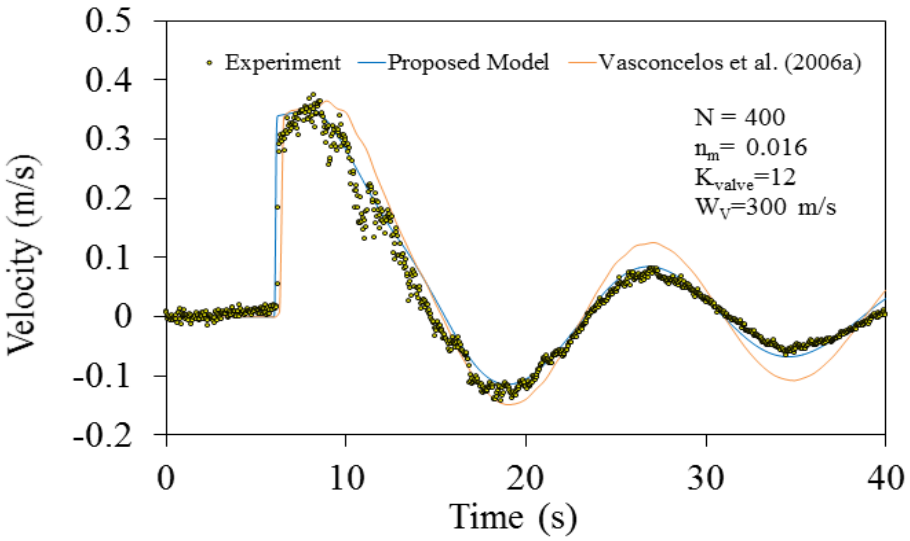

Figure 2.7

Comparing numerical and experimental pressure head time histories at 9.9 m from the upstream tank (acoustic speed = 300 m/s)

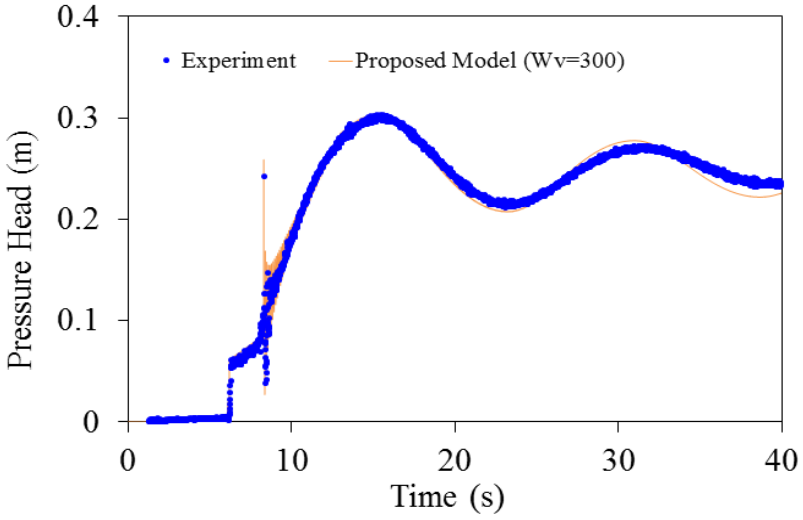

Figure 2.8

Comparing numerical and experimental pressure head time histories at 9.9 m from the upstream tank (acoustic speed = 500 m/s)

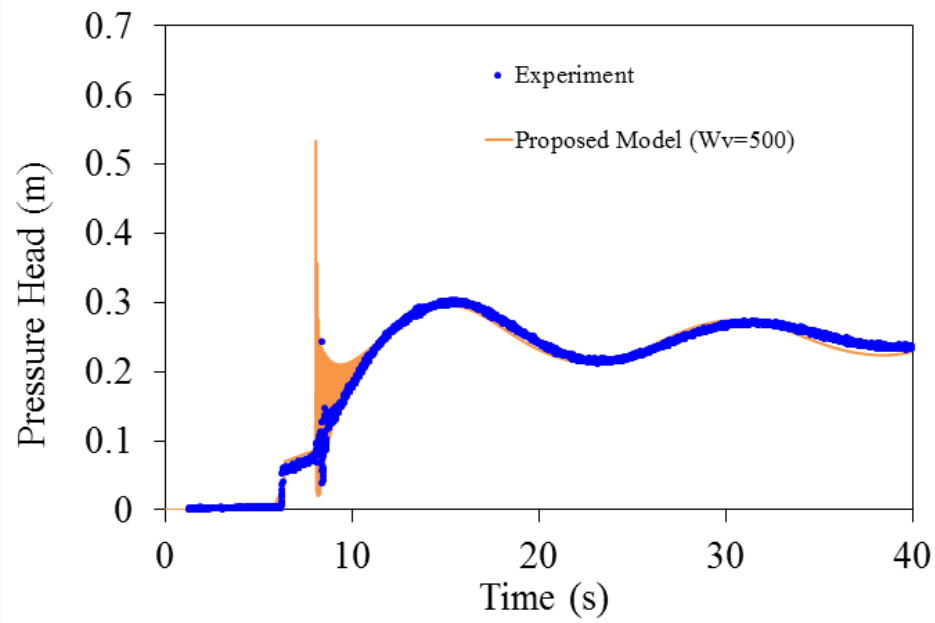

2.6.3 Test Case 3

In this test case, the experimental study conducted by Vasconcelos et al. (2009) is utilized to justify the validity of the proposed model in capturing non-oscillatory solution during pipe filling. The test rig is similar to the previous test case with two differences which are: 1) the pipe has an upslope of 0.1 and 2) there is no gate valve in the pipe (see Figure 2.9). A stagnant water column causes the initial water depth in the pipe to change from 8.2 cm in the upstream side to 6.7 cm in the downstream side. Rapid filling was implemented through applying a constant flow into the upstream tank. However, since the filling flow rate was not reported in the original work,

the upstream boundary condition is treated similar to the approach employed by Leon et al. (Leon and Ghidaoui, 2012). Leon et al. assumed that the flow at the upstream tank suddenly increased by 25 cm above the connecting pipe's bed and remains constant at this level for the rest of simulation.

Rapid filling is simulated with this set of parameters: NS = 12, N = 400 cells, a = 1000 m/s, Cr = 0.5, and n_m = 0.011. Figure 2.7 compares the hydraulic grade lines obtained from the proposed HLL solver and from the Hybrid-Flux approach proposed by Vasconcelos at al. (2009) at 6 s from the beginning of the filling. As can be seen in this figure, the proposed approach provides oscillation free solution at 1000 m/s but the Hybrid-Flux induced spurious numerical oscillations even at the acoustic speed of 100 m/s. It is worth noting that the numerical diffusion produced by the proposed approach in the open channel flow which occurs right after the filling bore is lesser than that induced by the Hybrid-flux method, confirming that the proposed approach admits optimal amount of numerical viscosity to the numerical scheme. Finally, Figure 2.10 depicts that the location of the filling bore replicated by the proposed approach at the time of 6 s is around one meter a head of that calculated by Vasconcelos et al. (2009), implying that the filling bore moves faster in the proposed approach than Vasconcelos et al.'s. To identify the root of the difference, the experimented water level time history in the downstream tank is compared with both the water level time histories obtained from the proposed HLL solver and from the Hybrid-Flux of Vasconcelos et al. As can be seen in Figure 2.11, the hydraulic bore arrival time to the downstream tank is correctly replicated by the proposed model; this means that the hydraulic bore speed is correctly captured by the proposed model.

Figure 2.9

Schematic of test case 3

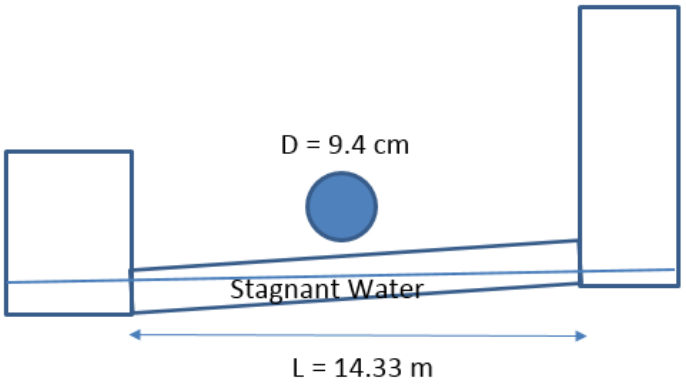

Figure 2.10

Hydraulic grade lines at the time of 6 s

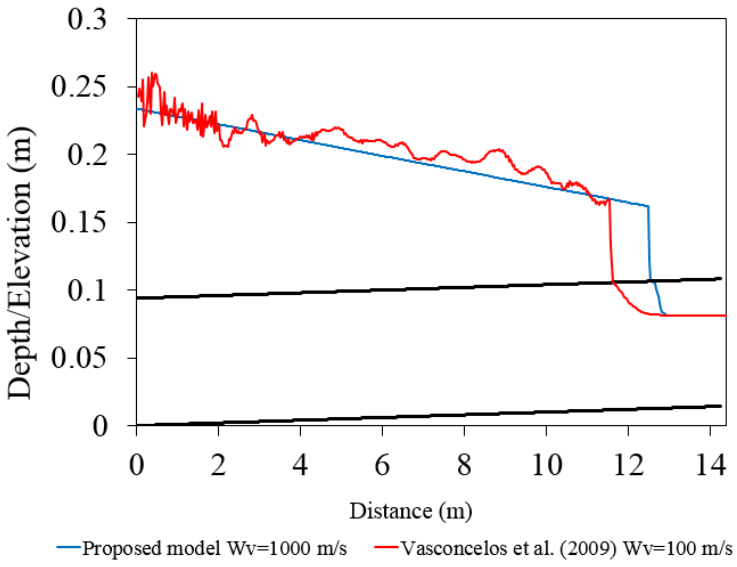

Figure 2.11

Water level time histories at the downstream tank

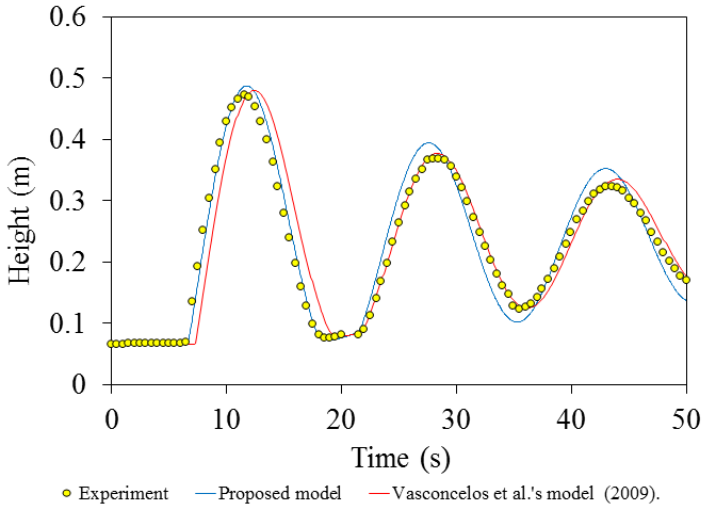

2.6.4 Test Case 4

The aim of conducting this test case is to verify that the proposed model can capture negative pressures. We consider a hypothetical frictionless-horizontal pipe-reservoir-valve system with the length; pipe diameter and acoustic speed of 400 m, 1 m and 1020 m/s, respectively (see Figure 2.12). The system initially runs at a steady state velocity of 4 m/s when the downstream valve is suddenly closed. This results in a waterhammer pressure spike which is running back and forth without being dissipated as the pipe system is considered frictionless. Due to its simplicity, this test case does have an analytic solution which can be utilized as a benchmark for verifying the proposed model's results. Figure 2.13 compares the time history of the calculated waterhammer pressure at the downstream end of the pipe with the analytical solution. It can be seen that the model accurately calculated the magnitude and frequency of the

induced waterhammer pressures. However, due to the artificial viscosity added to the numerical scheme, some non-physical numerical dissipation occurs that causes the edge of the calculated pressure head time history to be rounded.

Figure 2.12

Test case 4 schematic

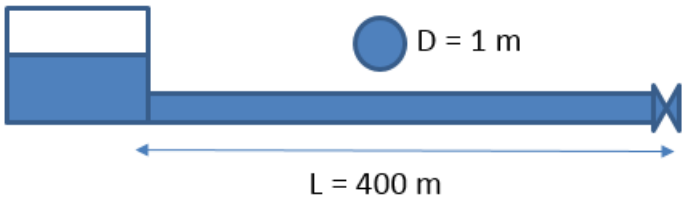

Figure 2.13

Waterhammer pressure oscillations

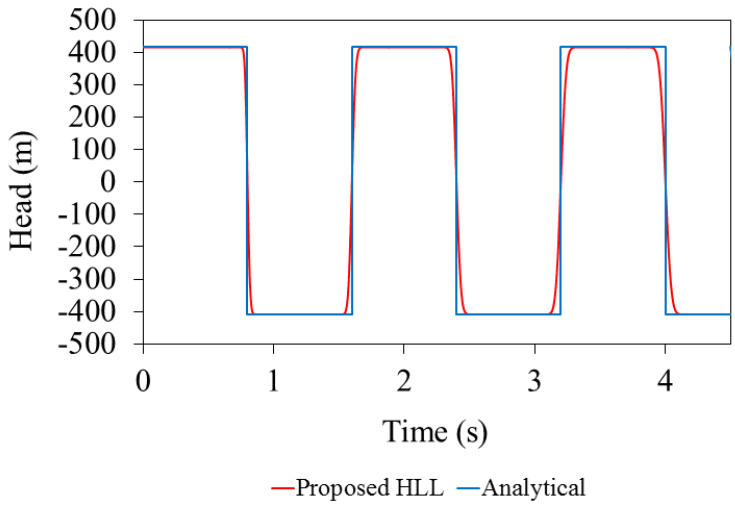

2.6.5 Test Case 5

In this test case, the ability of the proposed model in capturing negative pressures are tested through a hypothetical pipe system for which an analytical solution exists. The pipe system consists of two pipes with the profile shown in Figure 2.14 and the internal diameter of 0.3 m. An upstream reservoir with a constant head of 30 m is utilized to supply the pipe system during filling. A rapid filling is simulated with the setting parameters being N = 200 cells, NS = 4, a = 500 m/s and n_m = 0.009. The simulation is continued until the whole system is filled and as shown in Figure 2.15, the system reaches a steady state flow condition with a final flow rate of 0.1712 m^3/s. Figure 2.14 compares the calculated steady state Hydraulic Grade Line (HGL) with that obtained from a spreadsheet analysis. As it can be seen in Figure 2.14, the numerical results coincide the analytical solution showing that the model is correctly converging to the steady state condition. Obviously, the model also correctly captured the negative pressure occurred within the second half of the pipe.

Figure 2.14

Stablished steady state HGL at the flow rate of 0.1712 m

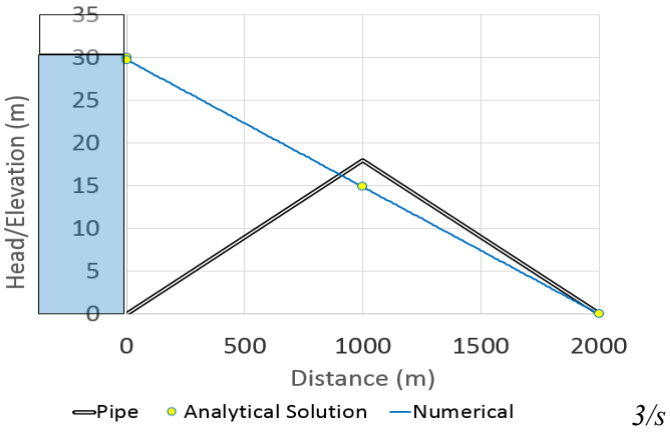

3/s

Figure 2.15

System flow rate time history

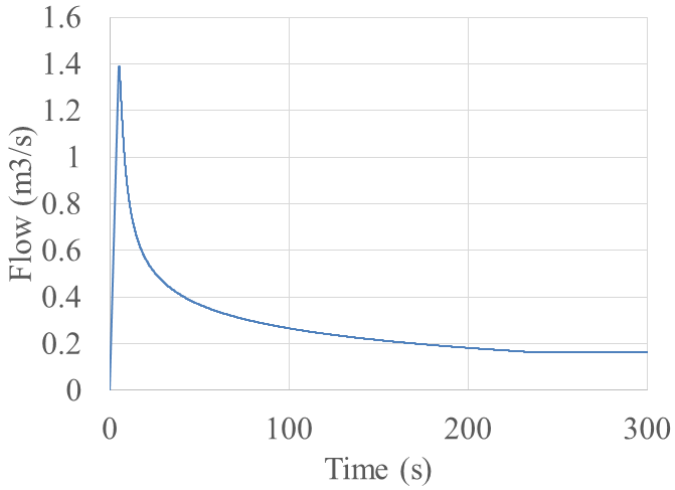

2.7 Discussion

Test case 1's results reveal that spurious numerical oscillations are induced when the flow regime is changed from open channel to pressurized flow. The numerical oscillations ware attributed to the fact that during the pipe pressurization, the wave velocity drastically increases when the flow is switched from open channel to pressurized flow; the higher the pipe's acoustic wave speed, the more intensified the numerical oscillations become. In such cases, the conventional Godunov finite volume scheme fails to dissipate the numerical oscillations, with extensive non-physical positive and negative pressure spikes appearing in the solution, which can eventually lead the procedure to the collapse of the computer code. Several studies tended to add artificial velocity only at the computational cell containing the pressurization front, but the results showed that this approach is unable to efficiently dissipate the numerical oscillations, particularly when the acoustic wave speed exceeds 150 m/s. This is far below the realistic pipe's

acoustic wave speed, which may exceed 1000 m/s, depending on the fluid properties, physical characteristics, and rigidity of each pipe. Rather than admitting the artificial viscosity at a local point, the modified HLL Riemann solution utilized in this research distributes artificial numerical viscosity over several computational cells around the cell containing the pressurization front. Test cases 1 and 3 justify that the proposed numerical model can dissipate the spurious numerical oscillations without producing significant data smearing.

To justify that the admitted artificial numerical viscosity does not dissipate the real pressure oscillations with a physical basis, we considered test case 2, which manifested both mass oscillations and waterhammer pressures. As test case 2's results imply, the proposed numerical scheme discriminates between physical and non-physical numerical oscillations and automatically controls the value of the artificial numerical viscosity without damping the physical pressure oscillations. It is worth mentioning that the artificial numerical viscosity can still affect physical pressure oscillations but the dissipation is too little to compromise the results. Test case 4's results showed that the model captures severe waterhammer pressure oscillations, and the admitted artificial viscosity also rounds the corner of the waterhammer pressure signals, which is ideally supposed to have rectangular shapes.

Finally, test cases 4 and 5 are used to confirm that the model enables capturing of negative pressures while controlling spurious numerical oscillations. As the results show, negative pressures are correctly replicated by the model, but the model is unable to capture water column separation. Test case 5's results clearly show that the induced negative pressure heads drop to nearly −400 m, but in reality, it is limited to the liquid vapor pressure head. As soon as

the pressure falls to the vapor pressure head, cavitation forms and the water column is locally separated. Replicating column separation requires more modification to the model, which is currently being perused by the authors.

2.8 Conclusion

In this paper, we proposed a numerical model to calculate transient mixed flow in close conduit systems. The TPA was utilized to enable the model to capture negative pressures. A first-order Godunov-type finite volume numerical scheme is utilized to numerically solve the governing equations. To dissipate the spurious numerical oscillations, we admit artificial numerical viscosity to the numerical scheme through applying a proposed HLL Riemann solver which is utilized for calculating the numerical fluxes at the computational cell interfaces. The proposed HLL solver controls the magnitude of the numerical viscosity through adjusting the left and right wave velocities. A wave velocity calculator is utilized to optimally distribute the numerical viscosity over several computational cells around the computational cell in which the pressurization front is located. The HLL solver admits significant artificial numerical viscosity when the pipe pressurization is imminent and automatically reduces it in other places; in this way, the numerical diffusion and data smearing are minimized.

Several test cases are presented to justify the validity of the model. The numerical results show that the proposed model completely dissipates the spurious numerical oscillations during flow transition, even at high pipe acoustic speeds over 1000 m/s. The results also imply that the model succeeds in capturing negative pressures during the course of transient flows. This concludes that the TPA with the proposed HLL solver provides a robust and efficient tool for

simulating and analyzing transient mixed flow in close conduit systems with a wide range of acoustic wave speeds.

Nevertheless, the proposed model cannot simulate column separation, which may occur when the negative pressure in the system falls close to the vapor pressure of the liquid. Including a column separation feature to the model is something that is being perused rigorously by the authors, and the results will be presented in another paper.

2.9 References

Abbott, M. B., & Minns, A. W. (1998). *Computational hydraulics.* Connecticut: Ashgate.

Arora, M., & Roe, P. L. (1997). On postshock oscillations due to shock capturing schemes in unsteady flows. *Journal of Computational Physics, 130*(1), 25-40.

Bourdarias, C. &. (2007). A finite volume scheme for a model coupling free surface and pressurised flows in pipes. *Journal of Computational and Applied Mathematics, 209*(1), 109-131.

Bousso, S., Daynou, M., & & Fuamba, M. (2013). Numerical modeling of mixed flows in storm water systems: critical review of literature. *Journal of Hydraulic Engineering, 139*(4), 385-396.

Capart, H., Sillen, X., & Zech, Y. (1997). Numerical and experimental water transients in sewer pipes. *Journal of Hydraulic Research, 35*(5), 659-672.

Cardle, J. A., & Song, C. S. (1988). Mathematical modelling of unsteady flow in storm sewers. *International Journal of Engineering Fluid Mechanics, 1*(4), 495–518.

Chaudhry, M. H. (1999). *Open channel flow.* Englewood Cliffs, N.J : Prentice-Hall.

Cunge, J. A., & Wegner, M. (1964). Numerical Integration of Bane de Saint-Venant's Flow Equations by Means of an Implicit Scheme of Finite Differences. Applications in the Case of Alternately Free and Pressurized Flow in a Tunnel. *La Houille Blanche, 1*, 33-39.

De Marchis, M., Fontanazza, C. M., Freni, G., La Loggia, G., & Napoli, E. &. (2010). A model of the filling process of an intermittent distribution network. *Urban Water Journal, 7*(6), 321-333.

Fuamba, M. (2002). Contribution on transient flow modelling in storm sewers. *Journal of hydraulic research, 40*(6), 685-693.

Garcia Navarro, P., Priestley, A., & Alcrudo, F. (1994). Implicit method for water flow modelling in channels and pipes. *Journal of Hydraulic Research, 32*(5), 721–742.

Guo, Q., & Song, C. S. (1990). Surging in urban storm drainage systems. *Journal of Hydraulic Engineering, 116*(12), 1523–1537.

Hyunuk, A., Seungsoo, L., Seong, J., Yeonsu, K., & Jaekyoung, N. (2018). Hybrid Numerical Scheme of Preissmann Slot Model. *water, 10*(7), 899.

Ji, Z. (1998). General hydrodynamic model for sewer/channel network systems. *Journal of Hydraulic Engineering, 124*(3), 307–315.

Jin, S., & Liu, J. G. (1996). The effects of numerical viscosities: I. Slowly moving shocks. *Journal of Computational Physics, 126*(2), 373-389.

Karni, S., & Čanić, S. (1997). Computations of slowly moving shocks. *Journal of Computational Physics, 136*(1), 132-139.

Kerger, F., Archambeau, P., Erpicum, S., Dewals, B. J., & Pirotton, M. (2011). An exact Riemann solver and a Godunov scheme for simulating highly transient mixed flows. *Journal of Computational and Applied Mathematics, 235*, 2030-2040.

Leon, A. S., & Ghidaoui, M. S. (2010). Discussion of Numerical Oscillations in Pipe-Filling Bore Predictions by Shock-Capturing Models by J. G. Vasconcelos, S. J. Wright, and P. L. Roe. *Journal of Hydraulic Engineering, 136*(6), 392-393.

León, A. S., Ghidaoui, M. S., Schmidt, A. R., & García, M. H. (2009). Application of Godunov-type schemes to transient mixed flows. *Journal of hydraulic research, 47*(2), 147-156.

Leon, A. S., Ghidaoui, M. S., Schmidt, A. R., & Garcia, M. H. (2010). A robust two equation model for transient mixed flows. *Journal of Hydraulic Research, 48*(1), 44 -56.

LeVeque, R. (2002). *Finite volume methods for hyperbolic problems.* Cambridge, UK: Cambridge Press.

Liou, C. P., & Hunt, W. A. (1996). Filling of pipelines with undulating elevation profiles. *Journal of Hydraulic Engineering, 122*(10), 534-539.

Malekpour, A., & B., K. W. (2011). Rapid filling analysis of pipelines with undulating profiles by the method of characteristic. *ISRN Applied Mathematics*, Article ID 930460, 16 pages, http://dx.doi.org/10.5402/2011/930460.

Malekpour, A., & Karney, B. (2015). Spurious Numerical Oscillations in the Preissmann Slot Method: Origin and Suppression. *Journal of Hydraulic Engineering, ASCE*.

Malekpour, A., Papa, F., & and Radulje, D. (2017). Uncertainty Analysis in Strom Sewer Collection Systems Using Monte Carlo Simulation and Parallel Computing. *WEAO 2017 Technical Conference.* Ottawa.

Mao, Z., Guan, G., & Yang, Z. (2020). Suppress Numerical Oscillations in Transient Mixed Flow Simulations with a Modified HLL Solver. *water, 12*(5), 1245.

Politano, M., Odgaard, A. J., & Klecan, W. (2007). Case study: Numerical evaluation of hydraulic transients in a combined sewer overflow tunnel system. *Journal of Hydraulic Engineering, 133*(10), 1103-1110.

Razak, T., & Karney, B. (2008). Filling of branched pipelines with undulating elevation profiles. *0th International Conference on Pressure Surges* (pp. 473–487). UK: BHR Groupe.

Sanders, B. F., & Bradford, S. F. (2010). Network implementation of the two-component pressure approach for transient flow in storm sewers. *Journal of Hydraulic Engineering, 137*(2), 158-172.

Sjöberg, A. (1982). Sewer network models dagvl-a and dagvl-diff. In B. C. Yen (Ed.), *Urban Stormwater Hydraulics and Hydrology* (pp. 127-136). Littleton, Colo.: Water Resource Publications.

Song, C. S., Cardle, J. A., & Leung, K. S. (1983). Transient mixed flow models for storm sewers. *Journal of Hydraulic Engineering, 109*(11), 1487–1504.

Toro, E. F. (2001). *Shock-capturing methods for free-surface shallow flows.* Chichester, New York: John Wiley.

Trajkovic, B., Ivetic, M., Calomino, F., & D'Ippolito, A. (1999). Investigation of transition from free surface to pressurized flow in a circular pipe. *Water Science and Technology, 39*(9), 105–112.

Vasconcelos, J. G., Wright, S. J., & Roe, P. L. (2006). Improved simulation of flow regime transition in sewers: two-component pressure approach. *Journal of Hydraulic Engineering, 132*(6), 553-562.

Vasconcelos, J. G., Wright, S. J., & Roe, P. L. (2009). Numerical oscillations in pipe-filling bore predictions by shock-capturing models. *Journal of Hydraulic Engineering, 135*(4), 296-305.

Wiggert, D. C. (1972). Transient flow in free-surface, pressurized systems. *Journal of Hydraulic Engineering, 98*(1), 11-27.

3 CHAPTER THREE

3.1 A Mixed Flow Analysis of Sewer Pipes with Different Shapes using a Non-Oscillatory Two-Component Pressure Approach (TPA)

3.2 Abstract

This paper aims to justify the performance of a non-oscillatory TPA-based model proposed by the authors for capturing transient mix flow in sewer systems consisting of a variety of pipe shapes. The model utilizes a first-order Godunov Finite volume numerical scheme in which an HLL (Harten, Lax, and van Leer) Riemann solver is used for calculating the fluxes at the cells' boundaries. The spurious numerical solution associated with the transient mix flow analysis is suppressed by enhancing the numerical viscosity of the scheme when the pipe pressurization is imminent. Due to the lack of experimental data for systems with other pipe shapes than circular and rectangular, a hypothetical pipe system for which analytical solutions exist is employed to verify the model performance. The results reveal that for all pipe shapes considered, the model provides oscillation-free solutions even at a high acoustic speed of 1,400 m/s. It is also observed that the numerical results are in perfect agreement with the analytical solution. The obtained results conclude that the proposed model can be utilized to capture transient responses of sewer systems with any pipe shape.

3.3 Introduction

Sewer pipe systems rarely run under steady-state flow conditions as the inflows into such systems change with time. In dry weather conditions, the flow gradually changes with time

inside the conduits, and quasi-steady open channel flow is established across the system. However, when a severe storm occurs, complex transient flows may be onset and the system undergoes flow regime transition from open channel to pressurized flow. The induced pressurization front serves as a moving piston and makes the air expelled out of the system through different components including, drop shafts, manholes, and outfalls. Fortunately, during pressurization, the available storage in the partially filled conduit can accommodate the transient flow energy and does not allow the energy to be stored in the pipe and liquid as strain and compression energy (Malekpour et al., 2014). In such conditions, the elastic feature of the flow does not play an important role even if the pace of transient is high, and the inertia and mass oscillation mainly govern the transient flow.

However, there are some situations in which the elastic feature of the flow becomes important. Two pressurization hydraulic bores moving in the opposite direction can easily trap a large air pocket in the conduit. As the entrapped air becomes pressurized, it may absorb a good portion of the transient energy and can significantly affect the hydraulics of the system. If the energized air pocket finds its way to the drop shafts or manholes, it can violently leave the system and produce geyseing (Wright et al., 2010; Wright et al., 2011). However, the presence of an air vent centered at the right position causes the air pocket to leave the system and remove the risk of geysering. On the other hand, when the last air escapes from the system the two adjacent hydraulic bores collide and depending on the velocities of the adjacent water columns significant water hammer pressures can occur (Malekpour & Karney, 2019). The generated water hammer pressure spike will propagate and affect the rest of the pipe located between two adjacent drop

shafts reflecting the pressure spike. The reflected wave may produce intense negative pressures followed by column separation in the system.

Available off-the-shelf software such as SWMM (Gironás et al., 2010), InfoWorks (Innovyze, 2020), etc. can calculate the most dominant transient flow governed by the flow inertia and mass oscillation in the system, but they are cripple in capturing those transient flow phenomena governed by the elastic feature of the flow. To fill this gap, though partially, some in-house computer programs have been emerged for performing surge analysis in sewer pipe systems (see Vasconcelos et al., 2015). These programs use either shock fitting or shock-capturing numerical strategies to solve the one-dimensional momentum and continuity equations governing the transient flow in sewer systems.

In the shock-capturing strategy, the pressurization front(s) which separate open channel and pressurized flow is traced with time through applying the discrete form of continuity, momentum, and/or energy on either side of the pressurization front (Bourdarias Gerbi, 2007; Leon et al., 2010; Politano, et al., 2007). Having calculated the location of the front, the open channel and pressurized flow on either side of the interface are calculated using their own set of governing equations. Song et al. (1983) employed the shock fitting method along with the method of characteristic for analyzing transient mixed flow in sewer systems. Although the method of characteristics can replicate the pressurized flow quite accurately, it fails to reasonably capture hydraulics bores in the open channel flow sections. Abbott & Minns (1998) showed that the method of characteristics cannot conserve mass when applied along a hydraulic bore. Leon et al. (2010) addresses this issue by solving the conservative form of the governing equations using

a finite volume numerical method. Although the proposed method succeeded in replicating both open channel and pressurized flow accurately, it suffers from the common disadvantage of shock fitting methods which is the difficultly in handling several interfaces in the system as well as in treating the interaction of the interfaces with each other and with the boundaries of the system. This has made the shock-capturing method be center of interest among the researchers.

In the shock-capturing method, both open channel and pressurized flow are treated using the same set of equations utilized for calculating transient open channel flows. The most popular method of this type is well-known as Preissmann Slot Method (PSM) (Kerger et al., 2011; Malekpour & Karney, 2015; Sjöberg, 1982), named after its inventor engineer Preissmann (Preissmann & Cunge, 1961). By a virtual narrow slot, on the crown of the pipe, the flow is assumed to always remain in open channel flow condition. The width of the slot is calculated in a way that open channel waves move as fast as their counterpart elastic waves in pressurized flows; the height of the water in the slot represents the pressure head of the flow. However, this approach cannot replicate negative pressures and as soon as negative pressures tend to occur, the flow switches to open channel flow. Kerger et al. resolved this problem by improving the PSM using a virtual negative slot and showed that their method can accurately replicate negative pressures. By splitting the pressure term in the momentum equation, Vasconcelos et al., (2006) proposed a novel approach, the Two-Component Pressure Approach (TPA), which can capture negative pressures during transient mixed-flow analysis.

Both PSM and TPA, however, generate spurious numerical oscillation when the flow regime changes from open channel to pressurized flow. The numerical oscillation intensifies as

the acoustic wave speed considered in the calculation increases, beyond a certain level it makes the solution unstable and worthless. One approach to control the numerical oscillation is to artificially reduce the wave speed but this approach is acceptable as long as the physics of the problem is not distorted. In a flow condition that is governed by the inertia and mass oscillation, the transient flow is independent of the wave speed and this approach works well, though due to a considered wider slot, some artificial storage is added to the system resulting in extra non-physical pressure attenuation (Ridgway & Kumpala, 2008). However, when the elastic feature of the transient flow becomes of significant importance, reducing the wave speed compromises the results by distorting the magnitude and distribution of the resulting pressures.

Vasconcelos et al (2009) proposed Numerical Filtering and Hybrid Flux approaches to suppress the spurious numerical oscillations and showed that these approaches can reasonably control the numerical oscillations if the acoustic wave is below a certain level (100 m/s). Malekpour and Karney (2015) proposed an approximate HLL solver which can remove the numerical oscillation in the PSM even when the acoustic speed exceeds 1000 m/s; the validity of his method has been independently confirmed by others (An et al., 2018).

3.4 Objective and Organization of the Research

Recently Khani et al. (2020) employed the approximate HLL solver proposed by Malekpour and Karney (2015) in conjunction with TPA and showed that the solver can effectively remove the numerical oscillations for as high acoustic wave speed as 1000 m/s, though the validity of the model was tested for pipes with circular sections and rectangular cross-sections. However, in real sewer pipe systems, a variety of pipe shapes can be used so further

investigation is required if this model can be utilized in practice. To fill this gap, this paper tends to verify whether the performance of the model is retained when applied to other pipe cross-sections.

The paper organization is as follows: Theoretical background including governing equations, TPA, and the numerical solution is first described, and the hypothetical example and its associated analytical solution utilized for validation of the produced numerical results are then and discussed. In the next stage, the numerical results are compared with the analytical solutions and finally, the conclusions are made.

3.5 Theoretical Backgrounds

3.5.1 Governing Equations

Unsteady flows in open channels are governed by the following partial differential equations representing the conservative form of the continuity and momentum equations (Chaudhry, 1999):

$$\frac{\partial U}{\partial t}+\frac{\partial F}{\partial x}=S \qquad 3\text{-}1$$

where the vectors U, F, and S are the flow variables, fluxes and source terms respectively and shown in the following:

$$U=\begin{bmatrix}A\\Q\end{bmatrix};F=\begin{bmatrix}Q\\\frac{Q^2}{A}+Agh\end{bmatrix};\ S=\begin{bmatrix}0\\gA(S_0-S_f)\end{bmatrix};\ S_f=\frac{Q^2n^2}{A^2R^{\frac{4}{3}}} \qquad 3\text{-}2$$

where A = flow cross sectional area, Q = flow rate, h = distance between the free surface and the centroid of the flow cross sectional area, S_0= pipe slope, S_f= energy grade line slope, R = flow hydraulic radius, n = Manning coefficient and g = gravitational acceleration.

3.5.2 TPA

By a smart trick, the above equation can be also used for calculating pressurized flows. In PSM, a narrow slot above the crown of the pipe allows the flow to remain in an open channel flow regime even when the pipe is surcharged. The width of the slot is selected narrow enough to make sure that, while the flow is in the slot the open channel wave velocity replicates the acoustic wave speed of the pipe. The following equation relates the slot width and pipe acoustic speed:

$$T_S = \frac{gA_f}{a^2} \qquad 3\text{-}3$$

where T_S, A_f, and a are the slot width, the cross-sectional area of the pipe and the acoustic speed of the pipe respectively.

In TPA (Khani et al., 2020), in order to use Equation (3-1) for pressurized flow, the flow depth in the momentum flux is split into two terms, as shown in the following.

$$F = \begin{bmatrix} Q \\ \frac{Q^2}{A} + Ag(h_c + h_s) \end{bmatrix} \qquad 3\text{-}4$$

In this equation, h_c represents the distance between the water surface and the centroid of the flow cross sectional area, and h_s measures the surcharging head. When the pipe carries open channel flows, the surcharging head is set to zero and the flux becomes identical to its original form presented in Equation (3-1). However, when the pipe is pressurized, h_c remains constant at

the maximum height of the pipe and h_s measures the pressure head of the system. Since the pipe can expand and contract when exposed to positive and negative surcharging pressure heads, the flow cross sectional area is a function of the pressure head and acoustic speed of the pipe and can be calculated using the following equation.

$$A = A_f \left(1 + \frac{g h_s}{a^2}\right) \quad 3\text{-}5$$

where a = pipe acoustic speed.

Note that when the pipe tends to be depressurized at a specific location with adequate ventilation, the flow is switched back to open channel flow and h_s is reset to 0. However, lack of ventilation causes the pipe to receive negative pressures and, in such conditions, h_s measures the magnitude of the negative pressure head and h_c remains unchanged and represents the maximum height of the pipe.

3.6 Numerical Solutions

In this work, the Godunov scheme is utilized to numerically solve the governing equations. The Godunov scheme is an explicit finite volume approach that is widely used in solving hyperbolic partial differential equations. The computational domain in this approach is discretized into some computation cells with a spatial length of Δx. The order of accuracy in the Godunov scheme depends on how the data is reconstructed in the computational cells. Piecewise constant data reconstruction provides the first order of accuracy while a piecewise linear data reconstruction leads to a second-order accurate solution. Since first-order numerical schemes are generally more dissipative than second-order schemes, they better fit into the existing application because as shown by Malekpour and Karney (2015), lack of adequate numerical viscosity of the

scheme during the pressurization of the conduit is the main cause of the production of the spurious numerical oscillations.

By discretizing Equation (3-1), unknowns at the current time level can explicitly be calculated based on the data retrieved from the previous timeline using the following equation:

$$U_i^{n+1} = U_i^n - \frac{\Delta t}{\Delta x}\left(F^n_{i+\frac{1}{2}} - F^n_{i-\frac{1}{2}}\right) + \Delta t \times S_i^n \qquad 3\text{-}6$$

Where subscript i is the computational cell number, $i + \frac{1}{2}$ and $i - \frac{1}{2}$ refer to the upstream and downstream boundaries of i_{th} cell respectively, n and $n + 1$ refer to the previous and current timelines respectively, and Δt is the computational time step.

In the Godunov scheme, the fluxes at the cell boundaries are calculated by solving the Riemann problem which is defined as a hyperbolic system of equations with a flow discontinuity. Although the exact Riemann solution is available for the current system of equations, considering the iterative nature of the solution, it compromises the efficiency of the numerical analysis. To resolve this problem, approximate Riemann solutions can also be utilized to speed up the calculations (Toro, 2001). Several approximate Riemann solutions have been proposed, including Roe, HLL, and Harten, Lax, and van Leer Contact HLLC (Toro, & Garcia-Navarro, 2007), among which the HLL Riemann solution is one of the most efficient ones, and thus we utilized it in this study.

The HLL Riemann solution assumes that the generated waves on either side of the discontinuity are both of shock wave type. Figure 3.1 describes the wave structure in the HLL solver.

Figure 3.1

Wave structure in the HLL solver

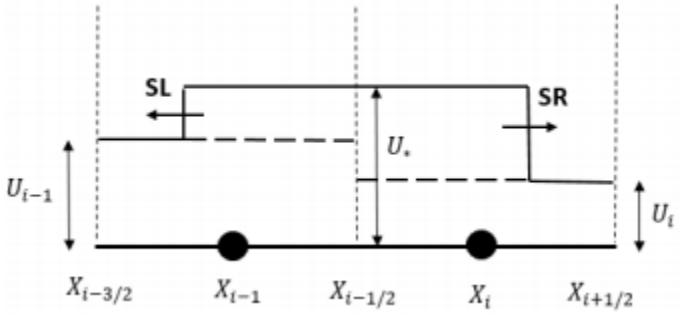

The speed of the left and write waves can be easily approximated by the following equations (Leon et al., 2009).

$$S_L = V_L - \Omega_L \quad \text{3-7}$$

$$S_R = V_R + \Omega_R \quad \text{3-8}$$

where indexes *L*, *R* refer to the left and right waves respectively and Ω_L and Ω_R can be calculating by the following equation:

$$\Omega_{K(K=L,R)} = \begin{cases} \sqrt{\frac{g[Y_G A_G - (h_s + h_c)_K A_K] A_G}{A_K (A_G - A_K)}} & if\ A_G > A_K \\ C_K & if\ A_G > A_K \end{cases} \quad \text{3-9}$$

C_K in Equation (3-9) is the gravity wave speed and calculated by the following equation and the index G, as can be discussed later, refers to a reference condition through which one can control the wave speeds.

$$C_K = \sqrt{gD_K} \tag{3-10}$$

where D is the hydraulic depth.

Having the S_L and S_R calculated, the fluxes can be approximated as follows:

$$F_* = \begin{cases} F_L & if\ S_L > 0 \\ \frac{S_R F_L - S_L F_R + S_L S_R (U_R - U_L)}{S_R - S_L} & if\ S_L \leq 0\ and\ S_R \geq 0 \\ F_R & if\ S_R < 0 \end{cases} \tag{3-11}$$

Although the fluxes presented in Equation (3-11) provide stable results over a wide range of flow conditions, it produces strong spurious numerical oscillations when the flow is being switched from open channel to pressurized flow. The induced oscillation is due to the significant change in the magnitude of the wave speed during the pressurization (Malekpour & Karney, 2015). It is also found that during the pressurization, the numerical scheme fails to admit adequate numerical viscosity to suppress the numerical oscillation. Obviously, to control the numerical oscillation, artificial viscosity has to be added to the scheme when the pressurization occurs.

In the Godunov type finite volume scheme, the amount of artificial viscosity of the scheme can be controlled by changing the wave speeds based on which the fluxes are calculated. Y_G in Equation (3-9) is to control the magnitude of the wave speed whenever required. Since the

numerical oscillation is set up during the pressurization, it seems that the best place to increase the artificial numerical viscosity is the computational cell containing the pressurization front. However, increasing artificial viscosity only at the cell containing pressurization front gives rise to spurious numerical oscillation in the neighbor cells. To resolve this issue, it was found that the artificial viscosity should be distributed around the computational cell with pressurization front.

If Y_G is greater than the height of the conduit, the wave velocity calculated by Equation (3-9) does not differ from the gravity wave velocity except in the vicinity of the conduit roof. In other words, by using Equation (3-9), significant artificial velocity is admitted to the numerical scheme only when the water surface in the conduit becomes very close to the conduit roof and the conduit is about to become pressurized. Extensive numerical experiments by Malekpour and Karney (2015) resulted in the following formula for calculating Y_G:

$$Y_G = K_a \times MAX\,[d_{i-NS}, d_{i-NS+1}, \dots, d_i, d_{i+1}, \dots d_{NS}] \qquad 3\text{-}12$$

where $d = h_c + h_s$.

By using the above equation, the maximum d is calculated within a number of cells (NS) located on either side of the i_{th} cell for which the wave velocity is being calculated. Y_G is then calculated by multiplying the maximum d by the factor K_a. In this way, numerical viscosity is distributed within a number of cells rather than being injected just in one cell. If all d*'s* are greater than the conduit height, the system is pressurized and a K_a. = 1.001 would provide reasonable results. When there is a pressurization front located within the cells, the numerical viscosity is further intensified by applying K_a = 1.4. The number of cells (NS) considered depends on the resolution of the computational grid and should be selected such that the

numerical viscosity is adequately distributed on either side of the computational cell for which the wave velocity is being calculated. Malekpour and Karney (2015) suggested that the number of cells should cover a distance equal to at least three times as large as the conduit height but in any case, it should not be less than three cells. If the i_{th} computational cell is found near a boundary, we should also incorporate the flow depth at the boundary point into Equation (3-12).

3.7 Conduit Geometry

As mentioned earlier, the aim of this paper is to justify if the non-oscillatory TPA model proposed by Khani et al. (2020) for calculating transient mix flow in circular and rectangular pipe cross sections performs equally well when other pipe shapes are used in the calculations. The most popular pipe shapes are assumed to be those supported by the program SWMM and presented in Figure 3.1. However, for the sake of generality, the custom shape whose dimensions can be defined by the users is also tested.

Figure 3.2

Conduit shapes considered in the study

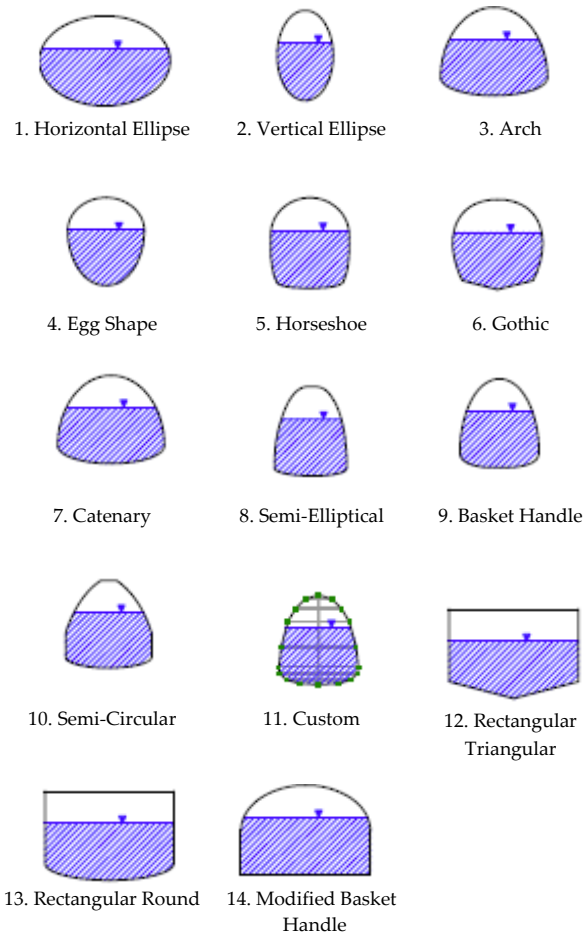

For the custom shape, the width of the conduit, W, at different heights needs to be defined; an example of such data is presented in Table 2. Note that the values of the table are non-dimensional with respect to the height of the conduit, Y_{full}.

Table 1

Non-Dimensional Geometry Information for the Custom Shaped considered in the Study

$\frac{Y}{Y_{full}}$	$\frac{W}{Y_{full}}$	$\frac{Y}{Y_{full}}$	$\frac{W}{Y_{full}}$
0.00	0.000	0.56	0.928
0.08	0.667	0.64	0.874
0.16	0.930	0.72	0.798
0.24	1.000	0.80	0.697
0.32	0.997	0.88	0.567
0.40	0.988	0.96	0.342
0.48	0.967	1.00	0.000

Shapes 1, 2, and 3 are all defined by the maximum height and maximum width of the pipe while shapes 4 to 10 can be defined by just the maximum height of the pipe. Shape 12 is characterized by three parameters including maximum height, top width and triangle height. Similarly, maximum height and top width define Shape 13 but instead of the triangle height, the bottom radius is used. Shape 14 is defined by maximum height, bottom width and top radius.

The numerical solution uses the information related to the pipe geometry including flow area, top width and hydraulic radius as a function of depth and flow depth as a function of flow area. For shapes 12, 13 and 14 all these parameters can be calculated analytically but for the other shapes, they should be interpolated from some pre-calculated tables. These tables are formed by calculating the geometry parameters at the incremental depths from the bottom to the top of the conduit. For the sake of generality, these data are stored in non-dimensional form with respect to the maximum height of the conduit. In this research, for the shapes 1 to 10, the data

used by SWMM (Rossman, 2017) are utilized. For the custom shape, the data defined by the user (an example of which is presented in Table 1) are employed to calculate the geometry-related parameters.

3.8 Model Verification

The validity of the proposed model, as well as its performance with regards to the suppression of the spurious numerical oscillations, were justified once before (Khani et al., 2020) through comparing the model results with the data obtained from a few experimental studies and analytical solutions but the investigation remained limited to the pipe systems with circular and rectangular shapes. Unfortunately, to the best of the authors' knowledge, there is no experimental study on transient mixed flow in pipes with other pipe shapes than rectangular circular. Thus, in this research analytical solution is employed as a benchmark for verifying the model performance.

The analytical solution consists of a horizontal-frictionless conduit with the maximum height and the total length of 1 and 500 m respectively. A reservoir at the upstream end of the pipe supplies the pipe and a reservoir at the downstream end collects the flow. The same water depth = 0.5 m at the upstream and downstream reservoirs made the pipe initially contains a stagnant water column with a depth of 0.5 m. By suddenly increasing the upstream reservoir level from 0.5 m to 6 m a hydraulic bore is setup and moves along the pipe with a constant speed called wave speed. Over a specific period, the location of the wavefront can be easily calculated using the wave speed.

Different components of the moving hydraulic bore can be analytically calculated by applying the discrete form of continuity and momentum equations on a frame of reference moving with the same speed as the hydraulic bore shown in Figure 3.1.

Figure 3.3

Schematic of the hypothetical pipe system utilized for validation of the model

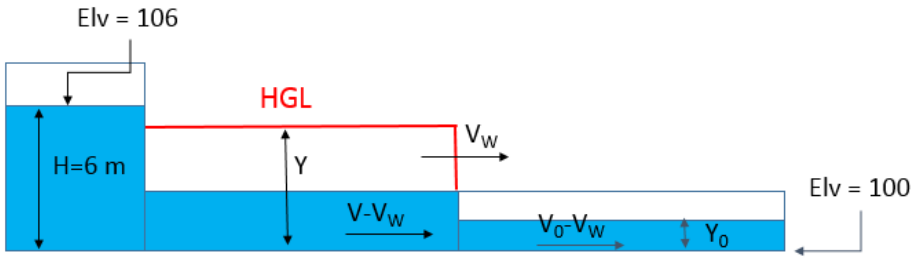

$$g\bar{Y}A - g\bar{Y}_0A_0 = (V - V_W)A\left(V - \overset{=0}{\bar{V}_0}\right) \qquad \textit{Momentum Equation} \qquad 3\text{-}13$$

$$\left(\overset{=0}{\bar{V}_0} - V_W\right)A_0 = (V - V_W)A \qquad \textit{Continuity Equation} \qquad 3\text{-}14$$

Where $\bar{Y}$ = distance between the *HGL* and the centroid of the pipe cross sectional area, $\bar{Y}_0$ = distance between the free surface and the centroid of the flow cross sectional area, A = pipe cross sectional area, V = flow velocity in the pressurized section and V_W = moving hydraulic bore speed.

The above equations contain three unknowns of V, V_W and Y and for being in the closed form they need an extra equation which is the energy balance on the upstream side of the system.

$$H = Y + \frac{V^2}{2g}$$ *The energy balance at the upstream end of the conduit* 3-15

To calculate the three unknowns of the problem, Equations 3-13 to 3-15 can be solved simultaneously by any iterative method such as the Newton-Raphson method. Having the speed of the hydraulic bore calculated, the location of the pressurization front can be calculated at any given time after the formation of the bore. This method was applied to the hypothetical pipe system with all pipe shapes shown in Figure 3.1 and the results are summarized in Table 2.

Table 2

Analytical Solution for Different Pipe Shapes

Pipe Shape	Dimensions (in meter)	Y (m)	HGL (m)	V (m/s)	Wv (m/s)	Location of the Bore (m)
1	I= 1; II=2	4.20	104.20	5.94	11.88	356.54
2	I=1; II=0.5	4.20	104.20	5.94	11.88	356.33
3	I=1; II=2	4.52	104.52	5.39	12.39	371.66
4	I=1	3.91	103.91	6.40	11.54	346.10
5	I=1	4.34	104.34	5.71	12.06	361.89
6	I=1	4.32	104.32	5.73	12.06	361.69
7	I=1	4.50	104.50	5.43	12.34	370.21
8	I=1	4.59	104.59	5.26	12.53	375.97
9	I=1	4.45	104.45	5.52	12.26	367.88
10	I=1	4.50	104.50	5.43	12.34	370.16
11	I=1	4.44	104.44	5.53	12.26	367.76
12	I=1; III=1; IV=0.3	3.69	103.69	6.73	11.37	341.22
13	I=1; III=1; VII=2	4.15	104.15	6.02	11.79	353.83
14	I=1; V=1; VI=10	4.22	104.22	5.91	11.87	356.13

Note: I = Maximum height; II=Maximum width; III=Top width; IV=Triangle height; V=Bottom width; VI=Top radius; VII=Bottom radius.

3.9 Numerical Results

For all test cases shown in Table 2, the model was run, and the hydraulic bore motion is numerically traced in 30 s. Since the spurious numerical oscillations are intensified at higher wave speeds, to make sure that the model provides oscillation free solutions, the most possible acoustic speed that can occur in pipes (1,400 m/s) is considered in the calculations. The numerical calculations are performed using 200 computational cells and the Courant number of 0.5 which resulted in a time step of 0.000911 s.

Figure 3.4

Comparing numerical results with the analytical solution for pipe shapes: a) Horizontal-Ellipse; b) Vertical-Ellipse; c) Arc

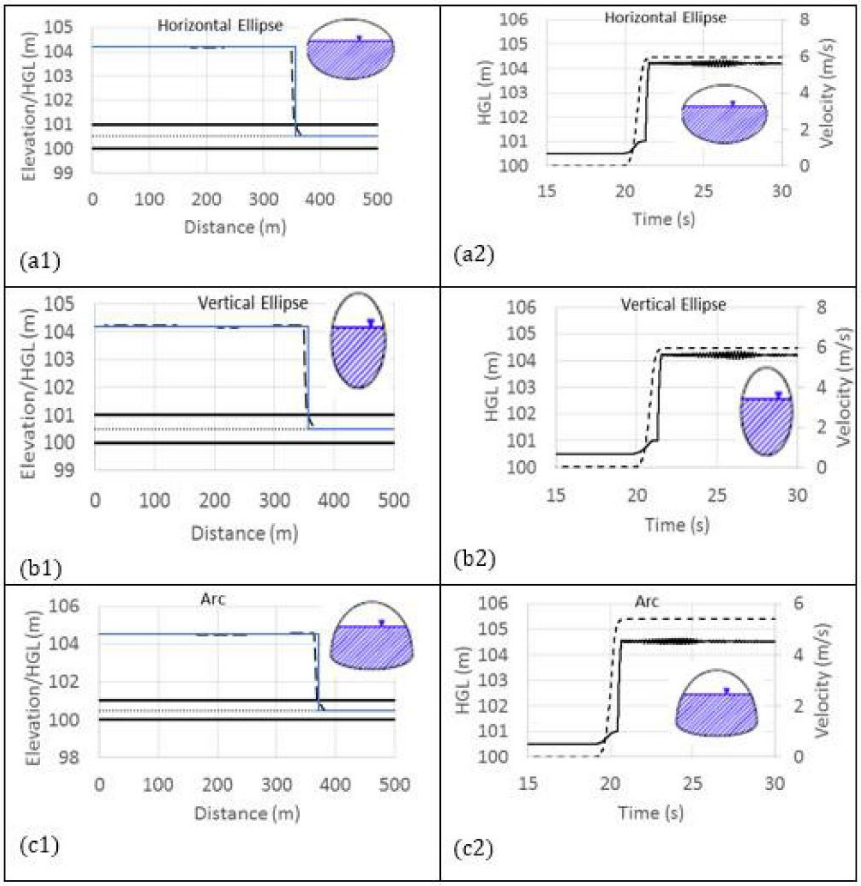

Figure 3.5

Comparing numerical results with the analytical solution for pipe shapes: a) Egg; b) Horseshoe; c) Gothic.

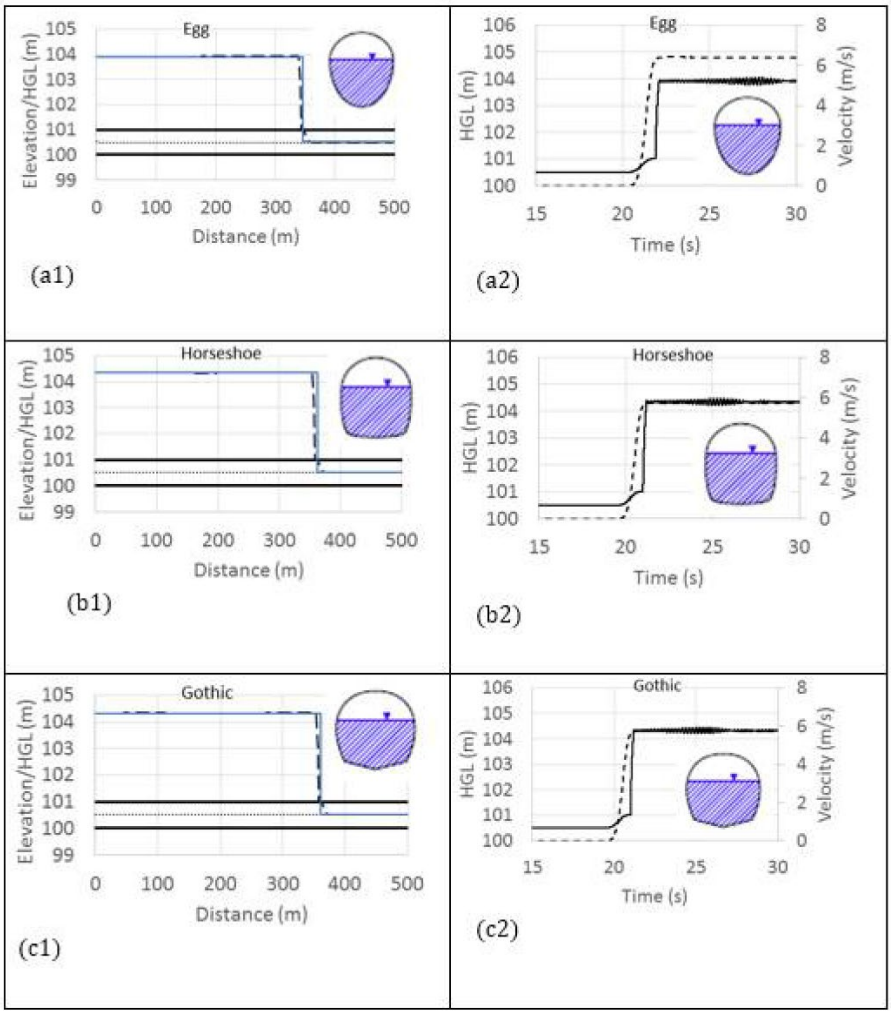

Figure 3.6

Comparing numerical results with the analytical solution for pipe shapes: a) Catenary; b) Semi-Elliptical; c) Basket Handle

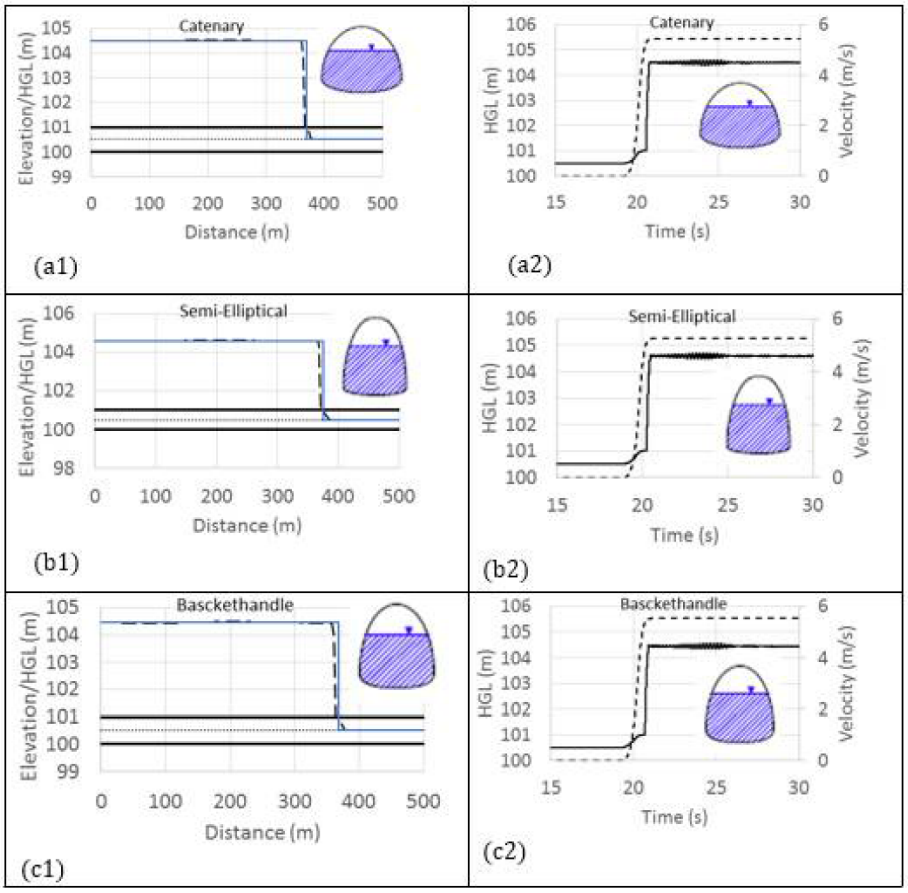

Figure 3.7

Comparing numerical results with the analytical solution for pipe shapes: a) Semi-Circular; b) Custom; c) Rectangular-Triangle

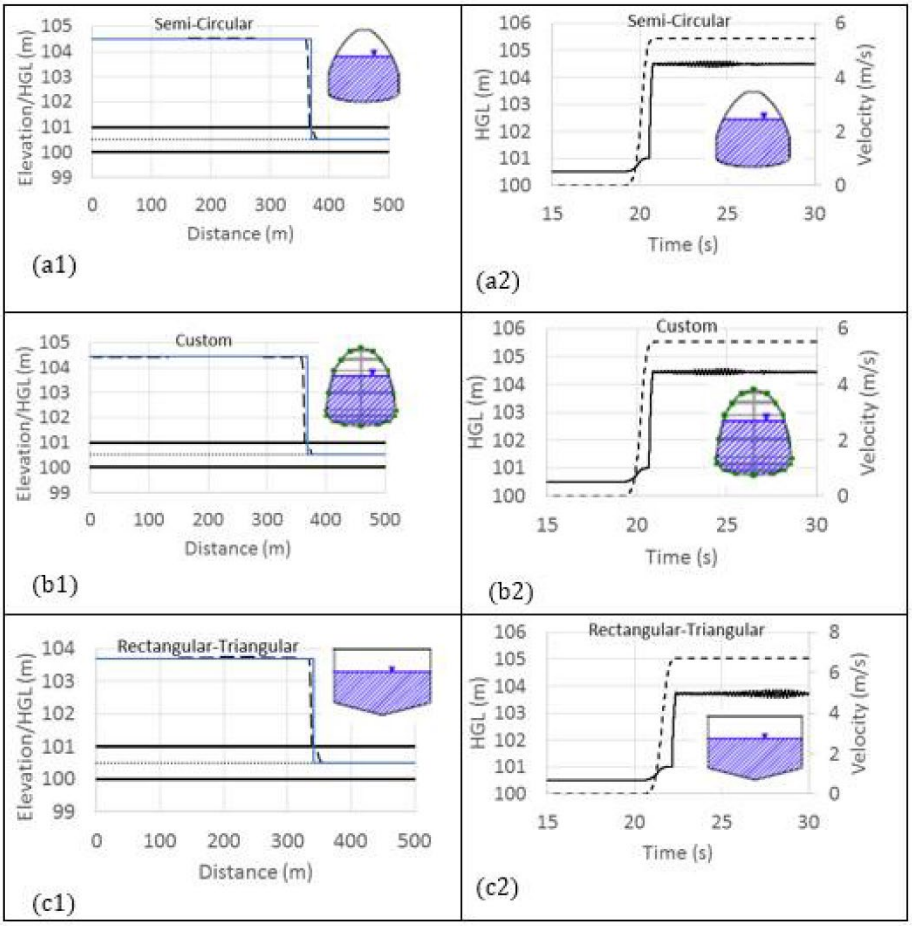

Figure 3.8

Comparing numerical results with the analytical solution for pipe shapes: a) Rectangular-Round; b) Modified-Basket Handle

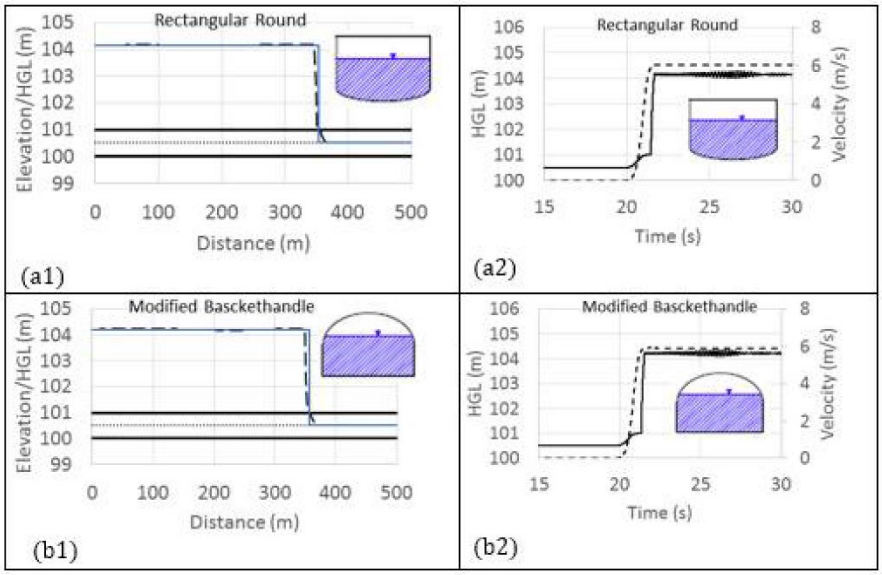

Figures 3.4 to 3.8 compare the numerical results with the analytical solutions. The figures on the left compare the hydraulic grade line calculated by the model with that of the analytical solution at 30 s after the start of the simulation. As it can be seen for all pipe shapes the numerical results are in excellent agreement with the analytical solution and there is no sign of numerical oscillation in the results. The figures on the right represent the time histories of the *HGL* and flow velocity at the middle of the conduit. It is obvious that no numerical oscillation is produced during the pressurization of the pipe for all pipe shapes considered. However, the time histories of the flow velocity contain tiny wiggles which are significant. The calculated velocities and the pressure heads of the water column behind the hydraulic bore are compared with those obtained from the analytical solution and the results are summarized in Table 3. The table shows

that the model captures the flow velocity for all pipe shapes quite accurately with an error ranging between 0.0702 and 0.1433 %. Likewise, the calculated pressure heads are in excellent agreement with the analytical solution and the errors change from 0.0350 to 1.2149 %.

Table 3

Comparing Numerical Results with Analytical Solution

Pipe Index	Y (Analytical) (m)	Y (Numerical) (m)	Error (%)	V (Analytical) (m/s)	V (Numerical) (m/s)	Error (%)
1	4.2003	4.1974	0.25	5.9423	5.9484	0.1032
2	4.2024	4.1784	0.50	5.9388	5.9447	0.0998
3	4.5198	4.5004	0.57	5.3891	5.3930	0.0734
4	3.9104	3.9417	0.64	6.4029	6.4121	0.1433
5	4.3367	4.3455	0.18	5.7125	5.7175	0.0861
6	4.3238	4.3253	0.32	5.7348	5.7399	0.0882
7	4.4973	4.5160	0.44	5.4298	5.4336	0.0702
8	4.5904	4.6066	0.56	5.2590	5.2655	0.1242
9	4.4480	4.4647	0.46	5.5183	5.5224	0.0746
10	4.4977	4.5161	0.42	5.4291	5.4330	0.0724
11	4.4403	4.4571	0.47	5.5319	5.5362	0.0772
12	3.6913	3.7362	0.86	6.7303	6.7130	0.2567
13	4.1505	4.1523	0.34	6.0239	6.0305	0.1092
14	4.2187	4.1926	0.61	5.9118	5.9171	0.0898

3.10 Summary and Conclusions

A TPA-based numerical model is proposed for capturing transient mixed flows in a variety of pipe shapes. The model utilizes the first order Godunov-Type finite volume scheme

to explicitly solve the governing equations. An HLL Riemann solver is proposed to calculate the numerical fluxes at the cells' boundaries. To suppress the spurious numerical oscillations, the solver automatically increases the amount of the numerical viscosity of the computational cells located in the vicinity of the pressurization front.

Due to the lack of experimental results, the model performance is evaluated by using a hypothetical pipe system for which an analytical solution exists. Since the numerical oscillations intensify with increasing the pace of pressurization of the pipe, the hypothetical system is intentionally designed to give rise to a fast-paced filling to make sure that the model is verified in the worst condition. Comparing the numerical results with the analytical solutions show that the model enables to successfully capture the hydraulics of the transient mixed flows quite accurately and can efficiently suppress the numerical oscillations even at as high acoustic pipe speed as 1,400 m/s.

The model can perform well even at the worst condition which is the combination of using very high pipe acoustic speeds and fast rates of pipe filling, confirms that it can be safely used for calculating transient mixed flows in real pipe systems which may consist of a verity of pipe shapes.

3.11 References

Abbott, M. B., and A. W. Minns. 1998. Computational hydraulics. Connecticut: Ashgate.

An, Hyunuk, Seungsoo Lee, Seong Jin Noh, Yeonsu Kim, and Jaekyoung Noh. 2018. "Hybrid numerical scheme of Preissmann slot model for transient mixed flows." Water 10: 899.

Bourdarias, Christian, and Stéphane Gerbi. 2007. "A finite volume scheme for a model coupling free surface and pressurized flows in pipes." Journal of computational and applied Mathematics 209: 109-131.

Chaudhry, M. H. 1999. Open channel flow. Englewood Cliffs, N.J: Prentice-Hall.

Gironás, Jorge, Larry A. Roesner, Lewis A. Rossman, and Jennifer Davis. 2010. "A new applications manual for the Storm Water Management Model (SWMM)." Gironás, Jorge, Larry A. Roesner, Lewis A. Rossman, and Jennifer Davis. "A new applications manual for the Storm Environmental Modelling & Software 6: 813-814.

Innovyze. 2020. "Product Family - Brochure-Letter-Sewer, Storm, Flood." InfoWorks. https://store.innovyze.com/StormwaterSewerFlood/InfoWoICM?cclcl=en_US.

Kerger, F., P. Archambeau, S. Erpicum, B. J. Dewals, and M. Pirotton. 2011. "An exact Riemann solver and a Godunov scheme for simulating highly transient mixed flows." Journal of Computational and Applied Mathematics 235: 2030-2040.

Khani, D., Y. H. Lim, and A. Malekpour. 2020. "Hydraulic Transient Analysis of Sewer Pipe Systems Using a Non-Oscillatory Two-Component Pressure Approach." Water 12: 2896. https://doi.org/10.3390/w12102896

Leon, A. S., M. S. Ghidaoui, A. R. Schmidt, and M. H. Garcia. 2010. "A robust two equation model for transient mixed flows." Journal of Hydraulic Research 48 (1): 44 -56.

León, A. S., M. S. Ghidaoui, A. R. Schmidt, and M. H. García. 2009. "Application of Godunov-type schemes to transient mixed flows." Journal of hydraulic research 47 (2): 147-156.

Malekpour, A., and B. Karney. 2015. "Spurious Numerical Oscillations in the Preissmann Slot Method: Origin and Suppression." Journal of Hydraulic Engineering, ASCE.

Malekpour, A., and B. W. Karney. 2019. "Complex interactions of water, air and its controlled removal during pipeline filling operations." Fluid Mechanics Research International Journal 3: 4-15.

Malekpour, A., F. Papa, D. Radulj, and B. and Karney. 2014. "Understanding hydraulic transients in sewer systems." 45th Annual WEAO Technical Symposium and OPCEA Exhibition. Toronto.

Politano, M., A. J. Odgaard, and W. Klecan. 2007. "Case study: Numerical evaluation of hydraulic transients in a combined sewer overflow tunnel system." Journal of Hydraulic Engineering 133 (10): 1103-1110.

Preissmann, M. A., and J. A. Cunge. 1961. "Calculation of wave propagation on electrical machines." 9th IAHR congress. Dubrovnik. 656-664.

Ridgway, R. E., and G. Kumpala. 2008. "Surge Modeling in Sewers Using Alternative Hydraulic Software Programs." Journal of Water Management Modeling. doi:10.14796/JWMM R228-10.

Rossman, Lewis A. 2017. Storm Water Management Model Reference Manual. Cincinnati: National Risk Management Research Laboratory, Office of Research and Development, US Environmental Protection Agency.

Sjöberg, A. 1982. "Sewer network models dagvl-a and dagvl-diff." Edited by B. C. Yen. Urban Stormwater Hydraulics and Hydrology. Littleton, Colo.: Water Resource Publications. 127-136.

Song, C. S. S., J. A. Cardle, and K. S. Leung. 1983. "Transient mixed flow models for storm sewers." Journal of Hydraulic Engineering 109 (11): 1487–1504.

Toro, E. F. 2001. Shock-capturing methods for free-surface shallow flows. Chichester, New York: John Wiley.

Toro, E. F., and P. Garcia-Navarro. 2007. "Godunov-type methods for free-surface shallow flows: A review." Journal of Hydraulic Research 45 (6): 736-751.

Vasconcelos, J. G., S. J. Wright, and P. L. Roe. 2006a. "Improved simulation of flow regime transition in sewers: two-component pressure approach." Journal of Hydraulic Engineering 132 (6): 553-562.

Vasconcelos, J. G., S. J. Wright, and P. L. Roe. 2009. "Numerical oscillations in pipe-filling bore predictions by shock-capturing models." Journal of Hydraulic Engineering 135 (4): 296-305.

Vasconcelos, Jose G., Peter R. Klaver, and Daniel J. Lautenbach. 2015. "Flow regime transition simulation incorporating entrapped air pocket effects." Urban Water Journal 12: 488-501.

Wright, S. J., J. W. Lewis, and J. G. Vasconcelos. 2010. "Geysering in rapidly filling storm-water tunnels." Journal of Hydraulic Engineering 137 (1): 112-115.

Wright, S. J., Lewis J. W., and J. G. Vasconcelos. 2011. "Physical processes resulting in geysers in rapidly filling storm-water tunnels." Journal of Irrigation and Drainage Engineering 137 (3): 199-202.

4 CHAPTER FOUR

4.1 Calculating Column Separation in Conduit Systems Using an Innovative Open Channel Based Model

4.2 Abstract

An innovative numerical model, called Modified Two-Component Pressure Approach (MTPA), is proposed to better capture the physics of column separation in conduit systems. Built based on the Two-Component Pressure Approach (TPA), the MTPA calculates both cavitating and pressurized flow using a single set of equations that governs unsteady flow in open channel flow. As opposed to shock-fitting- based models, in which a complex algorithm is needed to keep track of the interfaces separating the cavitating and liquid zones, the proposed model can capture both flow phases automatically. The first order Godunov type finite volume method is utilized to numerically solve the equations. A customized HLL Riemann solver is employed to calculate the fluxes at the computational cell boundaries and to dissipate potential post-shock oscillations generated when the cavity is collapsed and the open channel flow beneath the cavity is switched back to pressurized flow. The numerical results are shown to be in excellent agreement with both experimental data and the results obtained from the Discrete Gas Cavity Model (DGCM). A hypothetical test case is also presented to demonstrate the unique feature of the proposed model, which is the ability to simultaneously account for waterhammer, cavitating and open channels flow regimes, a feature making the model even superior to the DGCM.

4.3 Introduction

Cavitating flow occurs in pressurized pipe systems when the pressure drops to the vapor pressure of the liquid due to transient events such as pump power failure, rapid closing of a valve, the reflection of intensive positive water hammer pressures, etc. (Bergant et al., 2006). Since the pressure at the cavitating flow region remains constant at the vapor pressure, the liquid columns on either side of this zone become hydraulically disconnected. If the inflow to the cavitating zone is less than the outflow, vapor cavities form, and column separation occurs in the pipe. When the net inflow to the cavity becomes positive, the cavity starts to shrink. Once the cavity completely vanishes, the adjacent water columns are rejoined, and this may give rise to significant waterhammer pressures. The intensity of the induced positive pressure mainly depends on the velocity difference of the adjacent water columns at the moment the cavity is collapsed, as well as the magnitude of the pipe acoustic wave speed. The generated waterhammer pressure can be severe enough to rupture the pipe (Chuadhry, 1987).

Several experimental studies have been conducted on column separation in pressurized pipe systems since the phenomenon was first identified by Joukowsky early in the 20th century (Bergant et al., 2006); a few examples of which are: Simpson and Wylie (1991), Martin (1983), and Bergant and Simpson (1999), Adamkowski and Lewandowski (2012). The insight from the experimental studies had made the researchers propose a variety of numerical models for capturing the essential features of column separation (Bergant et al., 2006).

Among these models, Discrete Vapour Cavity Model (DVCM), Discrete Gas Cavity model (DGCM), and two-phase flow model are the most popular ones (Bergant et al., 2006). In the

DVCM, whenever the pressure at a computational node reduces to the vapor pressure, a vapor cavity condition is inserted at that computational node as an internal boundary condition. In the subsequent computational steps, the pressure at the computational node is held constant at the vapor pressure, and the evolution of the cavity volume is calculated through a simple continuity equation relating the cavity size to the inflow and outflow at the cavity.

To improve the performance of the DVCM, Provoost and Wylie (1981) proposed the DGCM. In this method, very small gas pockets are inserted in the computational nodes, and the evolution of the gas pockets is treated as internal boundary conditions. Expansion and contraction of the gas pockets replicate both the change in the acoustic wave speed occurring under two-phase flow conditions and the evolution of the cavity occurring when the vapor pressure is reached and the system experiences cavitating flow. Experiments show that the DGCM successfully simulates both discrete and distributed cavitating flows (Bergant and Simpson (1999); Simpson and Bergant (1994), Malekpour and Karney (2014a and 2014b).

Different types of two-phase flow models have been proposed to simulate cavitating flow and water column separation in pipe systems. Bergant and Simpson (1999) proposed a two-phase flow model called Generalized Interface Vapour Cavity Model (GIVCM). In this method, the distributed cavitating zone characterized with low void fraction and constant pressure (vapor pressure) is calculated by its own governing equations, and the liquid zone is calculated with the waterhammer equations. The interface between these two flow zones is tracked by an analytical approach within each time step.

In both DVCM and DGCM, the maximum size of the cavity must be small compared to the size of the computational cell. As shown by Simpson and Bergant (1994), if the cavity volume exceeds 10 % of the volume of the computational cell, the results are not valid, and the use of other alternative models appears to be inevitable. In such a case, the GIVCM proposed by Bergant and Simpson (1999) is a good choice as the interface determining the boundaries of the cavity can be shifted from one computational cell to another if needed. However, this approach still assumes that the cavity fills the whole cross-section of the pipe which is not confirmed by experimental study. Investigation on physical models revealed that the cavity forms on the top section of the pipe and the liquid beneath the cavity flow in an open channel flow regime. Nevertheless, GIVCM provides good results as long as the cavity size does not exceed a certain limit otherwise the results would be compromised and cannot be trusted.

Vasconcelos and Marwell (2011) proposed a TPA-based model to address one of the shortcomings of the existing models, which is the inability to simultaneously treat open channel and cavitating flow regimes. Small gas pockets postulated at the computational cells allow the proposed model to calculate the cells' wave velocity in response to pressure changes. When the pressure at a computational cell drops to the vapor pressure, the expansion of the gas pocket significantly reduces the wave velocity and keeps the pressure constant at the vapor pressures, the two characteristics of cavitating flows. However, the collapse of large vapor cavities is accounted for only at the pipe boundaries and is not permitted within the intermediate computational cells. Although the proposed model uses the TPA concept, when it comes to calculating column separation, it cannot be categorized as an open channel-based model and

suffers from some of the limitations associated with the DVCM and DGCM models. Indeed, large vapor cavities may be extended to a fairly long distance across a pipe, so an open channel flow-based model can better describe the physics of column separation.

In the conventional open channel flow-based models, the boundaries separating the cavitating and pressurized flows are tracked during the simulation. The hydraulic variables in these flow zones are calculated through solving open channel flow and waterhammer equations respectively. Baltzer (1967a and 1967b) proposed a model of this type that utilizes the method of characteristics to solve both the open channel and waterhammer equations. The results obtained by Baltzer imply that although the model is capable of describing the column separation more realistically, the amplitude and frequency of the pressure surge spikes captured by the model are not in agreement with experimental data. A few other researchers proposed different types of open channel flow-based models but none of them succeeded in calculating column separation with reasonable accuracy (Siemons, 1967; Kalkwijk et al., 1972; Mardsen and Fox, 1976). One of the major problems with open channel flow-based models is the difficulties in modeling the transition from the waterhammer region to the cavitating zone. This is perhaps one of the reasons why these types of models have not received further attention (Bergant et al., 2006). Other reasons, in the authors' point of view, are that the counterpart models provide promising results in a wide range of applications and are easier to implement, particularly in complex hydraulic systems.

To resolve the aforementioned problems, this paper proposes a novel open channel flow-based model called Modified Two-Component Pressure Approach (MTPA). The model is a

modified version of the TPA that can simultaneously calculate open channel, waterhammer, and cavitating flow zones with no necessity in keeping track of the interfaces separating those regions.

The organization of the paper is as follows: the TPA is briefly discussed, and the modification required for accounting for column separation is described. After discussing the numerical model, the MTPA results are verified using experimental data, the numerical results obtained from the DGCM, and a hypothetical test case. Finally, the paper outcomes are summarized, and conclusions are made.

4.4 Description of MTPA

One dimensional unsteady flow in open channels is governed by the following equations, which are well known as the conservative forms of the continuity and momentum equations Chaudhry (1999).

$$\frac{\partial A}{\partial t}+\frac{\partial Q}{\partial x}=0 \qquad Continuty\ Equation \qquad 4\text{-}1$$

$$\frac{\partial Q}{\partial t}+\frac{\partial\left(\frac{Q^2}{A}+Agh_c\right)}{\partial x}=gA(S_0-S_f) \qquad Momentum\ Equation \qquad 4\text{-}2$$

where, A= flow cross sectional area, Q = flow rate, h_c = distance between free surface and the centroid of the flow cross sectional area, g = gravitational acceleration, S_0 = pipe slope, and S_f = frictional slope which can be calculated by the following equation.

$$S_f = \frac{Q^2 n_m^2}{A^2 R_h^{\frac{4}{3}}} \quad 4\text{-}3$$

where n_m = Manning coefficient and R_h = hydraulic radius of the flow section.

The above equations govern unsteady flow in open channels, but with some modifications, they can handle pressurized flow as well. The key difference between open channel and pressurized flows is the velocity at which the information is propagated across the flow medium. Pressure waves move two orders of magnitude faster in pressurized flows than open channel flows because open channel and pressurized flows have different mass storage capacities. By changing the depth of flow, the liquid mass can be easily stored or released from open channel flow systems, which in turn, slowdowns the propagation of the information. However, due to the lack of free storage in pressurized systems, a small amount of liquid mass can be stored or released through the compression or stretching of the liquid column, and this speed up the pressure waves.

To make Equations 4-1 and 4-2 account for pressurized flow as well, Preissmann proposed a virtual-narrow slot on the crown of the pipe and assumed that when the pipe cross-section becomes full, the liquid remains in an open channel flow regime with the flow's top width as narrow as the slot width (Cunge and Wegner, 1964). In such conditions, the height of the water is analogous to the pressure head in pressurized flows and the width of the slot determines how fast the wave moves in the system. To replicate the wave motion in the pressurized flow, the width of the slot can be calculated as follows (Kerger et al., 2011):

$$T_S = \frac{gA_f}{a^2} \quad 4\text{-}4$$

where, T_S = slot width, A_f = cross sectional area of the pipe, and a = pipe acoustic wave speed.

The Preissmann Slot Method (PSM) has been shown to accurately capture waterhammer pressures (Leon et al., 2009; Malekpour and Karney, 2015), but it is incapable of maintaining negative pressures. As soon as the pressure is about to become negative, the flow would be switched back to open channel flows. To resolve this problem, Kerger et al. (2011) proposed the Negative Preissmann Slot Method (NPSM). In this approach, the water depth in the virtual slot can take negative values and measure negative pressure heads. In reality, however, pipes may be ventilated at specific points so negative pressures cannot be physically permitted. At these particular sections, the flow is turned into open channel flows while other parts of the pipe may still maintain negative pressures; the NPSM fails to handle such conditions. To resolve this issue, Vasconcelos et al. (2006a) proposed the TPA which can calculate both negative pressure and open channel flow simultaneously. To this end, the pressure head in the second term of the left-hand side of the momentum equation (Equation 4-2) is split into two separate components, as shown in Equation 4-5.

$$\frac{\partial Q}{\partial t} + \frac{\partial\left(\frac{Q^2}{A} + Ag[h_c + h_s]\right)}{\partial x} = gA(S_0 - S_f) \quad 4\text{-}5$$

When the flow is in the open channel flow regime, h_c measures the distance between the free surface and the centroid of the flow cross-sectional area, and h_s is set as 0. However, in pressurized flows, h_c is the distance between the crown of the pipe and the centroid of the pipe cross-section and h_s represents pressure heads. Note that when the hydraulic grade line is about

to fall below the grade of the pipe crown, the flow is allowed to either switch back to the open channel or remain in the pressurized regime. If the pipe is ventilated near a computational point, h_s is set to zero, and the flow regime is let to return to the open channel. Otherwise, h_c is kept constant at the pipe diameter, and h_s is assumed to measure negative pressures in the system.

In the PSM, the mass associated with the compression of the fluid is accumulated in the virtual slot, but the TPA accounts for the compression and stretch of the water column by changing the cross-sectional area of the pipe. The relation between h_s and the pipe cross-sectional area can be obtained by multiplying either side of Equation 4-4 by h_s and doing some algebra.

$$A = A_f \left(1 + \frac{g h_s}{a^2}\right) \qquad 4\text{-}6$$

One deficiency of the TPA is to allow the induced negative pressures to become significantly less than the vapor pressure. However, in reality, when the pressures reach the vapor pressure, cavitating flow forms and controls the pressure constant at the vapor pressure. The authors have found that with some modification of the TPA, it is possible to capture cavitating flow and column separation in the pressurized zone.

To facilitate explaining the modification, let us first examine how cavitating flows and column separation form in the pressurized zone. For this purpose, consider a horizontal pipe carrying water from one reservoir to another when the flow at the upstream side is suddenly cut off. Depending on the pipe length and the initial flow rate of the system, it takes some time for the water column to come to rest. Meantime, the pipe keeps feeding the downstream reservoir though with reducing the flow rate. Obviously, to compensate for the liquid mass leaving the

system, the pressure drops to withdraw liquid mass through squeezing the pipe and stretching the water column. However, when the vapor pressure of the liquid is reached, the pressure remains constant, and cavitating flows form. From this moment onwards, the liquid mass leaving the pipe from the downstream side is compensated for through the formation of a vapor cavity in the vicinity of the closed valve at the upstream side of the system. The mass conservation law enforces that the total flow mass leaving the system during water column deceleration should be almost equal to the volume of the vapor cavity created in the system.

It is worth noting that due to the gravity effect, the pipe receives higher pressures at the bottom than at the top. Consequently, vapor cavities initially form and spread near the upper portion of the pipe cross-section. The cavity becomes longer and deeper over time, but the liquid beneath the cavity flows in the open channel regime. As experimental studies also imply (Autrique and Rodal, 2013), the cavitating zone can be simulated more realistically using the open channel concept. In conventional models, such as DGCM and DVCP, it is assumed that as soon as the cavity forms it fills the whole section of the pipe; an assumption that is not physically sound.

Returning to the modification, as long as the pressure does not reach the vapor pressure of the liquid, Equations 4-5 and 4-1 can be used to calculate the transient pressure heads and flow rates across the system. When the pressure tends to drop below the vapor pressure of the liquid, Equation 4-5 no longer holds, and the following equation should be utilized instead.

$$\frac{\partial Q}{\partial t} + \frac{\partial\left(\frac{Q^2}{A} + g[Ah_c + A_f h_v]\right)}{\partial x} = gA(S_0 - S_f) \qquad 4\text{-}7$$

where h_v = vapor pressure head of the liquid.

Figure 4.1 demonstrates the pressure components applied on the pipe cross-section during column separation. As can be seen, the total force on the section is the superposition of two forces acting in opposite directions. The first one is due to the weight of the liquid with triangle distribution, and the second one is due to the vapor pressure applied on the whole section of the pipe.

Figure 4.1

Schematic of the pressure components applied on the flow and pipe section during cavitating flows

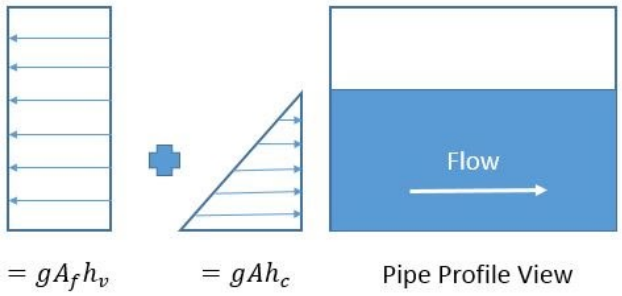

4.5 Numerical Solution

4.5.1 Finite Volume Implementation

The governing equations are numerically solved using the Godunov method, a finite volume-based numerical scheme widely utilized for solving hyperbolic partial differential equations (Toro, 2001; LeVeque, 2002). The first step in this approach is to discretize the flow

domain by numerous computational cells with the spatial distance and temporal steps of Δx, and Δt respectively. Choosing a data reconstruction method is of great importance in the Godunov scheme as it determines the order of accuracy. Piecewise data construction leads to first-order accuracy, and piecewise linear data reconstruction results in second-order accuracy. This study employs piecewise data reconstruction as the artificial viscosity admitted to removing the post-shock oscillations prevents achieving second-order accuracy (Khani et al., 2020). Discretization of the governing equations results in the following equations that can be utilized to explicitly calculate the flow area and the flow rate in the new timeline.

$$A_i^{n+1} = A_i^n - \frac{\Delta t}{\Delta x}\left(F^n_{i+\frac{1}{2}} - F^n_{i-\frac{1}{2}}\right) \quad 4\text{-}8$$

$$Q_i^{n+1} = Q_i^n - \frac{\Delta t}{\Delta x}\left(G^n_{i+\frac{1}{2}} - G^n_{i-\frac{1}{2}}\right) + \Delta t g A\left(S_0 - S_{f_i}{}^n\right) \quad 4\text{-}9$$

where i is computational cell number, $i+\frac{1}{2}$ and $i-\frac{1}{2}$ are referring to the downstream and upstream boundaries of the i^{th} cell respectively, n and $n+1$ are referring to the pervious and current timeline, F and G are mass and momentum fluxes respectively.

In the Godunov scheme, the fluxes at the cell boundaries are determined through solving the Riemann problem that includes a system of hyperbolic equations at a flow discontinuity with initial piecewise constant data (LeVeque, 2002). Among numerous approximate Riemann solutions, this study utilizes the Harten, Lax, and van Leer (HLL) due to its accuracy and ease of implementation (Toro, 2002). In the HLL solver, it is assumed that the generated waves on either side of a discontinuity are both shock waves. Figure 4.2 depicts the wave structure in the HLL solver.

Figure 4.2

Wave structure at the HLL solver

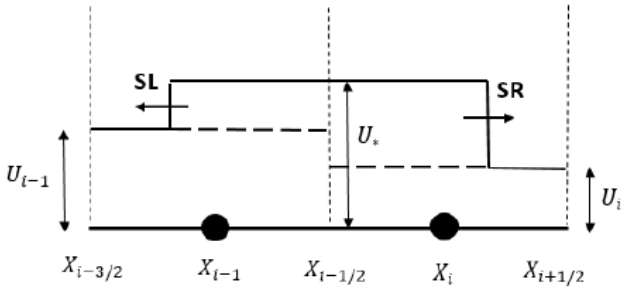

Left and right shock wave velocities can be calculated by the following formula:

$$S_L = \frac{\boldsymbol{\Gamma}_L - \boldsymbol{\Gamma}_*}{\boldsymbol{U}_L - \boldsymbol{U}_*} \quad \text{4-10}$$

$$S_R = \frac{\boldsymbol{\Gamma}_R - \boldsymbol{\Gamma}_*}{\boldsymbol{U}_R - \boldsymbol{U}_*} \quad \text{4-11}$$

where S_L and S_R are the left and right shock wave speeds respectively, $\boldsymbol{U}_L = \begin{bmatrix} A_L \\ Q_L \end{bmatrix}$ and $\boldsymbol{U}_R = \begin{bmatrix} A_R \\ Q_R \end{bmatrix}$ are dependent variables at the computational cells i and $i+1$ respectively, $\boldsymbol{\Gamma}_L = \begin{bmatrix} F_L \\ G_L \end{bmatrix}$ and $\boldsymbol{\Gamma}_R = \begin{bmatrix} F_R \\ G_R \end{bmatrix}$ are the fluxes at the computational cells $i-1$ and $i+1$ respectively and $\boldsymbol{U}_*$ is the dependent variables at the cell interface called star zone.

The fluxes at the star zone can be calculated through inspection of the wave structure. When the left and right waves move in opposite directions, the fluxes can be calculated by the simultaneous solutions of Equations 4-10 and 4-11. If the left wave moves to the right (SL > 0), the flow would be supercritical, and the fluxes at the star zone become equal to those of the left

cell. In case that the right wave moves to the left (SR < 0), the flow regime would be again supercritical, but the flow direction is opposite. In such a case, the fluxes at the star zone would equal those of the right cell. The calculation of the fluxes at the cell boundary is summarized in the following.

$$\boldsymbol{F}_* = \begin{cases} \boldsymbol{F}_L & if\ S_L\ > 0 \\ \frac{S_R\boldsymbol{F_L} - S_L\boldsymbol{F_R} + S_L S_R(\boldsymbol{U_R} - \boldsymbol{U_L})}{S_R - S_L} & if\ S_L \le 0\ and\ S_R\ \ge 0 \\ \boldsymbol{F}_R & if\ \ S_R\ < 0 \end{cases} \quad \text{4-12}$$

Malekpour and Karney (2015) showed that the drastic change of the wave speed during the pressurization of conduits produces significant sporous numerical oscillations even if a monotonous numerical scheme like the first-order Godunov scheme is utilized. Vasconcelos et al. (2009) proposed two measures for suppressing the numerical oscillations, but none of them were shown to be successful when the acoustic wave speed exceeds a certain limit (100-150 m/s). Malekpour and Karney (2015) proposed a customized HLL Riemann solver for calculating the numerical fluxes and showed that the numerical viscosity admitted by the solver can efficiently remove the numerical oscillations even at higher pipe acoustic speeds than 1000 m/s.

Khani et al. (2020) adapted the HLL solver proposed by Malekpour and Karney (2015) to suppress the numerical oscillations associated with the TPA and showed that it provides non-oscillatory solutions even at maximum possible acoustic speeds. They also showed that the model performs consistently for numerous shapes of conduits (Khani et al., 2021). The proposed HLL solver automatically increases the numerical viscosity of the scheme when flow pressurization is imminent. In the HLL solver, the intensity of the numerical viscosity admitted to the numerical scheme is controlled by the magnitude of the right and left wave velocities. To admit the optimal

amount of numerical viscosity, Khani et al. (2020 and 2021) proposed a simple strategy for calculating the left and right wave velocities in both waterhammer and open channel flow regions. In the following research, this approach is slightly adjusted to account for the cavitating flow region as well.

$$S_L = V_L - \Omega_L \; ; \; S_R = V_R + \Omega_R \tag{4-13}$$

$$\Omega_{K(L,R)} = \sqrt{\frac{g[Y_G A_G - (h_C + |h_s|)_K A_K] A_G}{A_K (A_G - A_K)}} \qquad if \; h_s < 0 \; and \; h_s > 0 \tag{4-14}$$

where sub-index G refers to the variables that are the function of Y_G.

Equation 4-14 shows that Y_G determines the magnitudes of the left and right waves which in turn control the artificial viscosity of the scheme. Khani et al. (2020 and 2021) demonstrated that calculating Y_G by the following equation can admit the optimal amount of numerical viscosity.

$$Y_G = K_a \times MAX\,[d_{i-NS}, d_{i-NS+1}, \dots, d_i, d_{i+1}, \dots d_{NS}] \tag{4-15}$$

where $d = h_c + |h_s|$, NS = the number of cells located on either side of the i^{th} cell and K_a = amplification factor.

For a computational cell that carries open channel flow, K_a takes a value of 1.001 if the cell is away from a pressurization front by more than NS computational cells, otherwise, K_a is considered as 1.4. For the cells running under full flow conditions, K_a also takes a value of 1.001. It is worth mentioning that NS depends on the resolution of the computational grid and should be selected such that the numerical viscosity is adequately distributed on either side of the i^{th} computational cell for which the wave velocity is being calculated.

4.6 Boundary Conditions

Boundary conditions are the essential part of numerical modeling and can significantly affect the numerical results because any change in the pressure and flow rates of the system is enforced at the boundaries. That how some physical boundaries such as constant water level reservoirs, pipe dead-ends, pumps, etc. interact with the pipe system is determined through the simultaneous solution of the equations governing the hydraulics of both the boundary and the pipe flow.

The test cases utilized for validating the proposed model includes two simple boundary conditions, constant water level reservoirs and pipe dead-ends. Thus, these two boundary conditions are dealt with herein. In constant water level reservoirs, the HGL remains constant at the boundary, and the velocity or flow rate at this point needs to be calculated. If the reservoir is located at the downstream end of the system, the positive characteristic equation can be simply used to calculate the flow velocity at the boundary otherwise the negative characteristics equation is utilized. The discrete forms of the positive and negative characteristics lines are brought in the following:

$$C^{+}: V_B + \frac{g}{a} H_B = V_n + \frac{g}{a} H_n \qquad 4\text{-}16$$

$$C^{-}: V_B - \frac{g}{a} H_B = V_1 - \frac{g}{a} H_1 \qquad 4\text{-}17$$

where V_B , V_1 and V_n are flow velocities at the boundary, first and last computational cells respectively and, H_B, H_1 and H_n are piezometric heads at the boundary, first and last computational cells respectively.

Using the characteristics equations, the flow velocity at the boundary can be calculated by the following equations.

$$V_B = V_1 + \frac{g}{a}(H_r - H_1) \qquad Upstream\ Reservoir \tag{4-18}$$

$$V_B = V_1 + \frac{g}{a}(H_n - H_r) \qquad Downstream\ Reservoir \tag{4-19}$$

Having the V_B calculated, the mass and momentum fluxes can be calculated for the boundary.

Calculating flow variables at a dead-end is a bit more challenging because at dead-ends the flow cannot always remain in the waterhammer regime, and cavitating and consequent column separation makes the flow switch to open channel flow while the pressure remains constant at the vapor pressure. If the flow is in waterhammer regime, the HGL at the dead-end can be easily calculated by assuming the velocity is zero at the boundary.

$$H_B = H_1 - \frac{a}{g}V_1 \qquad Upstream\ deadend \tag{4-20}$$

$$H_B = H_n + \frac{a}{g}V_n \qquad Downstream\ deadend \tag{4-21}$$

When a vapour cavity forms at the dead-end, the flow turns into the open channel regime, and the characteristics equations should be written as follows:

$$C^+: V_B + \Phi_B = V_n + \Phi_n \tag{4-22}$$

$$C^-: V_B - \Phi_B = V_1 - \Phi_1 \tag{4-23}$$

where Φ is the Riemann invariant and can be calculated using the following equation.

$$\Phi = \int_0^y \frac{\sqrt{gD}}{A} dA \tag{4-24}$$

where y = depth of flow and D = hydraulic depth.

By setting $V_B = 0$ and plugging Equation 4-24 into Equations 4-22 and 4-23 the following equations are reached.

$$\int_0^{y_B} \frac{\sqrt{gD_B}}{A_B} dA = V_n + \int_0^{y_n} \frac{\sqrt{gD_n}}{A_n} dA \qquad Downstream\ deadend \qquad 4\text{-}25$$

$$\int_0^{y_B} \frac{\sqrt{gD_B}}{A_B} dA = \int_0^{y_1} \frac{\sqrt{gD_1}}{A_1} dA - V_1 \qquad Upstream\ deadend \qquad 4\text{-}26$$

Each of the above equations has just one unknown which is the depth of the flow at the boundary, y_B. However, the equations cannot be solved explicitly, and an iterative method such as the Newton-Raphson method should be employed to calculate y_B. Having $h_c = y_B$ and knowing that $V_B = 0$ and P_s equals the vapor pressure, the mass and momentum fluxes at the boundary can be easily calculated.

4.7 Numerical Results

The MTPA is first validated by comparing the numerical results with both the experimental data conducted by Bergant and Simpson (1999) and the numerical results obtained from the well-known DGCM. As shown in Figure 3, the test rig consists of two pressurized tanks whose pressures are kept constant during the test. The two tanks were connected by a copper pipe with internal diameter, length, wave velocity, and upward slope of 22.1 mm, 37.23 m, 1319 m/s, and 5.6% respectively. Column separation is induced by suddenly closing the downstream valve when a steady-state condition is established across the system. The experiments were conducted for the initial steady-state flow velocities of 0.3, 0.71 and 1.4 m/s. During the

experiment, the pressure head at Tank 2 is kept constant at 22 m. The pressure head time histories conducted at points $H_{v,1}$ and H_{mp} are utilized for numerical verification.

Figure 4.3

Bergant and Simpson (1999) test rig configuration

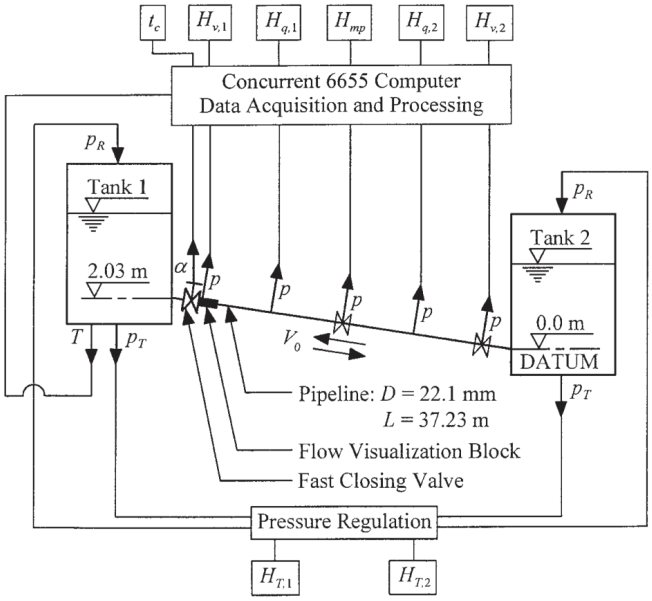

The numerical simulations are conducted with both DGCM and MTPA, and the results are summarized in Figures 4.4 to 4.6. Both models use 50 computational cells. NS = 4 and K_a = 1.4 are used in calculating the numerical fluxes in the proposed model. As can be seen, the proposed model results are in excellent agreement with the experimental data. It is also seen that the proposed model replicates the amplitude and frequency of the resulting waterhammer pressure spikes slightly better than the DGCM. However, the model appears to dissipate the small pressure fluctuations that occur between two subsequent pressure spikes. This is attributed to the

extra numerical viscosity admitted to the model and will be further discussed later in the discussion section.

To show how the model captures the shape of the cavity formed on the upper portion of the pipe cross-section, another set of experimental data conducted by Bergant and Simpson (1999a) is utilized. The test rig is similar to the one shown in Figure 4.3 but the flow is moving in the opposite direction from Tank 1 to Tank 2. The pressure head at Tanks 2 was kept constant at 32 m until the steady-state flow with the velocity of 1.5 m/s is established across the system. Transient flow is then induced by suddenly closing the valve at the upstream end of the system. Figure 4.7 compares the numerical results with the experimental data and the numerical results obtained from DGCM. As can be seen, MTPA accurately captures the magnitude and amplitude of the induced waterhammer pressure spikes and are in excellent agreement with the results obtained from DGCM.

Note that, since 50 computational cells are used, the vapor cavity formed right after the closed valve is captured within just two computational cells. To allow the cavity to be extended over several computational cells, another simulation is conducted with a spatial length of around 1 cm, resulting in 3750 computational cells. Figures 4.8 and 4.9 exhibit a few snapshots of the cavity captured at different timelines during both cavity expansion and contraction stages, respectively.

Figure 4.4

Piezometric head time histories for the initial velocity =1.4 m/s. a) H_(v,1) (DGCM); b) H_(v,1) (MTPA); c) H_mp (DGCM); d) H_mp (MTPA)

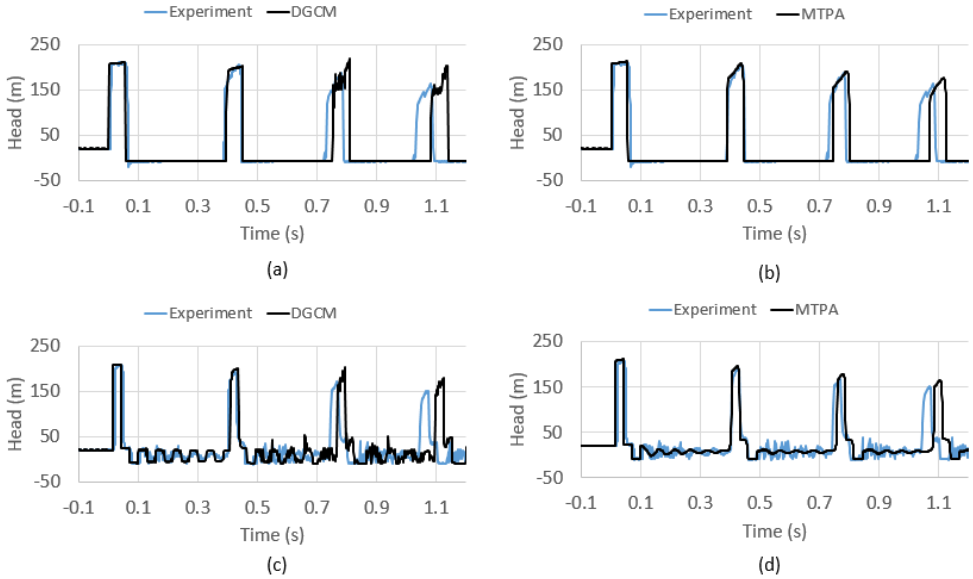

Figure 4.5

Piezometric head time histories for the initial velocity = 0.71 m/s. a) H_(v,1) (DGCM); b) H_(v,1) (MTPA); c) H_mp (DGCM); d) H_mp (MTPA)

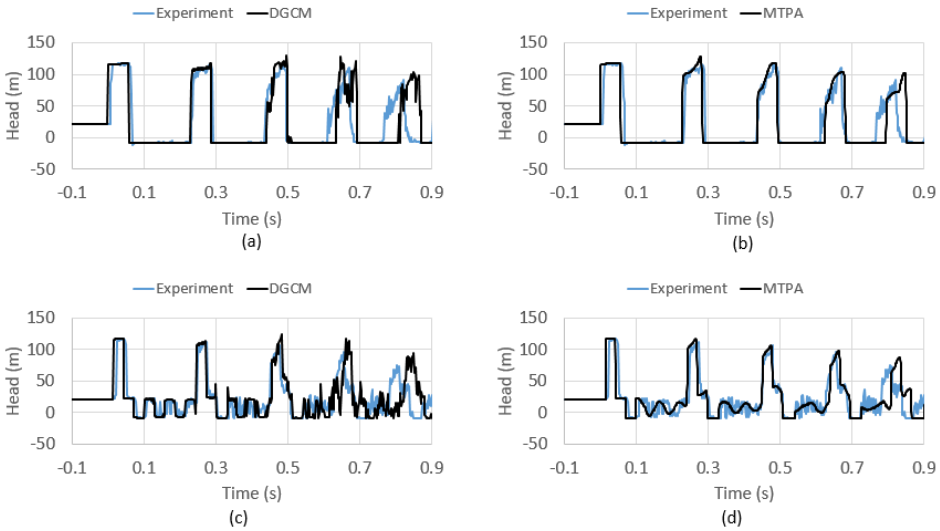

Figure 4.6

Piezometric head time histories for the initial velocity = 0.3 m/s. a) H_(v,1) (DGCM); b) H_(v,1) (MTPA); c) H_mp (DGCM); d) H_mp (MTPA)

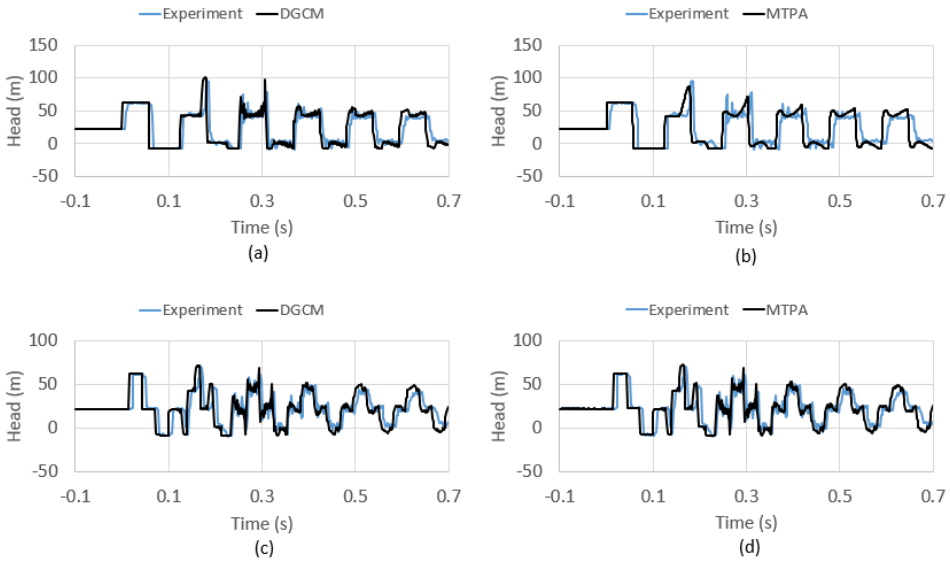

Figure 4.7

Piezometric head time histories for the initial velocity = 1.5 m/s. a) H_(v,1) (DGCM); b) H_(v,1) (MTPA); c) H_mp (DGCM); d) H_mp (MTPA)

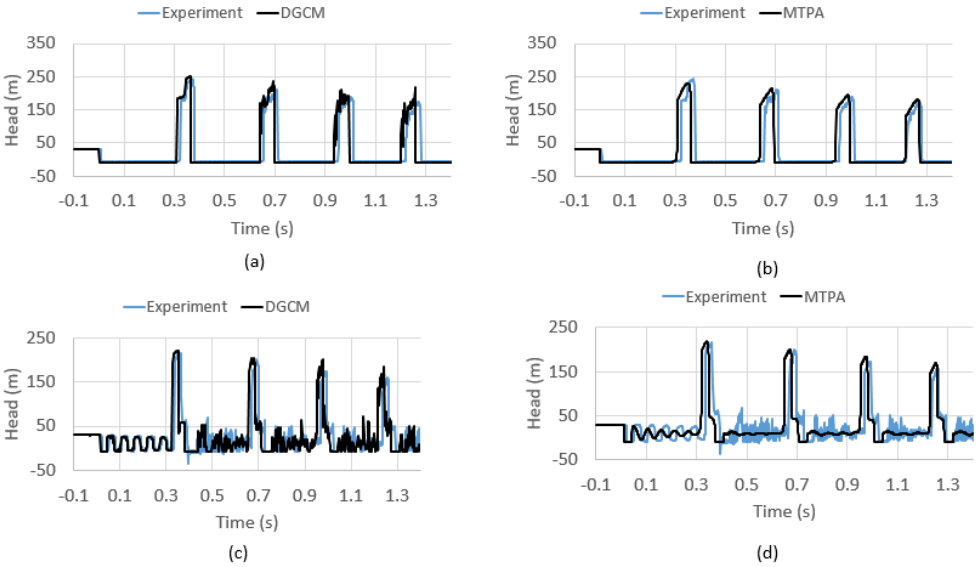

Figure 4.8

Snapshots of the cavity captured by the model during the cavity expansion

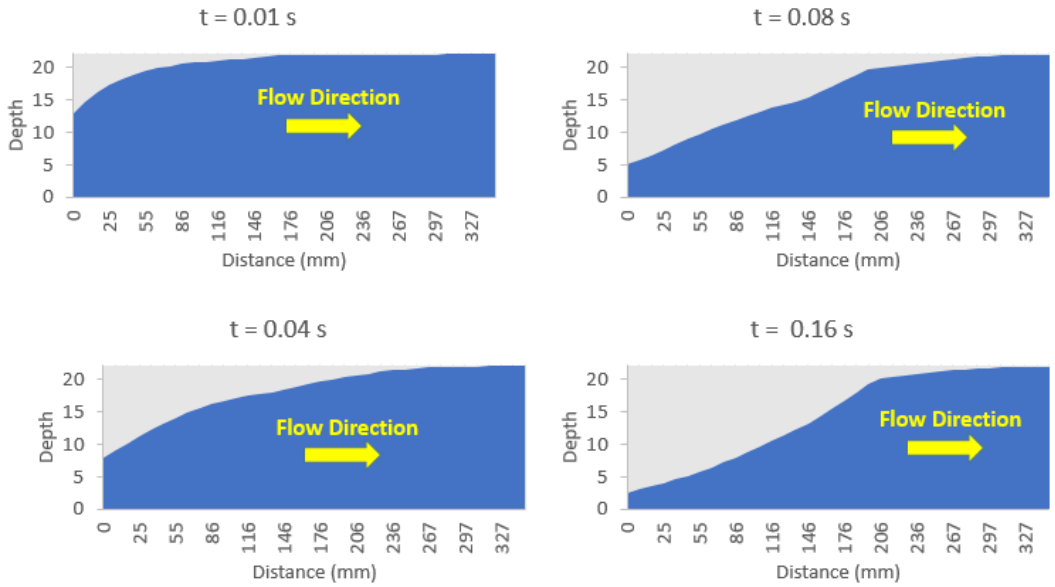

Figure 4.9

Snapshots of the cavity captured by the model during the cavity contraction

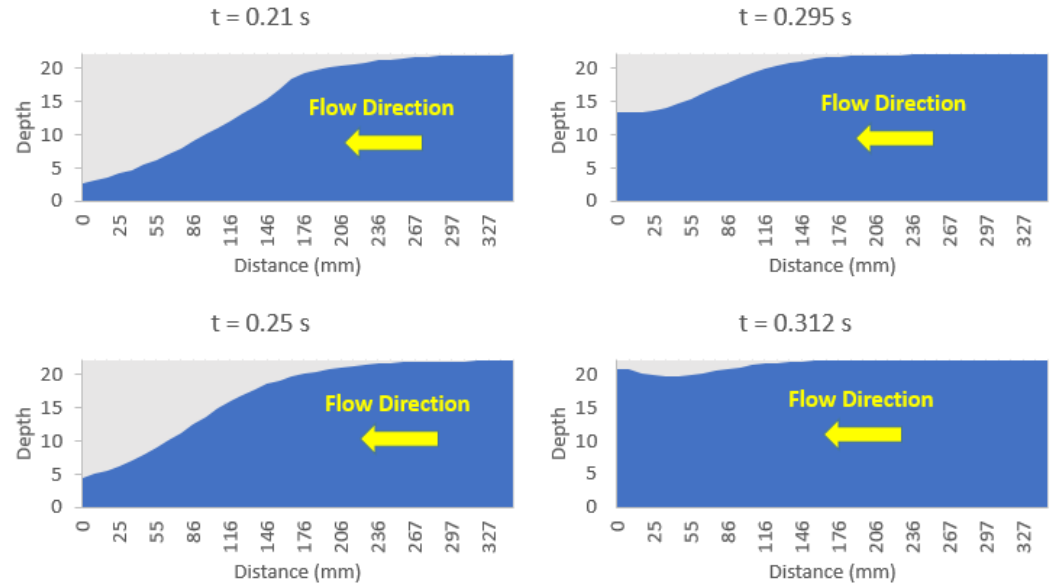

Another test case is utilized to verify the ability of the MTPA in calculating column separation when a vapor cavity develops in the middle of a pipe. Figure 4.10 shows a hypothetical pipe system in which a horizontal-frictionless box shape conduit with the sides of 1m connects two storage tanks in its upstream and downstream ends. The conduit has a length of 400 m and contains a stagnant water column with a depth of 0.6 m. The transient flow starts by suddenly bringing up the water levels at the storage tanks by 3.6 m. Consequently, two identical hydraulic bores form in the vicinity of the tanks and move in the opposite direction toward the middle of the conduit. By applying the momentum and energy equations, the speed and upstream depth of the hydraulic bores are calculated as 10.08 m/s and 3.167 m, respectively (Malekpour and Karney, 2005).

The MTPA was employed to simulate the transient flow in the system. The simulation was performed with the number of computational cells, and acoustic wave speed of 400 and 1000 m/s, respectively. Ka, *NS*, and the Courant number considered are 1.4, 4, and 0.9, respectively. Figure 4.11 compares the numerical and analytical results before the hydraulic bores collide. As can be seen, the model accurately captures the hydraulic bores without producing post-shock oscillations relevant to the original TPA.

Figure 4.12 also depicts the resulting water hammer pressure spikes at the middle of the pipe where the hydraulic bores collide. The Figure implies that that the first pressure spike due to the collusion of the hydraulic bores is reflected at the tanks and initiates column separation in the middle of the pipe. Although there are no experimental data to confirm the numerical results, the results can be validated to some extend analytically. Obviously, the first pressure spike following

the collision of the hydraulic bores can be calculated by the Joukowsky equation. The analytical solution shows that the flow velocity behind the hydraulic bore is 4.0329 m/s (Malekpour and Karney, 2015) which in turn results in a waterhammer pressure head of 411.11 m, confirming the numerical result. This pressure spike should repeat itself following the subsequent cavity collapse because the system is considered frictionless. However, the numerical results show that the pressure amplitude slightly reduces with time which is attributed to the artificial numerical viscosity added to the model to suppress the potential post-shock oscillations.

Figures 4.13 and 4.14 also demonstrate snapshots of the cavity during its formation and collapse. It is seen that the cavity spreads over almost 50 meters of the conduit. To the authors' best of knowledge, the occurrence of such a large cavity had not been identified in the middle of a pipe before. The common belief has been that large cavities dominantly form at pipe dead-ends and the junctions connecting the pipes with different slopes.

4.8 Discussions

As shown in Figures 4.4 to 4.7, although the MTPA and DGCM captured both the amplitude and frequency of the pressure head spikes with almost the same accuracy, the MTPA dissipates the small pressure head oscillations occurring between the two subsequent pressure spikes. As discussed before, to remove post-shock numerical oscillations which may occur after the collapse of cavities, additional numerical viscosity is admitted through a customized HLL solver. However, this additional numerical viscosity is intensified when the pipe is on the verge of pressurization and depressurization. During the occurrence of two subsequent pressure spikes, the pressure head in the pipeline is bouncing between the vapor pressure head and the head of the

downstream tank, making the HLL solver automatically increase the numerical viscosity during this period. However, following the generation of a pressure spike whole pipeline receives the pressure rise, and the model reduces the numerical viscosity to a minimum amount. This explains why the model is significantly dissipative just between two subsequent pressure spikes.

Furthermore, for the sake of removing the small numerical wiggles that appeared in the solution, the MTPA used the Courant number of 0.9 while the DGCM was run with the Courant number of 1. It is well known that the accuracy of a first-order numerical model diminishes as the Courant number decreases. This can be compensated for by increasing the number of computational cells. Figure 4.15 compares the pressure head time histories associated with the second test cases and at the middle of the pipe, for the number of computational cells of 3750 and 50. The figure concludes that increasing the number of computational cells makes the model accurately capture the pressure head oscillations between the subsequent pressure spikes. It is worth noting that only 100 computational cells were adequate to accurately replicate the pressure oscillations but for the sake of capturing the evolution of the cavity with a higher resolution (shown in Figures 4.8 and 4.9), too many computational cells were employed.

Figure 4.10

Piezometric head time histories at H_mp for the initial velocity = 1.5 m/s. a) 50 computational cells; b) 3750 computational cells

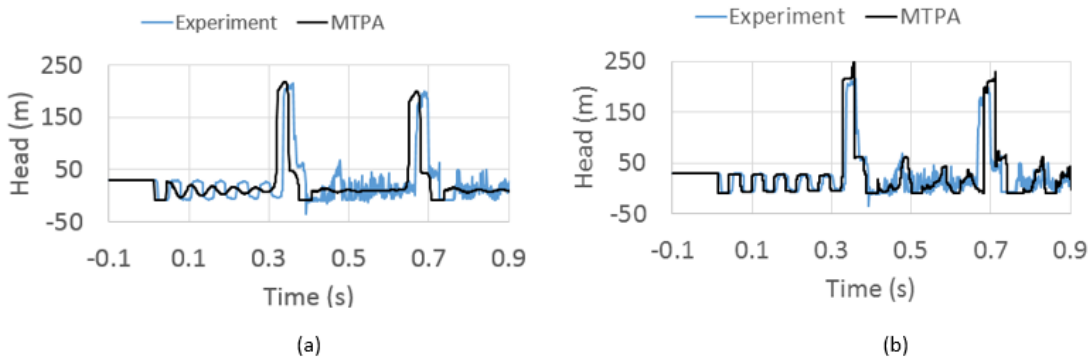

4.9 Summary and Conclusions

An innovative numerical model is proposed to better capture the physics of column separation. The model is built based on the TPA and treats both cavitating and waterhammer flow regimes using a single set of equations that governs unsteady flows in open channel flow. As opposed to shock-fitting-based models in which a complex algorithm is needed to keep track of the interfaces separating the cavitating and liquid zones, the proposed model can capture both flow regimes automatically. The first-order Godunov type finite volume method is utilized to numerically solve the equations. A customized HLL Riemann solver is employed to calculate the fluxes at the computational cell boundaries and to dissipate potential post-shock oscillations when the cavity is about to collapse and the open channel flow below the cavity is switched back to the full flow regime.

The model is validated by comparing the numerical results with the experiment. The comparison shows that the numerical results are in excellent agreement with the experimental data, implying that the model can be used as a reliable tool for calculating column separation in

pipe systems. The numerical results also are compared with those obtained from the DGCM and an excellent agreement is consistently observed. However, due to the artificial numerical viscosity admitted to the model, the model significantly damps the small pressure oscillation occurring between two subsequent pressure spikes. Nevertheless, by increasing the number of computational cells the problem can be resolved.

The MTPA has an obvious superiority over the open-channel-based models proposed by others because they are all based on the shock-fitting algorithm which is very cumbersome to implement while the MTPA enjoys using a shock-capturing algorithm which is very easy to develop even in complex liquid systems. In addition, the MTPA is far more accurate than other shock-fitting-based models and provides comparable results to the DGCM. A unique feature of the MTPA is that it can simultaneously account for waterhammer, cavitating flow and free surface flow regimes, a feature making the MTPA even superior to the DGCM.

Finally, although the MTPA can better replicate the physics of column separation, it provides comparable results to the DGCM. This arises the question that under what circumstances the MTPA is expected to provide better results? The preliminary results from an ongoing study by the authors have revealed that in larger pipe sizes and/or when large vapor cavities are extended over long and steep pipes, the MTPA performs far better than the DGCM. The details are beyond the scope of this paper and are planned to be published in a separate paper in the future.

4.10 References

Adamkowski, A., and M. Lewandowski. 2012. "Investigation of hydraulic transients in a pipeline with column separation." Journal of Hydraulic Engineering 138 (11): 935-944.

Autrique, R., and E. Rodal. 2013. "Laboratory studies of water column separation." IOP Conference Series: Materials Science and Engineering. IOP Publishing. 022022.

Baltzer, R. A. 1967a. "Column separation accompanying liquid transients in pipes." Journal of Basic Engineering 837-846.

Baltzer, R.A. 1967b. A study of column separation accompanying transient flow of liquids in pipes. PhD Thesis. Michigan: University of Michigan.

Bergant, A., A. R. Simpson, and A. S. Tijsseling. 2006. "Water hammer with column separation: A historical review." Journal of Fluids and structures 22: 135-171.

Bergant, A., and A. R. Simpson. 1999a. "Cavitation inception in pipeline column separation." 28th IAHR Congress. Graz, Austria: CD-ROM.

Bergant, A., and A. R. Simpson. 1999. "Pipeline column separation flow regimes." Journal of Hydraulic Engineering 125 (8): 835–848.

Chaudhry, M. H. 1999. Open channel flow. Englewood Cliffs, N.J : Prentice-Hall.

Chaudhry, M.H. 1987. Applied Hydraulic Transients. New York: Van Nostrana Reinhold Co.

Cunge, J. A., and M. Wegner. 1964. "Numerical Integration of Bane de Saint-Venant's Flow Equations by Means of an Implicit Scheme of Finite Differences. Applications in the Case of Alternately Free and Pressurized Flow in a Tunnel." La Houille Blanche 1: 33-39.

Kalkwijk, J.P.Th., C. Kranenburg, C.B. Vreugdenhil, and A.H. De Vries. 1972. Cavitation caused by water hammer in horizontal. Delft: Delft Hydraulics Laboratory,Publication No. 97.

Karni, S., and S. Čanić. 1997. "Computations of slowly moving shocks." Journal of Computational Physics 136 (1): 132-139.

Kerger, F., P. Archambeau, S. Erpicum, B. J. Dewals, and M. Pirotton. 2011. "An exact Riemann solver and a Godunov scheme for simulating highly transient mixed flows." Journal of Computational and Applied Mathematics 235: 2030-2040.

Khani, D, Y. H. Lim, and A. Malekpour. 2020. "Hydraulic Transient Analysis of Sewer Pipe Systems Using a Non-Oscillatory Two-Component Pressure Approach." Water 12 (10): 2896.

Khani, D., Y. H. Lim, and A. Malekpour. 2021. "A Mixed Flow Analysis of Sewer Pipes with Different Shapes Using a Non-Oscillatory Two-Component Pressure Approach (TPA)." Modelling 2 (4): 467-481.

León, A. S., M. S. Ghidaoui, A. R. Schmidt, and M. H. García. 2009. "Application of Godunov-type schemes to transient mixed flows." Journal of hydraulic research 47 (2): 147-156.

LeVeque, R.J. 2002. Finite volume methods for hyperbolic problems. Cambridge, UK: Cambridge Press.

Malekpour, A., and B. Karney. 2015. "Spurious Numerical Oscillations in the Preissmann Slot Method: Origin and Suppression." Journal of Hydraulic Engineering, ASCE.

Malekpour, A., and B. W. Karney. 2014b. "Column separation and rejoinder during rapid pipeline filling induced by a partial flow blockage." Journal of Hydraulic Research 52 (5): 693-704.

Malekpour, A., and B. W. Karney. 2014a. "Profile-induced column separation and rejoining during rapid pipeline filling." Journal of Hydraulic Engineering 140 (11).

Marsden, N.J., and J.A. Fox. 1976. "An alternative approach to the problem of column separation in an elevated section of pipeline." Second International Conference on Pressure Surges. London: BHRA. 1–13.

Martin, C.S. 1983. "Experimental investigation of column separation with rapid closure of downstream valve." Fourth International Conference on Pressure Surges. Cranfield, UK: BHRA Fluid Engineering. 77–88.

Provoost, G. A., and E. B. Wylie. 1981. "Discrete gas model to represent distributed free gas in liquids." 5th International Symposium on Water Column Separation. Obernach, West Germany. 28-30.

Siemons, J. 1967. "The phenomenon of cavitation in a horizontal pipe-line due to a sudden pump-failure." Journal of Hydraulic research 5 (2): 135-152.

Simpson, A.R., and A. Bergant. 1994. "Numerical comparison of pipe column-separation models." Journal of Hydraulic Engineering 120 (3): 361–377.

Simpson, A.R., and E.B. Wylie. 1991. "Large water-hammer pressures for column separation in pipelines." Journal of Hydraulic Engineering 117 (10): 1310–1316.

Toro, E. F. 2001. Shock-capturing methods for free-surface shallow flows. Chichester, New York: John Wiley.

Vasconcelos, G. J., and T. B. D. Marwell. 2011. "Innovative simulation of unsteady low-pressure flows in water mains." Journal of Hydraulic Engineering 137 (11): 1490-1499.

Vasconcelos, J. G., S. J. Wright, and P. L. Roe. 2006. Current Issues on modeling extreme inflows in stormwater systems in Intelligent Modeling of Urban Water Systems, Monogrph 14. Guelph, Ontario: CHI.

Vasconcelos, J. G., S. J. Wright, and P. L. Roe. 2009. "Numerical oscillations in pipe-filling bore predictions by shock-capturing models." Journal of Hydraulic Engineering 135 (4): 296-305.

5 CHAPTER FIVE

5.1 Investigating the Performance of the Modified Two-Component Pressure Approach in Capturing Column Separation with Large Vapor Cavities

5.2 Abstract

This paper aims to investigate the performance of the Modified Two-Component Pressure Approach (MTPA), recently proposed by the authors, in capturing column separation with large vapor cavities. The MTPA calculates both the cavitating and waterhammer flow regions using a single set of equations that governs unsteady flow in open channels. Comparing the results with experimental data, the results obtained from the Discrete Gas Cavity Model (DGCM), and analytical solutions reveals that: 1) the proposed model can accurately capture the evolution of large vapor cavities in pipe systems; 2) the model provides more accurate results compared to the DGCM, particularly as the pipe size increases; 3) under some circumstances the DGCM fails to capture the cavitating flow region correctly while the proposed model accurately calculates the hydraulics of the pipe system. Finally, the results exhibit the obvious superiority of the proposed model over the DGCM and the conventional open channel-based models.

5.3 Introduction

Pressurized pipe systems may receive negative pressures under different circumstances. Pump trip and power failure, rapid closing of valves, and load rejection in hydropower systems are a few examples of transient events that can trigger down surges that propagate across the system with the pipe acoustic wave speed (Wylie and Streeter, 1993; Chaudhry, 1987). Negative

pressures develop if the hydraulic grade line falls below the pipe grade. When the negative pressure reaches the vapor pressure of the liquid, cavitating flow forms and makes the pressure remain constant at the vapor pressure. The cavitating flow region disconnects the hydraulics grade line, whereby the liquid columns on either side of the cavity can accelerate and decelerate independently (Bergant et al., 2016). The flow imbalance at the cavitating zone causes the vapor cavities to grow and column separation to form. Once the cavity is collapsed, the adjacent water columns collide and produce significant water hammer pressure spikes with the intensity that depends on the velocity difference of the water columns and the magnitude of the acoustic wave speed. The resulting pressures are severe enough to compromise the integrity of the pipe system (Chaudhry, 1987).

Due to its destructive nature column separation has been received several experimental and numerical investigations since it was first identified by Joukowsky early in the 20th century (Bergant et al., 2006). Simpson and Wylie (1991), Martin (1983), and Bergant and Simpson (1999), Adamkowski and Lewandowski (2012), and Autrique and Rodal (2013), among others, experimented with column separation and shed light on this complex phenomenon. The insight from the experimental studies had made the researchers propose a variety of numerical models for capturing the essential features of column separation in pipe systems (Bergant and Simpson, 2006). Among these models, the two most popular numerical approaches utilized in the industry are the Discrete Vapor Cavity Model (DVCM) and Discrete Gas Cavity Model (DGCM). The models have been validated by comparing the numerical results with the experiment (Wylie, 1984; Brgant and Simpson, 1994; Simpson and Bergant, 1994; Provoost and Wylie, 1981; Adamkowski and Lewandowski, 2012; Bergant and Simpson, 1999). Although both models simulate column separation pretty well, the DGCM is superior to the DGCM in that it

significantly smooths the non-physical numerical oscillation generated by the DVCM. The annihilation of multiple cavities formed in the distributed cavitation region can explain the cause of the numerical oscillations (Bergant et al., 2006).

However, Simpson and Bergant (1994) showed that both the DVCM and DGCM could compromise the accuracy of the resulting pressure peaks if any cavity volume exceeds 10% of the computational cell volume. In pipe systems in which the production of large cavities is expected, increasing the spatial length of computational cells may resolve this problem (Simpson and Bergant, 1994). Yet, coarse meshes can decrease the model efficiency, except at the Courant number =1. In complex pipe systems that comprise several pipes with different lengths and acoustic wave speeds, it is almost impossible to enforce a Courant number of 1 in all pipes (Wylie and Streeter, 1991). However, the Courant numbers of less than one still compromises the efficiency of numerical models (LeVeque, 2002; Ghidaoui and Karney, 2014), suggesting that using a course mesh may not be a good solution. Another potential remedy is to employ two-phase flow models (Wylie and Steeter, 1991; Bergant and Simpson, 1999). To this end, Bergant and Simpson (1999) proposed the Generalized Interface Vapour Cavity Model (GIVCM) that tracks the interfaces separating the cavitating and liquid zones and calculates the flow variables in the regions using the relevant governing equations. Although the model provides accurate results, it is hard to implement, particularly in complex pipe systems in which the track of several interfaces needs to be kept.

A few common assumptions made in developing the GIVCM, DVCM, and DGCM may still compromise the accuracy of the results under specific flow conditions. The first assumption in the models is that the cavities fill the whole pipe cross-section while forming (Wylie and Streeter, 1991). However, experiments show that they start developing near the crown of the

pipes. This conceptual difference causes the models to underestimate the extension of the cavities. Next, the models assume that the whole pipe cross-section experiences the vapor pressure during cavitating flow, which is not physically sound. In fact, due to the gravity effect, the upper layers of the liquid in the pipe receive lower pressures. As will be shown, this assumption causes the models to overestimate the frequency of the resulting pressure spikes. Last, the models fail to calculate column separation in the pipe systems, in which both pressurized and open channel flow regimes co-exist.

Vasconcelos and Marwell (2011) proposed a modified version of the TPA which can simultaneously calculate open channel and cavitating flow regimes. The model relates pipe acoustic speed to the pressure through a small gas pocket considered at each computational cell. Following pressure drop at a computational cell, the gas pocket expands, and the wave speed reduces. When the vapor pressure is reached, the gas pocket no longer expands whereby the pressure is kept constant at the vapor pressure, the two characteristics of cavitating flows. However, this model does not allow cavity formation and collapse at the intermediate computational cells, and column separation is treated only at pipe boundaries with the same approach utilized in the DVCM. Although the model can capture open channel flow, when it comes to calculating column separation the model cannot be categorized as an open-channel-based model and suffers from some of the limitations associated with the DVCM and DGCM models.

The open channel flow-based model appears to address the shortcomings discussed earlier, but they have not received adequate attention so far. Early versions of these models employed the shock-fitting approach to keep track of the boundaries separating various flow regimes that can occur during the transient flow. The models then calculate each flow region

with its relevant governing equations. Baltzer (1967a, and 1967b) proposed a shock-fitting model to simulate water column separation in pressurized pipe systems. The proposed model utilizes the method of characteristics to solve both the open channel and water hammer equations. Although the model succeeded in capturing the shape of the cavity, it failed to accurately replicate the frequency and amplitude of the pressure spikes experimented on in the lab. Siemons (1967a and 1967b), Kalkwijk et al. (1972), Marsden and Fox (1967), among others (see Bergant et al., 2016), proposed some shock-fitting based models, but their mode could not provide reasonable accuracy. The key challenge with the shock-fitting models is to calculate the locations where the cavitating flow region is transferred to the water hammer region. This challenge and the fact that the shock-fitting models are hard to implement in the context of the complex pipe systems can perhaps explain why the open channel-based models have not received further attention since then (Bergant et al., 2006).

To resolve the challenges of the open-channel-based models, Khani et al. (2022) proposed the Modified Two-Component Pressure Approach (MTPA). The proposed model can simultaneously calculate open channel, water hammer, and cavitating flow regimes using a single set of equations that govern unsteady flow in open channels. They showed that the MTPA allows simulating column separation with a level of accuracy comparable to DGCM's though the conclusion was made based on validating both models with the data obtained from experimenting with a test rig having a small pipe diameter. However, the question arises as to how the MTPA differs from the DGCM when applied to real pipe systems?

The goal of the following paper is to investigate the performance of the MTPA in the pipelines with larger pipe diameters that may produce the hydraulic circumstances under which large cavities may form and spread. To this end, the MTPA is further tested with the aid of a

larger-scale test rig and with some hypothetical test cases designed to reveal in what ways the MTPA can better replicate column separation in pipe systems.

The organization of this paper is as follows: The concept of the MTPA and the employed numerical method is first discussed. The numerical results are then evaluated using experimental data and the results obtained from the DGCM. The discrepancy of the results obtained from the MTPA and DGCM are highlighted, and the underlying cusses are discussed. Finally, the outcomes of the paper are summarized, and conclusions are made.

5.4 MTPA

The Two-Component Pressure Method (TPA) is proposed to address the limitation of the Preissmann Slot Method (PSM) in capturing negative pressures (Vasconcelos et al., 2006). The TPA enjoys using the same set of equations that govern unsteady flow in open channels, though with slight modification. As shown in Equation 5-2, the pressure term in the momentum equation is split into two components that include the effect of pressure head and water depth distinctively.

$$\frac{\partial A}{\partial t}+\frac{\partial Q}{\partial x}=0 \qquad Continuty\ Equation \qquad 5\text{-}1$$

$$\frac{\partial Q}{\partial t}+\frac{\partial\left(\frac{Q^2}{A}+Ag[h_c+h_s]\right)}{\partial x}=gA(S_0-S_f) \qquad Momentum\ Equation \qquad 5\text{-}2$$

where, A= flow cross sectional area, Q = flow rate, h_c = the distance between the free surface and the centroid of the flow cross-sectional, h_s = pressure head, g = gravitational acceleration, S_0 = pipe slope and S_f = frictional slope which can be calculated by the following equation.

$$S_f = \frac{Q^2 {n_m}^2}{A^2 {R_h}^{\frac{4}{3}}} \quad 5\text{-}3$$

where n_m = Manning coefficient and R_h = hydraulic radius of the flow.

When the hydraulic grade line is about to fall below the pipe grade, the flow can either remain pressurized or turn to the free surface regime depending on the ventilation condition of the pipe at that location. If the pipe cannot be ventilated, h_s accounts for negative pressures and h_c remains constant at the pipe diameter. Otherwise, h_c represents the depth of the flow, and h_s is set to zero.

In pressurized flows, when the pipe receives an overpressure, the resulting unbalanced liquid mass is accommodated through the compression of the liquid and expansion of the pipe cross-section. However, negative pressures withdraw liquid mass from the pipe system by squeezing the pipe and stretching the liquid. In the TPA, the following equation relates the pressure head to the pipe cross-section expansion/contraction (Vasconcelos et al., 2006).

$$h_s = \left[\frac{A - A_f}{A_f}\right]\frac{a^2}{g} \quad 5\text{-}4$$

where a = acoustic wave speed, and A_f = pipe cross-sectional area.

The TPA has been successfully used for capturing negative pressures (Vasconcelos et al., 2006; Vasconcelos and Wright, 2007; Sanders and Bradford, 2010; Khani et al., 2020 and 2021) but it cannot account for cavitating flow and column separation. In reality, whenever the pressure reaches the vapor pressure of the liquid, cavitating flow forms and maintains the pressure constant at the vapor pressure. However, the TPA responds to this condition by allowing the pressure drops far below the vapor pressure, which is not physically sound.

Khani et al. (2022) proposed a modified version of the TPA (MTPA), which can account for cavitating flow and column separation. In the MTPA, Equations 5-1 and 5-2 can calculate the transient pressure heads and flow rates across the system as long as the pressures are above the vapor pressure. Otherwise, Equation 5-2 no longer holds, and the following equation should be utilized instead.

$$\frac{\partial Q}{\partial t} + \frac{\partial\left(\frac{Q^2}{A} + g[Ah_c + A_f h_v]\right)}{\partial x} = gA\,(S_0 - S_f\,) \qquad 5\text{-}5$$

where h_v = vapor pressure head of the liquid.

Figure 5.1 demonstrates the pressure components applied on the pipe cross-section during column separation. As can be seen, the total force on the section comprises two forces acting in opposite directions. The weight of the water pushes the flow cross-section, while the vapor pressure sucks the whole pipe cross-section.

Figure 5.1

Schematic of the pressure components applied on the flow and pipe section during cavitating flows

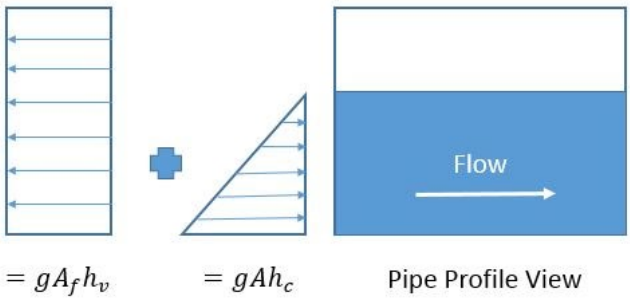

5.5 Numerical Solution

5.5.1 Finite Volume Implementation

The Godunov scheme is employed to solve the governing equations. It is an upwind finite volume-based numerical scheme that is widely used for solving hyperbolic partial differential equations (Toro, 2001; LeVeque, 2002). In this method, the spatial domain of the computation is discretized to several computational cells with a spatial distance of Δx, and the temporal domain is split by a constant time interval of Δt. To alleviate the potential spurious numerical oscillations, the scheme is implemented with first-order accuracy through applying piecewise constant data reconstruction at the computational cells.

By discretizing the governing equations, unknowns at the current time level can be explicitly calculated based on the data retrieved from the previous timeline using the following equation:

$$A_i^{n+1} = A_i^n - \frac{\Delta t}{\Delta x}\left(F^n_{i+\frac{1}{2}} - F^n_{i-\frac{1}{2}}\right) \quad 5\text{-}6$$

$$Q_i^{n+1} = Q_i^n - \frac{\Delta t}{\Delta x}\left(G^n_{i+\frac{1}{2}} - G^n_{i-\frac{1}{2}}\right) + \Delta t g A\left(S_0 - S_{f_i}^{\ n}\right) \quad 5\text{-}7$$

where i is computational cell number, $i+\frac{1}{2}$ and $i-\frac{1}{2}$ are referring to the downstream and upstream boundaries of the i^{th} cell respectively, n and $n+1$ are referring to the pervious and current timelines respectively, and F and G are mass and momentum fluxes respectively.

In the Godunov scheme, the mass and momentum fluxes in Equations 5-6 and 5-7 should be calculated by solving the Riemann problem at the cells' boundaries (Toro, 2002). Khani et al. (2020) adapted the HLL solver proposed by Malekpour and Karney (2015) to suppress the numerical oscillations associated with the TPA and showed that it provides non-oscillatory

solutions even at the maximum possible acoustic pipe speeds. They also showed that the model performs consistently for different shapes of conduits (Khani et al., 2021).

The fluxes in the HLL solver are generally calculated through a procedure summarized in Equation 5-8.

$$= \boldsymbol{\Gamma}_L \quad if\ S_L > 0$$

$$= \frac{S_R \boldsymbol{\Gamma}_L - S_L \boldsymbol{\Gamma}_R + \boldsymbol{S_L S_R}(\boldsymbol{U_R} - \boldsymbol{U_L})}{\boldsymbol{S_R} - \boldsymbol{S_L}} \quad if\ S_L \leq 0\ and\ S_R \geq 0 \qquad 5\text{-}8$$

$$= \boldsymbol{\Gamma}_R \quad if\ S_R < 0$$

where S_L and S_R are the left and right shock wave speeds respectively, $\boldsymbol{U}_L = \begin{bmatrix} A_L \\ Q_L \end{bmatrix}$ and $\boldsymbol{U}_R = \begin{bmatrix} A_R \\ Q_R \end{bmatrix}$ are dependent variables at the computational cells $i-1$ and $i+1$ respectively, and $\boldsymbol{\Gamma}_L = \begin{bmatrix} F_L \\ G_L \end{bmatrix}$ and $\boldsymbol{\Gamma}_R = \begin{bmatrix} F_R \\ G_R \end{bmatrix}$ are the fluxes at the computational cells $i-1$ and $i+1$ respectively.

The amount of the numerical viscosity admitted to the numerical scheme is controlled by the magnitude of the right and left wave velocities (Malekpour and Karney, 2015). To include the optimal amount of numerical viscosity, Khani et al. (2020, 2021) proposed a simple strategy for calculating the left and right wave speeds in both water hammer and open channel flow regions. The left and right wave speeds are calculated using the following equations.

$$S_L = V_L - \Omega_L\ ;\ S_R = V_R + \Omega_R \qquad 5\text{-}9$$

$$\Omega_{K(L,R)} = \sqrt{\frac{g[Y_G A_G - (h_C + |h_S|)_K A_K] A_G}{A_K (A_G - A_K)}} \qquad 5\text{-}10$$

where variables with sub-index G are the function of Y_G that needs to be estimated.

Malekpour and Karney (2015) showed that Equation 5-10 significantly augments wave speeds only when the water depth is close to the pipe crown. This implies that by using Equation 5-10 the artificial viscosity admitted to the numerical scheme increases when the flow is about to switch from open channel to full flow. Khani et al. (2020) showed that calculating Y_G by the following equation can admit the optimal amount of numerical viscosity.

$$Y_G = K_a \times MAX\,[d_{i-NS}, d_{i-NS+1}, \dots, d_i, d_{i+1}, \dots d_{NS}] \qquad 5\text{-}11$$

where $d = h_c + |h_s|$.

In Equation 5-11, NS is the number of computational cells among which the artificial viscosity is distributed. Numerical exploration shows that NS should be selected such that the numerical viscosity spread over a length 3 or 4 times higher than the pipe height. In any way, the NS should not be less than 3. Numerical exploration also reveals that in the computational cells carrying free surface flow, K_a can take a value of around 1.4 if a pressurization front exists within NS computational cells on either side of the target computational cell. Otherwise, NS can be considered as 1.001.

5.6 Boundary Conditions

The test rig and test cases utilized for validating the proposed model contain several boundary conditions including constant water level reservoirs, dead-ends, and junctions. The formulation of the boundary conditions is described in the following:

5.6.1 Constant water level reservoirs

A constant water level reservoir serves as a wave reflector in pipe systems and fixes the HGL of the pipe at the connection. Given the HGL is known at the connection point, the flow velocity can be calculated using the positive or negative characteristic equations depending on

whether the reservoir located on the upstream or downstream of the pipe. The discrete forms of the characteristic equation are brought in the following

$$C^+: V_B + \frac{g}{a}H_B = V_n + \frac{g}{a}H_n \quad 5\text{-}12$$

$$C^-: V_B - \frac{g}{a}H_B = V_1 - \frac{g}{a}H_1 \quad 5\text{-}13$$

where V_B , V_1 and V_n are flow velocities at the boundary, first and last computational cells, respectively and, H_B, H_1 and H_n are piezometric heads at the boundary, first and last computational cells, respectively.

Using the characteristics equations, the flow velocity at the boundary can be calculated by the following equations.

$$V_B = V_1 + \frac{g}{a}(H_r - H_1) \qquad Upstream\ reservoire \quad 5\text{-}14$$

$$V_B = V_n + \frac{g}{a}(H_n - H_r) \qquad Downstream\ Reservoir \quad 5\text{-}15$$

Having V_B calculated, the mass and momentum fluxes can be calculated for the boundary.

5.6.2 Dead Ends

At dead ends, the flow velocity is zero, and depending on the flow regime, either the flow depth or pressure head needs to be determined. When cavitating flow forms at a dead end, the flow depth beneath the cavity formed at the dead-end is unknown. Otherwise, the water hammer region prevails, and the pressure head needs to be calculated. In the latter case, the HGL is calculated by setting the boundary velocity to zero in the positive and negative characteristic equations (Equations 5-12 and 5-13), as shown below.

$$H_B = H_1 - \frac{a}{g}V_1 \qquad Upstream\ deadend \quad 5\text{-}16$$

$$H_B = H_n + \frac{a}{g}V_n \qquad Downstream\ deadend \quad 5\text{-}17$$

When a vapour cavity forms at the dead-end, the flow turns into the open channel regime, and the characteristic equations should be written as follows:

$$C^+: V_B + \Phi_B = V_n + \Phi_n \quad \text{5-18}$$

$$C^-: V_B - \Phi_B = V_1 - \Phi_1 \quad \text{5-19}$$

where Φ can be calculated using the following equation.

$$\Phi = \int_0^y \frac{\sqrt{gD}}{A} dA \quad \text{5-20}$$

where y = flow depth and D = hydraulic depth.

By setting V_B = 0 and plugging Equation 5-20 into Equations 5-18 and 5-19, the following equations are reached.

$$\int_0^{y_B} \frac{\sqrt{gD_B}}{A_B} dA = V_n + \int_0^{y_n} \frac{\sqrt{gD_n}}{A_n} dA \qquad Downstream\ deadend \quad \text{5-21}$$

$$\int_0^{y_B} \frac{\sqrt{gD_B}}{A_B} dA = \int_0^{y_1} \frac{\sqrt{gD_1}}{A_1} dA - V_1 \qquad Upstream\ deadend \quad \text{5-22}$$

Each of the above equations contains just one unknown which is the depth of the flow at the boundary, y_B. However, the equations cannot be solved explicitly, and an iterative method such as the Newton-Raphson method should be employed to calculate the unknown.

5.6.3 Junctions

A Junction refers to a point where two pipes are connected. When the junction and the adjacent pipes are in the waterhammer regime, the associated pressure head and flow velocity can be easily calculated by simultaneous solution of the discrete form of the positive and negative characteristics equations. However, when a vapor cavity forms at the junction, calculating the flow parameters is challenging and depend on whether the flow in the pipes is

sub- or supercritical. In the following, the junction boundary condition is formulated for all possible flow conditions. However, the formulation is limited to junctions with identical pipe diameters and pipe acoustic wave speeds, as is in all test cases utilized in this paper.

For junctions working in the waterhammer region, the HGL and flow velocity can be calculated by simultaneous solutions of Equations 5-12 and 5-13.

$$H_B = \frac{H_n+H_1}{2} + \frac{a}{g}\left(\frac{V_n-V_1}{2}\right) \quad 5\text{-}23$$

$$V_B = \frac{V_n+V_1}{2} + \frac{g}{a}\left(\frac{H_n-H_1}{2}\right) \quad 5\text{-}24$$

When the junction works in the cavitating flow regime and the flow in both pipes is subcritical, the flow depth and velocity are calculated by solving Equations 5-21 and 5-22 simultaneously. Since no explicit solution exists for solving these equations, the Newton-Raphson is used to calculate the unknowns. If the flow in the upstream pipe is subcritical and the downstream pipe runs under supercritical flow, critical depth would form at the junction. In this case, the flow velocity and depth are calculated by solving the following equation.

$$V_c + \Phi_c = V_n + \Phi_n \quad 5\text{-}25$$

where V_c and Φ_c can be calculated by the following equation. Subscript $_c$ refers to the critical flow condition.

$$V_C = \sqrt{gD_c} \quad 5\text{-}26$$

$$\Phi_c = \int_0^{y_c} \frac{\sqrt{gD_c}}{A} dA \quad 5\text{-}27$$

where D_c = critical hydraulic depth and y_c is critical depth.

The Newton-Raphson method is employed to solve Equation 5-25 for the critical depth. When the critical depth is calculated, the critical velocity would be obtained from Equation 5-26. Note that the HGL at the junction can be calculated by adding the bottom elevation of the junction to the critical depth.

In case that the flow in the downstream pipe is subcritical, but the flow runs at supercritical flow in the upstream pipe, the critical flow would be formed at the junction though the fluid moves in the opposite direction. In such a case, the following equation can be used to calculate the critical depth.

$$V_c - \Phi_c = V_1 - \Phi_1 \qquad 5\text{-}28$$

Having V_c, and y_c calculated, the fluxes at the junction boundary can be calculated.

5.7 Numerical Results

Khani et al. (2022) validated the MTPA by comparing the numerical results with the experimental data conducted by Bergant and Simpson (1999) and the numerical results obtained from the DGCM. They showed that the MTPA results are in excellent agreement with both experiment and the results obtained from the DGCM. However, the validity of the MTPA in capturing the evolution of the vapor cavity was not tested since Bergant and Simpson (1999) did not record the time history of the vapor cavity. To this end, the experimental study conducted by Autrique and Rodal (2013) is employed to test this aspect of the model. As shown in Figure 5.3, the test rig consists of two pressurized tanks connected by a pipe with a length, diameter, and acoustic speed of 277 m, 0.1 m, and 989 m/s, respectively. For the sake of video recording of the evolution of the vapor cavity, a transparent PVC pipe is utilized in the first 9 m of the test rig, whereas steel pipes are used for the rest of the system. At the upstream end of the system, the

pipe vertical profile is configured like a hump to let the vapor cavity concentrate in the transparent zone rather than being spread far downstream side. The detail of the pipe profile in this section is shown in Figure 5.3. The transient pressures are logged using the pressure transducers located at points T1, T2, and T4 shown in Figure 5.2.

Figure 5.2

Test rig configuration (adapted from Autrique and Rodal, 2013)

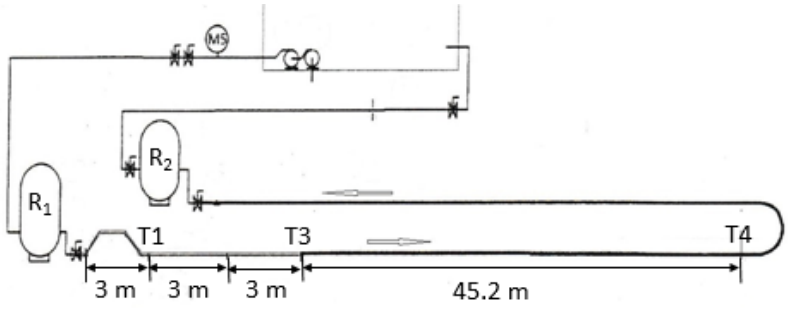

Figure 5.3

Pipe Configuration at the upstream end of the test rig (adapted from Autrique and Rodal, 2013)

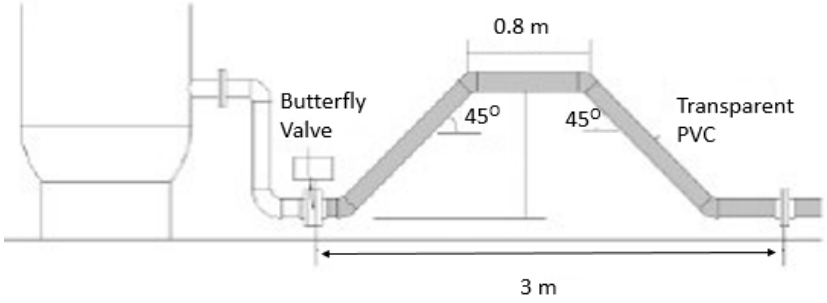

Experiments with column separation were conducted with the two flow rates of 8.2 and 18 L/s. To this end, following the establishment of the steady-state flow in the system, the butterfly valve at the upstream side of the pipe is suddenly closed and the resulting transient pressures are recorded at points T1, T3, and T4. At the steady flow, the pressures at the upstream

and downstream tanks are measured as 1.2 and 0.8 kg/cm2, respectively for the flow rate = 8.2 L/s and as 3 and 1 kg/cm2, respectively for the flow rate = 18 L/s.

Considering the vapor pressure of the water = -8 m (Autrique and Rodal, 2013), the numerical simulations are performed with both the DGCM and MTPA for the flow rates of 8.2 and 18 L/s, and the results are summarized in Figures 5.4 to 5.11. To capture the evolution of the cavity with an adequate level of accuracy, a fine computational grid with the spatial length of 0.1 m is used in both models, resulting in a time step of around 0.0001 s. NS = 4 and K_a = 1.4 are used in calculating the numerical fluxes in the MTPA.

Figures 5.4 to 5.6 shows that for the flow rate = 8.2 L/s, the pressure time histories are in good agreement with both experimental and those obtained from the DGCM. As shown in Figure 5.7, the shape of the cavity at times 1.48 s and 3.02 s are also captured very well compared to the experiment.

However, for the flow rate = 18 L/s, except in the first pressure cycle, the results captured by both the MTPA and DGCM do not agree well with the experiment. As shown in Figures 5.8 to 5-10, both numerical models overestimate the frequency of the amplitude of the pressure spikes induced following water column rejoining. Nevertheless, as shown in Figure 5.11, the MTPA calculates the evolution of the cavity in the first cycle very well at both time levels of 3.51 and 6.01 s.

The videos show that extensive air comes out of solution when negative pressures occur in the system. The release of air which is not accounted for in both models may change the transient responses of the system during cavitating flow and perhaps can explain the discrepancy between the numerical results and experiment. Nevertheless, this is just a hypothesis that is subjected to verification.

Figure 5.4

Comparing calculated pressure head time histories with experiments at point T1 and flow rate = 8.2 L/s; a) MTPA. B) DGCM

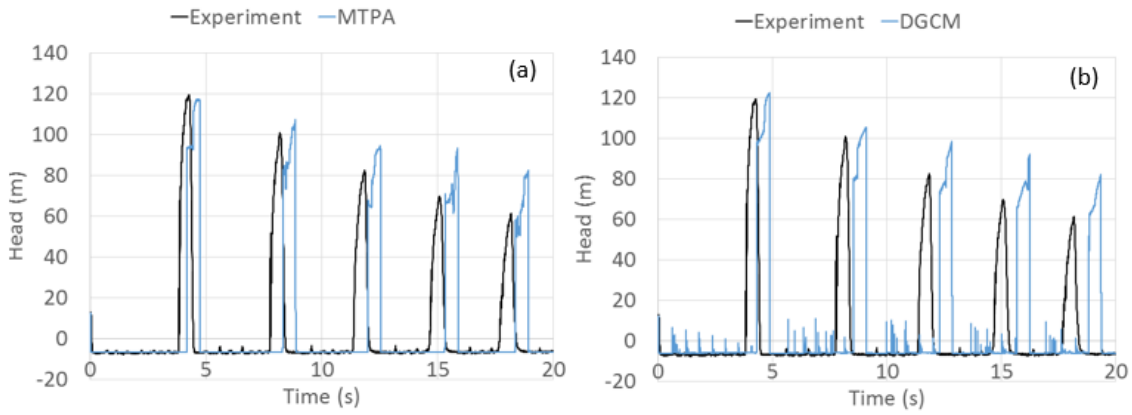

Figure 5.5

Comparing calculated pressure head time histories with experiments at point T3 and flow rate = 8.2 L/s; a) MTPA. B) DGCM

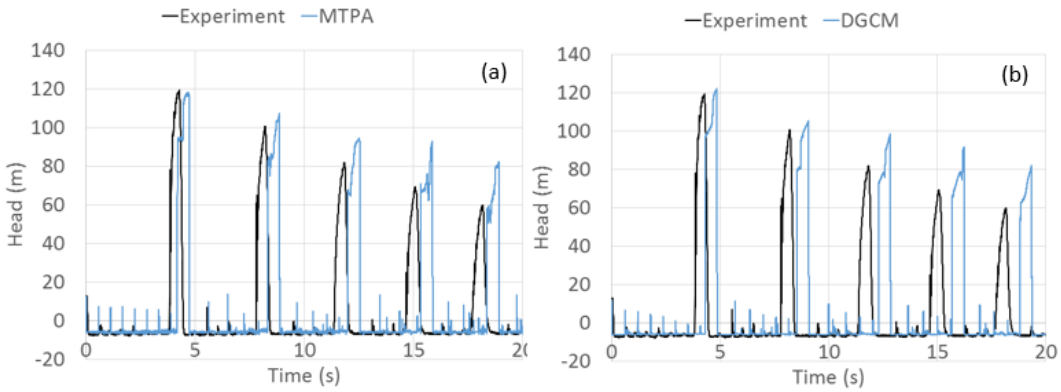

Figure 5.6

Comparing calculated pressure head time histories with experiments at point T4 and flow rate = 8.2 L/s; a) MTPA. B) DGCM

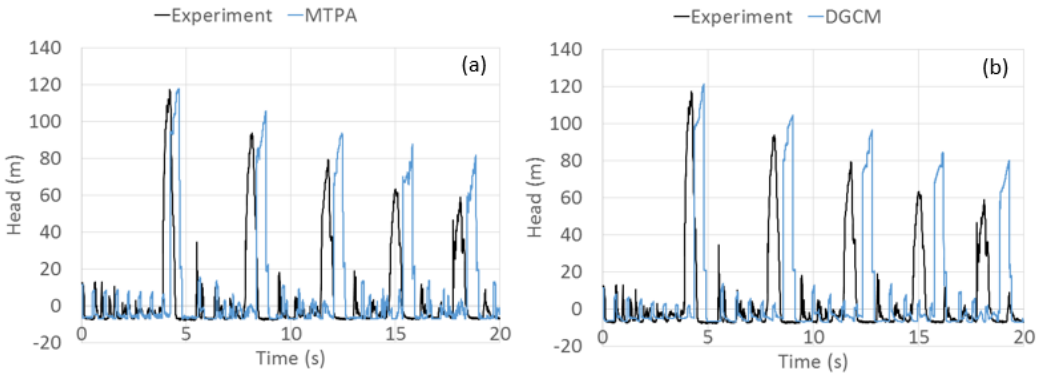

Figure 5.7

Snapshots of the cavity during expansion (a) and contraction (b) stages at flow rate =8.2 L/s

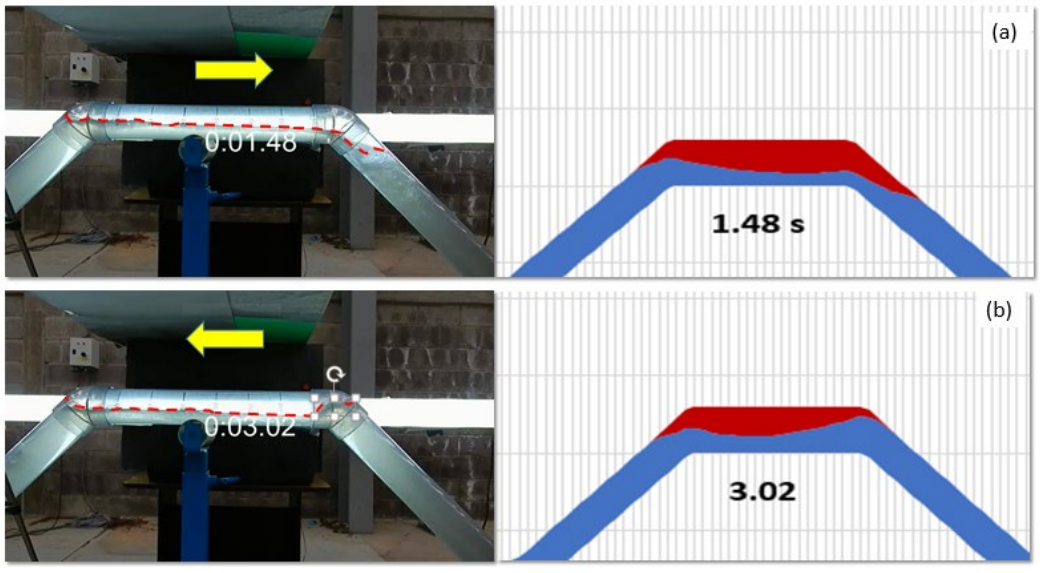

Figure 5.8

Comparing calculated pressure head time histories with experiments at point T1 and flow rate = 18 L/s; a) MTPA. B) DGCM

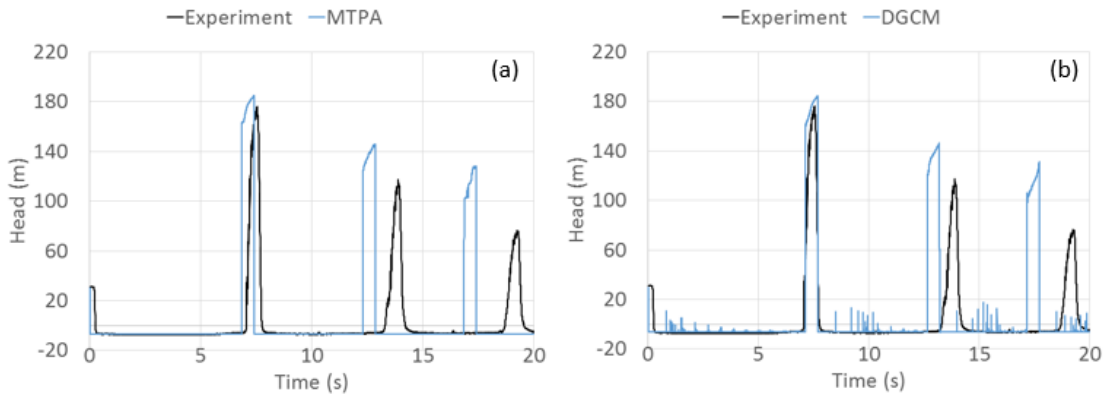

Figure 5.9

Comparing calculated pressure head time histories with experiments at point T3 and flow rate = 18 L/s; a) MTPA. B) DGCM

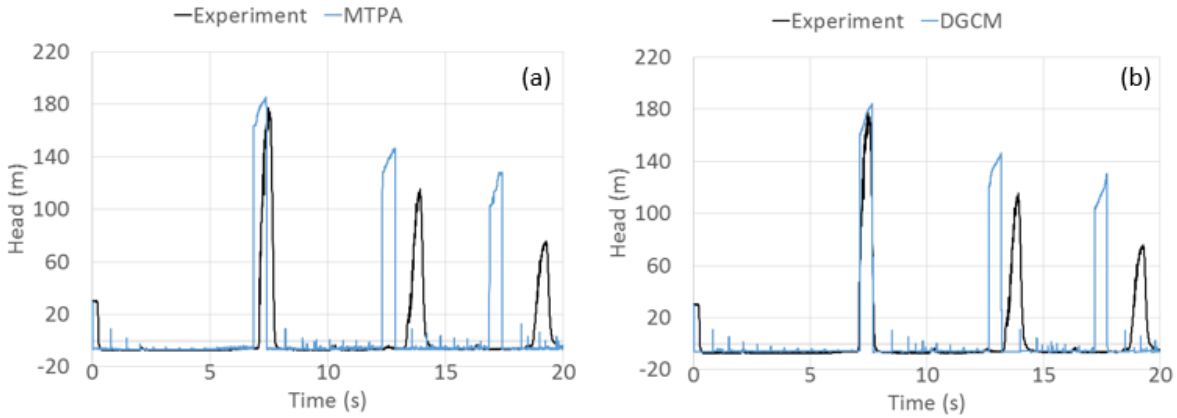

Figure 5.10

Comparing calculated pressure head time histories with experiments at point T4 and flow rate = 18 L/s; a) MTPA. B) DGCM

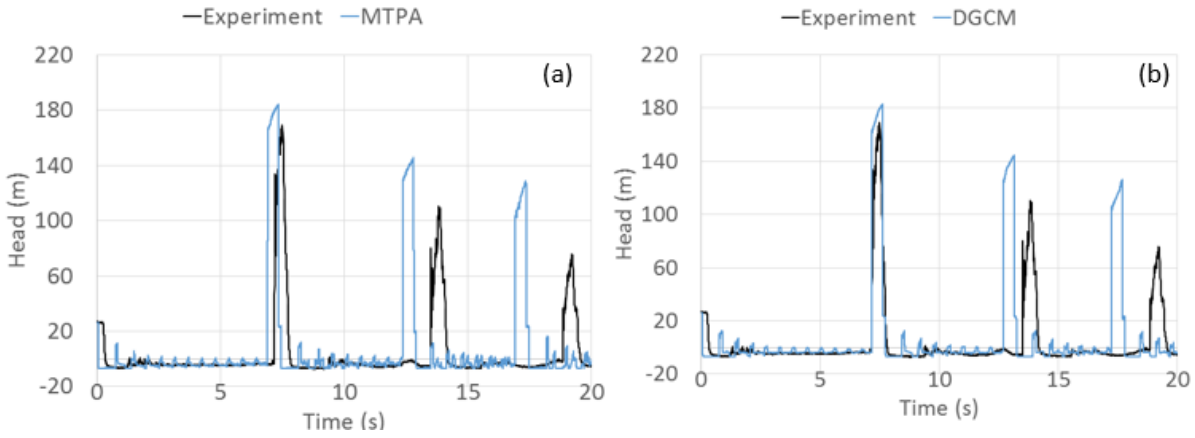

Figure 5.11

Snapshots of the cavity during expansion (a) and contraction (b) stages at flow rate = 18 L/s

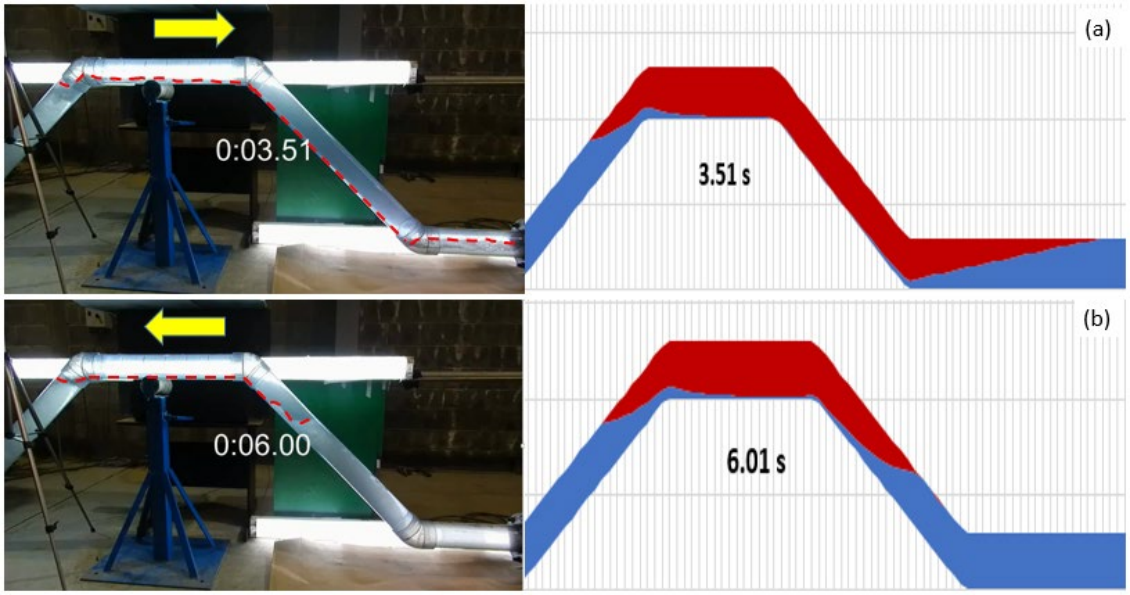

It is seen that the MTPA results are in good agreement with those obtained from the DGCM. Khani et al. (2022) also came up with a similar conclusion though they made the

comparison in the context of a test rig with a small pipe diameter. This raises the question as to if the MTPA can better capture the physics of column separation, under what circumstances, the MTPA performance surpasses the DGCM's? The following test cases are presented to address this question.

The simple pipe system shown in Figure 5.12 consists of two fix level reservoirs connected with a horizontal pipe with length, diameter, and acoustic wave speed of 1000 m, 1 m, and 1000 m/s respectively. Water column separation is induced by suddenly closing the upstream valve when the system is working in a steady state condition. Three different analyses are performed with the aid of both MTPA and DGCM for the pipe diameters of 1, 1.5, and 2 m. The initial steady-state flow velocity in all three cases is identical and equal to 2 m/s. The water depths at the upstream reservoir for the pipe diameters of 1, 1.5, and 2 m are 7.42, 6.5, and 6.07 m respectively. Both the MTPA and DGCM models are run with 100 computational cells but different Currant numbers of 0.9 and 1 respectively. NS = 4 and K_a = 1.4 are used in calculating the numerical fluxes in the MTPA.

Figure 5.12

The schematic of the pipe system utilized in the second test case

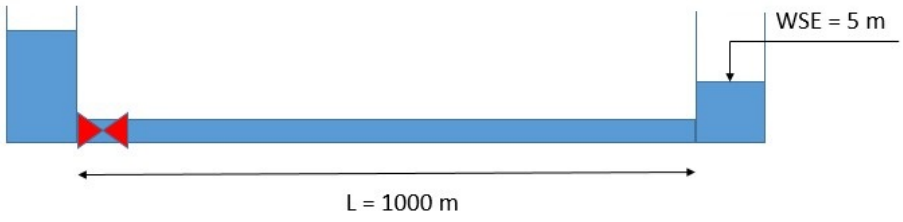

Figure 5.13

Comparing the results from MTPA and DGCM; a) pipe diam. = 1 m; b) pipe diam. = 1.5 m; c) pipe diam. = 2 m

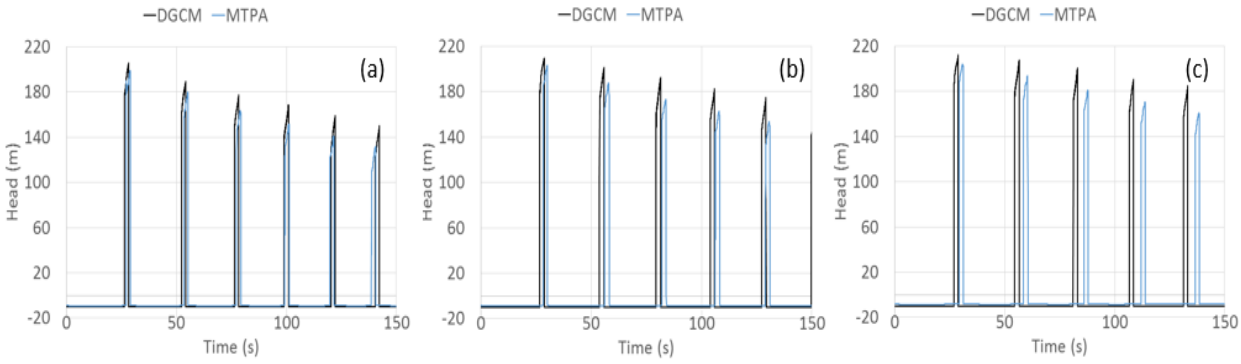

Figure 5.14 shows that at pipe diameter = 1 m, the frequency of the calculated pressure spikes is almost identical in both models but due to using a lower Currant number and additional numerical viscosity admitted to removing the potential spurious numerical oscillations, the MTPA dissipates the transient energy slightly faster. The results also reveal that with increasing the pipe diameter the discrepancy between the frequencies of the pressure spikes becomes greater. The underlying cause of the discrepancies can be explained by considering how negative pressures are applied to the pipe in each model.

To facilitate the discussion, it is necessary to first explain the factors affecting the frequency of the pressure spikes in the context of the pipe system under study. Following rapid closing of the valve, the moving water column cannot come to rest instantaneously because of its significant inertia. This makes a vapor cavity form just the downstream side of the valve to compensate for the mass flow leaving the system in this period. When the water column eventually stops, the whole pipe experiences full vacuum pressure, and the pressure gradient between the downstream reservoir and the pipe causes the water to start moving in the opposite

direction. The accelerating water column gradually reduces the size of the vapor cavity and when the cavity eventually vanishes, the water column is arrested at the closed valve whereby a significant waterhammer pressure spike is induced. This explains that the duration between two subsequent pressure spikes is two times as long as the time required for the water column velocity to change from the initial velocity to zero. By neglecting the effect of friction, the deceleration time can be calculated by the following equation, derived from the momentum equation.

$$\Delta T = \frac{L}{g} \times \frac{V_0}{\Delta H} \qquad 5\text{-}29$$

where, ΔT = deceleration time, V_0 = initial velocity of the water column, and ΔH = is the pressure head difference under which the water column decelerates.

Equation 5-29 reveals that the key factors affecting the deceleration time are the water column length and initial velocity as well as ΔH which is the difference between the pipe's upstream and downstream pressures heads. Nevertheless, since both models use the same water column length and initial velocity, the discrepancy is attributed to the pressure head difference. In the DCGM, the upstream pressure during the water column deceleration is independent of the pipe diameter and remains constant at the vapor pressure of the liquid. However, since the MTPA includes the effect of gravity on the pipe cross section pressure, the upstream pressure is no longer constant and depends on the pipe diameter. As shown in Figure 5.1, with increasing the pipe diameter, the negative pressure at the cavity location becomes less intense, causing the declaration time to increase. This well explains why the DCGM further compromises the frequency of the waterhammer pressure spikes as the pipe diameter becomes larger and larger.

The next test case is a hypothetical pipe system configured to reveal another shortcoming of the conventional column separation models such as DGCM. As shown in Figure 5.14, the system consists of two pipes connecting two reservoirs with two different water level elevations of 1002 and 900 m. The pipes have the same diameter and acoustic wave speed of 1 m and 1000 m/s but different lengths of 400 and 1000 m. It is assumed that a closed valve at the downstream end keeps the whole water column at rest with a constant hydraulic grade line of 1002 m.

Following the sudden opening of the valve, the system is expected to reach a steady-state flow condition when all resulting transient flow energy is damped out. Two distinct numerical analyses are performed with the DGCM and MTPA to calculate the steady-steady flow. Figure 5.15 compares the steady-state hydraulic grade lines calculated by the DGCM and MTPA. Although no experimental data are available to assess the results, it is easy to show that the DGCM is converged to a wrong solution, whereas the MTPA correctly captured the final steady-state condition in the system. To prove this, consider Figure 5.16, representing the flow rates calculated by the models across the pipe system. It is seen that both models identically captured the flow rate of around 4.6 m3/s in the first pipe while the DCGM calculated a far higher flow rate in the second pipe (around 8 m3/s). The DCGM fails to capture the extension of the cavity across the second pipe with the steep slope and lets the cavity remain stationary at the high point. Since the pressure at the high point remains constant at the vapor pressure of the liquid, the hydraulic grade line on either side of the high point takes different slopes which are associated with two different flows. This means that although the whole system reaches a steady-state condition, the cavity keeps growing. On the other hand, the MTPA allows a large cavity, as shown in Figure 5.17, to form in the steep pipe whereby the extra driving head of the system is dissipated in the open channel flow region formed beneath the cavity. The cavitating flow is also

switched to the pressurized flow regime at a point at which the elevation of the pipe provides an adequate driving head to push the flow toward the downstream reservoir.

Figure 5.14

Schematic of the pipe system considered in test case 3

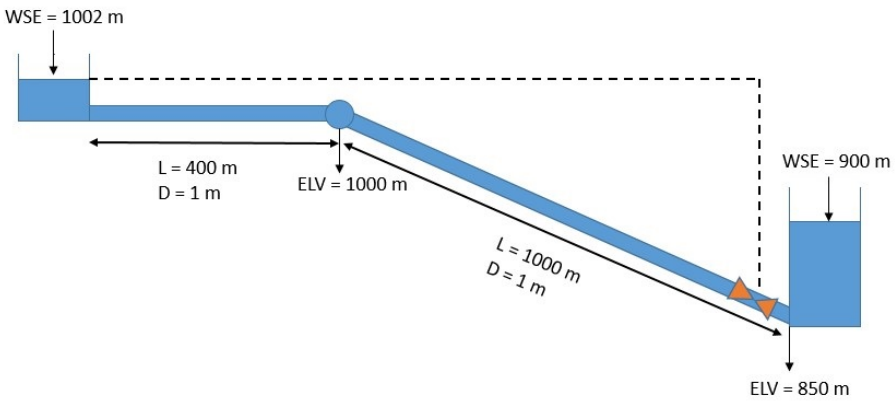

Figure 5.15

Steady-state HGLs calculated by the DGCM and MTPA

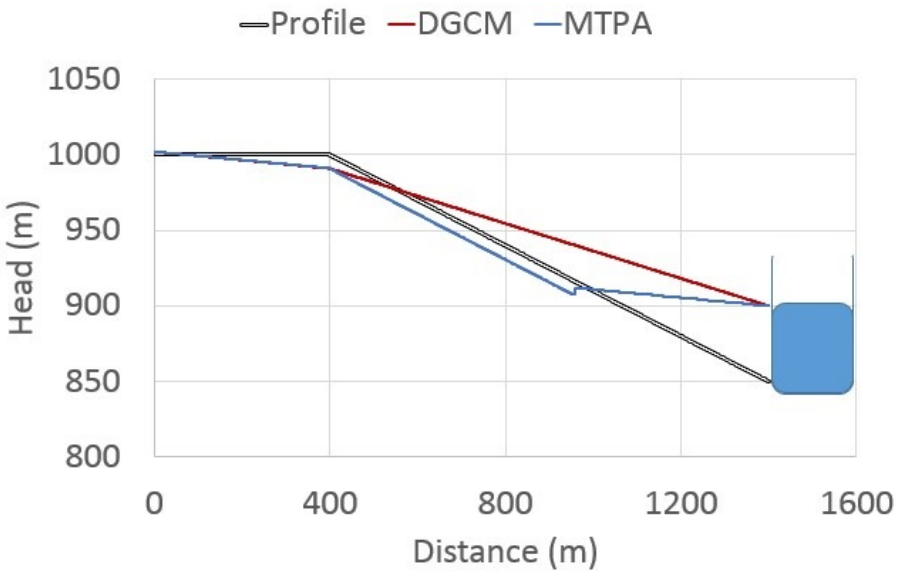

Figure 5.16

Calculated flow rates by the DGCM and MTPA across the pipeline

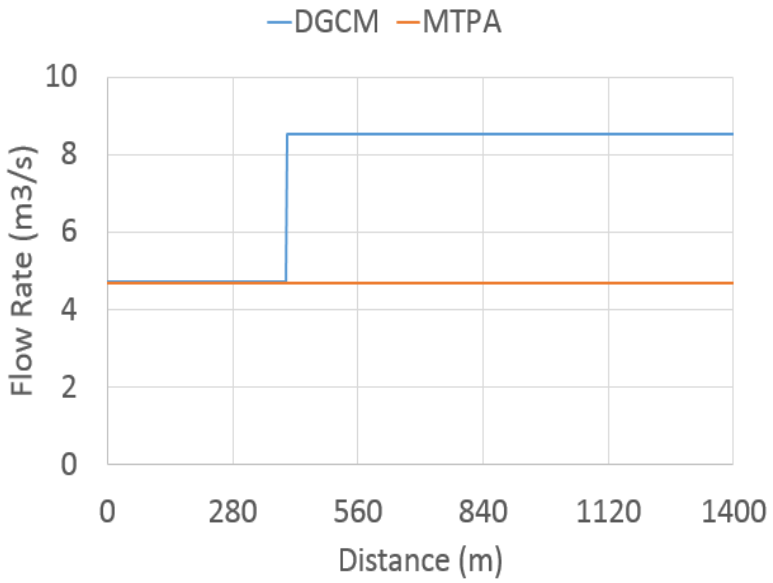

Figure 5.17

The distributed cavity calculated by the MTPA

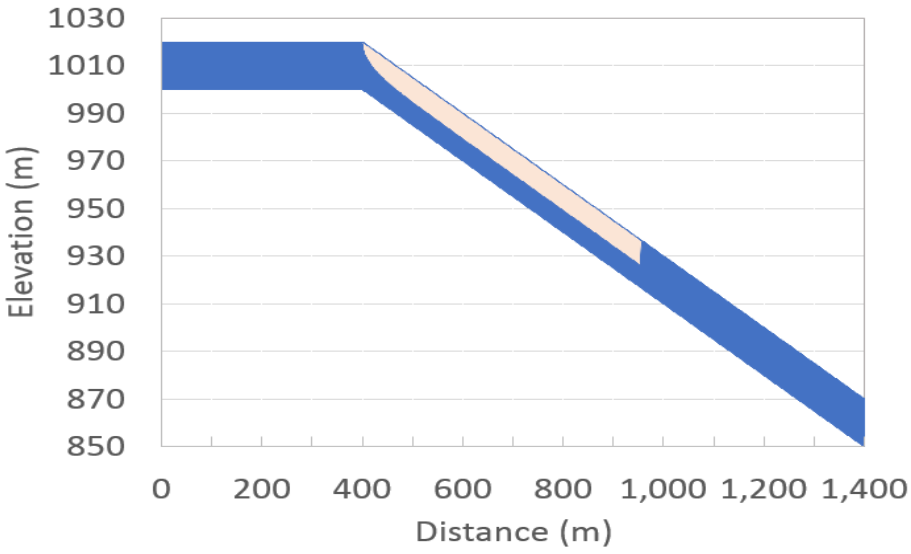

5.8 Summary and Conclusions

This paper investigates the performance of the MTPA recently proposed by the authors in capturing column separation in pipe systems with large vapor cavities. The MTPA calculates both cavitating and pressurized flow using a single set of equations that governs unsteady flow in open channel flow. The first-order Godunov type finite volume method is utilized to numerically solve the governing equations. A customized HLL Riemann solver is employed to calculate the fluxes at the computational cell boundaries and to dissipate potential post-shock oscillations that may occur when the cavity collapses and the open channel flow beneath vapor cavities converts to pressurized flow.

The model results are compared using the experimental data conducted with a large-scale test rig in which a large vapor cavity spreads over a long distance in the pipe. The results show that the model can successfully calculate the evolution of the cavity with reasonable accuracy. To further evaluate the performance of the model, the numerical results from the proposed model and the DGCM are compared in the context of some hypothetical problems. The results show that both the DGCM and MTPA provide identical results in pipe systems with smaller pipe diameters. However, with increasing the pipe diameter, the DGCM comes to compromise the frequency of the resulting pressure spikes induced following water column rejoining. The results show that regardless of the pipe diameter, the DGCM keeps the pressure constant at the vapor pressure on the pipe cross section whereby the water column acceleration and deceleration times remain unaffected. The MTPA resolves the problem by including the effect of the water depth in calculating the total pressure acting on the pipe section. This modification causes the acceleration and deceleration times to become longer as the pipe diameter increases. This paper also concludes that conventional models such as the DGCM fails to correctly capture the physics of

the cavitating flow when a large cavity is extended in a pipe with a steep slope. To prove this, the numerical results from the proposed model and the DGCM are compared in the context of a hypothetical problem for which an analytical solution exists. The hypothetical problem is designed to converge to a steady-state condition with cavitating flows established in a good portion of the pipe. The results show that for this case, the DGCM converges to a wrong solution while the MTPA accurately calculates the hydraulics of the problem.

Finally, the MTPA has shown to be a powerful tool for calculating column separation with an obvious superiority over the open-channel-based models proposed before, because they are all based on the shock-fitting algorithm which is very cumbersome to implement while the MTPA enjoys using a shock-capturing algorithm which is easy to develop even in complex liquid pipe systems. Furthermore, the MTPA is shown to provide more precise results than other conventional models such as the DGCM. A particular feature of the MTPA is that it can concurrently account for waterhammer, cavitating flow, and free surface flow regimes.

5.9 References

Adamkowski, A., & Lewandowski, M. (2012). Investigation of hydraulic transients in a pipeline with column separation. Journal of Hydraulic Engineering, 138(11), 935-944.

Autrique, R., & Rodal, E. (2013). Laboratory studies of water column separation. IOP Conference Series: Materials Science and Engineering. 52, p. 022022. IOP Publishing.

Baltzer, R. (1967b). A study of column separation accompanying transient flow of liquids in pipes. PhD Thesis. Michigan: University of Michigan.

Baltzer, R. A. (1967a). Column separation accompanying liquid transients in pipes. Journal of Basic Engineering, 837-846.

Bergant, A., & Simpson, A. R. (1999). Pipeline column separation flow regimes. Journal of Hydraulic Engineering, 125(8), 835–848.

Bergant, A., & Simpson, A. R. (1999a). Cavitation inception in pipeline column separation. 28th IAHR Congress. Graz, Austria: CD-ROM.

Bergant, A., Simpson, A. R., & Tijsseling, A. S. (2006). Water hammer with column separation: A historical review. Journal of Fluids and structures, 22, 135-171.

Chaudhry, M. (1987). Applied Hydraulic Transients. New York: Van Nostrana Reinhold Co.

Chaudhry, M. H. (1999). Open channel flow. Englewood Cliffs, N.J: Prentice-Hall.

Cunge, J. A., & Wegner, M. (1964). Numerical Integration of Bane de Saint-Venant's Flow Equations by Means of an Implicit Scheme of Finite Differences. Applications in the Case of Alternately Free and Pressurized Flow in a Tunnel. La Houille Blanche, 1, 33-39.

Kalkwijk, J., Kranenburg, C., Vreugdenhil, C., & De Vries, A. (1972). Cavitation caused by water hammer in horizontal. Delft: Delft Hydraulics Laboratory,Publication No. 97.

Karni, S., & Čanić, S. (1997). Computations of slowly moving shocks. Journal of Computational Physics, 136(1), 132-139.

Kerger, F., Archambeau, P., Erpicum, S., Dewals, B. J., & Pirotton, M. (2011). An exact Riemann solver and a Godunov scheme for simulating highly transient mixed flows. Journal of Computational and Applied Mathematics, 235, 2030-2040.

Khani, D., Lim, Y. H., & Malekpour, A. (2020). Hydraulic Transient Analysis of Sewer Pipe Systems Using a Non-Oscillatory Two-Component Pressure Approach. Water, 12(10), 2896.

Khani, D., Lim, Y. H., & Malekpour, A. (2021). A Mixed Flow Analysis of Sewer Pipes with Different Shapes Using a Non-Oscillatory Two-Component Pressure Approach (TPA). Modelling, 2(4), 467-481.

León, A. S., Ghidaoui, M. S., Schmidt, A. R., & García, M. H. (2009). Application of Godunov-type schemes to transient mixed flows. Journal of hydraulic research, 47(2), 147-156.

LeVeque, R. (2002). Finite volume methods for hyperbolic problems. Cambridge, UK: Cambridge Press.

Malekpour, A., & Karney, B. (2015). Spurious Numerical Oscillations in the Preissmann Slot Method: Origin and Suppression. Journal of Hydraulic Engineering, ASCE.

Malekpour, A., & Karney, B. W. (2014a). Profile-induced column separation and rejoining during rapid pipeline filling. Journal of Hydraulic Engineering, 140(11).

Malekpour, A., & Karney, B. W. (2014b). Column separation and rejoinder during rapid pipeline filling induced by a partial flow blockage. Journal of Hydraulic Research, 52(5), 693-704.

Marsden, N., & Fox, J. (1976). An alternative approach to the problem of column separation in an elevated section of pipeline. Second International Conference on Pressure Surges (pp. 1–13). London: BHRA.

Martin, C. (1983). Experimental investigation of column separation with rapid closure of downstream valve. Fourth International Conference on Pressure Surges (pp. 77–88). Cranfield, UK: BHRA Fluid Engineering.

Provoost, G. A., & Wylie, E. B. (1981). Discrete gas model to represent distributed free gas in liquids. 5th International Symposium on Water Column Separation, 1, pp. 28-30. Obernach, West Germany.

Siemons, J. (1967). The phenomenon of cavitation in a horizontal pipe-line due to a sudden pump-failure. Journal of Hydraulic research, 5(2), 135-152.

Simpson, A., & Bergant, A. (1994). Numerical comparison of pipe column-separation models. Journal of Hydraulic Engineering, 120(3), 361–377.

Simpson, A., & Wylie, E. (1991). Large water-hammer pressures for column separation in pipelines. Journal of Hydraulic Engineering, 117(10), 1310–1316.

Toro, E. F. (2001). Shock-capturing methods for free-surface shallow flows. Chichester, New York: John Wiley.

Vasconcelos, G. J., & Marwell, T. B. (2011). Innovative simulation of unsteady low-pressure flows in water mains. Journal of Hydraulic Engineering, 137(11), 1490-1499.

Vasconcelos, J. G., Wright, S. J., & Roe, P. L. (2006). Current Issues on modeling extreme inflows in stormwater systems in Intelligent Modeling of Urban Water Systems, Monogrph 14. Guelph, Ontario: CHI.

Vasconcelos, J. G., Wright, S. J., & Roe, P. L. (2009). Numerical oscillations in pipe-filling bore predictions by shock-capturing models. Journal of Hydraulic Engineering, 135(4), 296-305.

6 CHAPTER SIX

6.1 Calculating Column Separation in Liquid Pipelines Using a 1D-CFD Coupled Model

6.2 Abstract

This paper proposes a coupled 1D-CFD model for calculating column separation. ANSYS Fluent is utilized to calculate two-phase flow analysis, and the Method of Characteristics and the Discrete Gas Cavity Model (DGCM) are employed to conduct 1D transient analysis. The results show that the proposed model with both 2D and 3D CFD analysis captures the transient responses of the system with almost identical accuracy that are both in very good agreement with the experiment. The results of a pure CFD analysis are employed to evaluate the performance of the proposed model in capturing the shape of the vapor cavity. The comparison shows that although the results are in general agreement, the vapor cavity in the pure CFD model is established and grown on top of a film of liquid while in the proposed model the cavity in someplace fills the whole pipe cross-section. The results obtained from the Modified Two-Component Pressure Approach (MTPA) also confirm the results from the pure CFD analysis. The discrepancy may be attributed to the uniform velocity distribution considered at the interface between 1D and CFD zones. Nevertheless, this is just a hypothesis that warrants a detailed investigation.

6.3 Introduction

Negative pressures may occur in liquid pipe systems under a variety of circumstances, examples of which include pumping power failure, hydropower load rejection, rapid closing of an inline valve, etc. (Chaudhry, 1987; Wylie et al., 1993). When the pressure at a particular point of the pipe drops to the vapor pressure of the liquid, the liquid column locally ruptures, and the resulting vapor cavity causes the liquid to be separated. During the column separation, the pressure at the cavitating zone remains constant at the vapor pressure, allowing the liquid water columns on either side of the cavity to move independently and gain different velocities, whereby the cavity size changes (Bergant et al., 2006). Eventually, a positive pressure condition in the system causes the cavity to collapse and let the separated water columns rejoin. Rejoining the liquid column can induce significant water hammer pressure with an intensity that depends on the difference in the liquid column's velocities as well as the acoustic wave speed of the pipe. The induced water hammer pressure can be strong enough to rupture the pipe and associated joints.

Due to its destructive nature, column separation has been the subject of a handful of research, both numerically (Wylie, 1984; Brgant and Simpson, 1994; Simpson and Bergant, 1994; Provoost and Wylie, 1981; Adamkowski and Lewandowski, 2012; Bergant and Simpson, 1999; Khani et al., 2022a; Khani et a., 2022b; Vasconcelos and Marwell, 2011) and experimentally (Simpson and Wylie, 1991; Martin, 1983; Bergant and Simpson, 1999; Adamkowski and Lewandowski, 2012; and Autrique and Rodal, 2013), since it was first identified by Joukowsky. Several numerical models have been proposed for calculating column separation, among which Discrete Vapor Cavity Model (DVCM) and Discrete Gas Cavity Model (DGCM) are the most popular approaches used in research and industry (Bergant et al., 2006). In

DVCM, a vapor cavity is inserted in the computation node when the pressure drops to the vapor pressure. By keeping the pressure of the cavity constant at the vapor pressure, the size of the cavity at a given time is calculated by a simple mass balance approach. If the size of the cavity becomes nil or negative, the cavity is removed, and the liquid column rejoining is replicated. In DGCM, a permeant-infinitesimal gas cavity assumed in each computational allows for automatically capturing column separation and rejoining everywhere across the pipe length. Although the validity of these models has been widely approved by experimental studies, they cannot provide accurate results in case a large cavity is extended over a long distance across a pipe with a steep slope. Khani et al. (2022b) presented a hypothetical test case in which the system is working under a steady-state-cavitating flow regime and showed that in such cases, extensive energy dissipation occurs in the cavitating zone that cannot be accounted for by either the DVCM or the DGCM. Khani also demonstrated that in this case, the DGCM captures a steady-state flow which is far off the true solution.

To improve the performance of DVCM and DGCM, different types of open-channel-based models have been proposed (Baltzer, 1967a, and 1967b; Siemons,1967; Kalkwijk et al., 1972; Marsden and Fox, 1967). At each computational time level, the models utilize a shock-fitting approach to trace the interface between the cavitating flow and waterhammer zones. Once the location of the interface is calculated, the flow parameters on either side of the interface are calculated using different sets of governing equations, the open channel flow equations for the cavitating zone, and the waterhammer equations for the waterhammer region. However, the obtained results did not agree well with the experiments due to the challenge associated with calculating the location of the interface. Khani et al. (2022a) proposed the Modified Two-Component Pressure Approach (MTPA) that utilizes the open channel flow equations in both

cavitating and water hammer flow regions. The model employs a shock-capturing approach which can automatically calculate both the interface between the water hammer and cavitating flow regions as well as the spread of the cavity across the pipe. The model results were shown to be in excellent agreement with both experiments and analytical solutions, implying that the MTPA can provide reasonable results even in the circumstances the DVCM and DGCM provide poor results. However, when cavitating flow occurs in a highly three-dimensional flow field such as a large Turbine's draft tube, the MTPA no longer provides reasonable results; in such cases, using Computational Fluid Dynamics (CFD) analysis appears to be inevitable.

CFD analysis has not been received significant attention in the realm of column separation probably because 1D models can alternatively cover a wide range of applications. Nevertheless, a few researchers tried to investigate the performance of CFD in capturing the key aspects of cavitating flow and column separation in pipe systems. Tang et al. (2020) and Wang et al. (2016) utilized 2D CFD analysis for calculating column separation that occurs following the rapid closing of a valve in a simple reservoir-pipe-valve system and found that not only can CFD accurately capture the time history of the resulting transient pressures, but it also can successfully account for the spread of the vapor cavity across the pipe. Warda et al. (2020) employed a 3D CFD analysis for calculating column separation in a laboratory-scale pipe system and concluded that CFD can capture key features of cavitating flow and column separation quite accurately. However, CFD analysis is quite expensive, at least at present, in terms of computational resources. Wang et al. (2016) demonstrated that it takes a few days for a personal computer to complete 0.6 s of transient analysis in a pipe with an internal diameter and length of 0.02 and 30 m, respectively. This implies that CFD is inefficient in practice due to the scale of

pipe systems and the fact that an engineering design is iterative and may need numerous simulations.

Coupling CFD with 1D analysis appears to be an efficient solution to significantly reduce the computational time. This idea is grown based on the fact that mass, momentum, and energy are dominantly transferred in the longitude dimension of the pipe and the information exchanged in the radial dimension of the pipe is not of insignificant importance. In CFD-1D analysis, the limited part of the system with the significant 3D feature is calculated by the CFD analysis, and the rest of the system is handled by the 1D analysis; the two computational approaches exchange the information at each computational time level through the interface connecting 1D and CFD domains. This method has been successfully employed for calculating transient flow in liquid pipe systems (Mandair, 2020). For example, Zhang and Cheng (2012) applied 1D-3D analysis to different components of hydropower systems. Zhang et al. (2014) successfully utilized 1D-3D analysis in transient analysis of a pumped-storage system. Wu et al. (2015) applied 1D-3D coupling for steady-state and transient flow analysis in a pumped pipeline. Maddahian et al. (2021) employed 1D-3D analysis in rapid pressurization of a pipe system with an entrapped air pocket and showed that the modeling results are in excellent agreement with experiments. To the best of the authors' knowledge, the 1D-3D coupling approach has not been utilized for calculating column separation so far.

Thus, this paper aims to shed light on the performance of 1D-CFD coupling in simulating liquid column separation analysis in pipe systems including water pipe systems. The organization of this paper is as follows: the theoretical background is first presented, and the numerical results are then discussed. Finally, the research is summarized, and conclusions are made.

6.4 Theoretical Background

6.4.1 DGCM

Transient flow in liquid pipe system is governed by the following 1D equation aka waterhammer equations (Wylie et al., 1993):

$$\frac{\partial V}{\partial t} + g\frac{\partial H}{\partial x} + \frac{f}{2D}|V|V = 0 \quad (6\text{-}1)$$

$$\frac{\partial H}{\partial t} + \frac{a^2}{g}\frac{\partial V}{\partial x} = 0 \quad (6\text{-}2)$$

where V = velocity, H = piezometric head, D = pipe diameter, a = elastic wave velocity, g = gravitational acceleration, f = friction factor in Darcy-Weisbach equation, and x,t = distance and time independent variables respectively.

These equations hold as long as the pressure exceeds the vapor pressure of the liquid. Otherwise, cavitating flow and column separation occur, and the equations fail to replicate the physics of the flow. There are several approaches to include the column separation feature in the water hammer equations, among which DGCM is the more popular and accurate one. In DGCM, a small gas pocket assumed in each computational cell can account for column separation in the system.

To numerically implement DGCM, the well-known Method of Characteristics (MOC) is utilized. The first step in the MOC is to discretize the computational domain into numerous computational cells, as shown in Figure 6-1, with identical spatial and temporal increments, Δx and Δt, respectively. The unknown flow parameters at the computational points at time t_{n+1} can be then explicitly calculated based on the information from the previous timeline.

Figure 6.1

Schematic of computational cells in the method of characteristics and DGCM

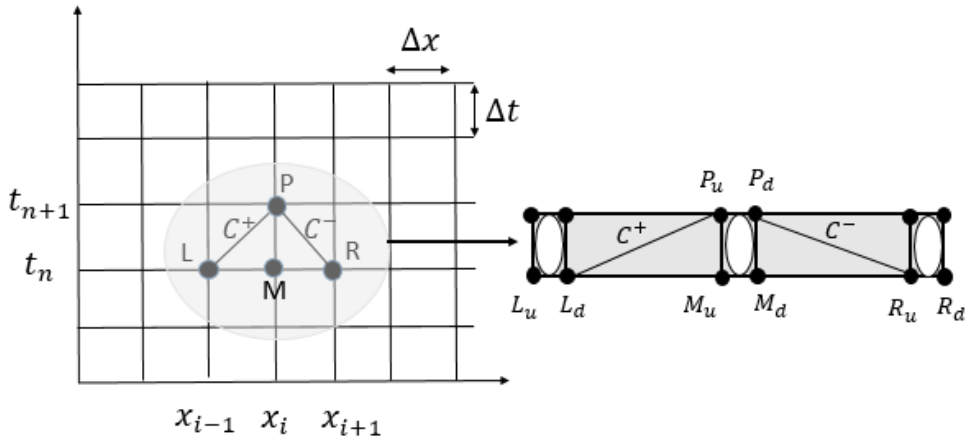

The four unknowns at a given point (P) include the flow rates on either side of the gas pocket, the piezometric head, and the volume of the gas pocket and can be calculated by the following discretized equations called positive and negative characteristic equations, continuity equation and the gas equation of state.

$$C^+: H_{Pu} = H_{Pd} = C_1 - C_2 Q_{Pu} \quad (6\text{-}3)$$

$$C^-: H_{Pd} = C_3 + C_4 Q_{Pd} \quad (6\text{-}4)$$

$$(\forall_P)_{t+\Delta t} = (\forall_P)_t + [\psi(Q_{Pd} - Q_{Pu})_{t+\Delta t} + (1-\psi)(Q_{Md} - Q_{Mu})_t] \times \Delta t \quad (6\text{-}5)$$

$$(\forall_P)_{t+\Delta t} = \frac{P_0^* \alpha_0 \forall_R}{\rho g (H_{Pd} - Z_{Pd} - H_V)} \quad (6\text{-}6)$$

with

$$C_1 = H_{Ld} + \frac{a}{gA} Q_{Ld} \quad ; \quad C_2 = \frac{a}{gA} + \frac{f\Delta x}{2gDA^2} |Q_{Ld}|$$

$$C_3 = H_{Ru} - \frac{a}{g} Q_{Ru} \quad ; \quad C_4 = \frac{a}{gA} + \frac{f\Delta x}{2gDA^2} |Q_{Ru}|$$

where Q_{Pu}, Q_{Pd} = flow rates at the upstream and downstream side of the gas pocket at point P, respectively, $H_{Pu} = H_{Pd}$ = piezometric head at the upstream and downstream side of the gas pocket at point P, respectively, $Z_{Pu} = Z_{Pd}$ = pipe elevation upstream and downstream side of the gas pocket at point P, respectively, Q_{Ld} = flow rate at the downstream side of the gas pocket at point L, H_{Ld} = piezometric head at the downstream side of the gas pocket at point L, Q_{Ru} = flow rate at the upstream side of the gas pocket at point R, H_{Ru} = piezometric head at the upstream side of the gas pocket at point R, A = pipe cross sectional area, D = pipe diameter, ρ = water density, $\forall_P$= gas pocket volume at point P, H_V = gas vapour pressure head, α_0 = initial gas void fraction, $\forall_R$ = computational cell volume, P_0^* = reference pressure, Δt = computational time step, S_0 = pipe slope, S_f = energy slope, g = gravitational acceleration, $t, t + \Delta t$ = indexes referring to the previous and current time lines, respectively.

By combining Equations 6-3 to 6-6 and doing some algebra the following equation is reached.

$$(H_{Pd} - Z_{Pd} - H_V)^2 + 2B_1(H_{Pd} - Z_{Pd} - H_V) - B_4 = 0 \qquad 6\text{-}7$$

The analytical solution of the above equation is as follow.

$$H_{Pd} - Z_{P1d} - H_V = -B_1\left(1 + \sqrt{1 + B_B}\right) \ if \ B_1 \leq 0 \qquad 6\text{-}8$$

$$H_{Pd} - Z_{P1d} - H_V = -B_1\left(1 - \sqrt{1 + B_B}\right) \ if \ B_1 > 0 \qquad 6\text{-}9$$

where

$$B_1 = B_2C_4C_2B_V + 0.5(Z_{Pd} + H_V) - B_2(C_2C_3 + C_4C_1); \quad B_B = \frac{B_4}{B_1^2}$$

$$B_2 = \frac{0.5}{C_2 + C_4}; \ B_V = \frac{(\forall_P)_t}{\psi \Delta t} + \frac{1-\psi}{\psi}(Q_{Pd} - Q_{Pu})_t; \ B_4 = \frac{P_0^* \alpha_0 \forall_R B_2 C_4 C_2}{0.5\rho g \psi \Delta t}$$

In cases with high gas volume and very low pressure or very low volume but high

pressure, indicated by $|B_B| \ll 1$, Equations 6-8 or 6-9 may provide inaccurate results due to miscalculation of the radical. The appropriate results in such cases can be achieved through the linearization of the original equations (Wylie et al. 1993):

$$H_{Pd} - Z_{Pd} - H_V = -2B_1 - \frac{B_4}{2B_1} \qquad if\ B_1 \leq 0 \qquad 6\text{-}10$$

$$H_{Pd} - Z_{Pd} - H_V = \frac{B_4}{2B_1} \qquad if\ B_1 > 0 \qquad 6\text{-}11$$

Having H_{Pd} calculated, Q_{Pu}, Q_{Pd}, and $\forall_P$ can be calculated by Equations 6-3, 6-4, and 6-5, respectively.

6.4.2 MTPA

The Two-Component Pressure Approach (TPA) was proposed by Vasconcelos et al. (2006) to address the limitation of the Preissmann Slot Method (PSM) in capturing negative pressures (Cunge and Wegner, 1964; Kerger et al., 2011). In this method, the conservative form of the equations that govern unsteady flow in open channels are rearranged as follows:

$$\frac{\partial A}{\partial t} + \frac{\partial Q}{\partial x} = 0 \qquad Continuty\ Equation \qquad 6\text{-}12$$

$$\frac{\partial Q}{\partial t} + \frac{\partial\left(\frac{Q^2}{A} + Ag[h_c + h_s]\right)}{\partial x} = gA(S_0 - S_f) \qquad Momentum\ Equation \qquad 6\text{-}13$$

where, A= flow cross sectional area, Q = flow rate, h_c = the distance between the free surface and the centroid of the flow cross-sectional, h_s = pressure head, g = gravitational acceleration, S_0 =

pipe slope and S_f = frictional slope which can be calculated by the following equation.

$$S_f = \frac{Q^2 {n_m}^2}{A^2 R_h^{\frac{4}{3}}} \quad \text{6-14}$$

where n_m = Manning coefficient and R_h = hydraulic radius of the flow.

Splitting the pressure term in the momentum equation allows TPA to account for both pressurized and open channel flows, with h_s representing the pressure of the conduit in pressurized flow and h_c measuring the flow depth in the open channel flow regime. In TPA the pressure head and pipe acoustic wave speed are related by the following equation (Vasconcelos et al., 2006).

$$h_s = \left[\frac{A - A_f}{A_f}\right] \frac{a^2}{g} \quad \text{6-15}$$

where a = acoustic wave speed, and A_f = pipe cross-sectional area.

Many researchers have successfully utilized the TPA for capturing mixed-flow and negative pressures in close conduit systems (Vasconcelos et al., 2006; Vasconcelos and Wright, 2007; Sanders and Bradford, 2010; Khani et al., 2020 and 2021). However, TPA still cannot replicate the physics of the flow when column separation occurs in the system. In such cases, the TPA generates negative pressures that are far below the vapour pressure of the liquid, which is not physically sound.

To fill this gap, Khani et al. (2022) proposed a modified version of the TPA (MTPA) which can account for cavitating flow and column separation. In the MTPA, Equations 6-1 and 6-2 can calculate the transient pressure heads and flow rates across the system as long as the pressures are above the vapor pressure. Otherwise, Equation 6-2 no longer holds, and the following equation should be utilized instead.

$$\frac{\partial Q}{\partial t} + \frac{\partial\left(\frac{Q^2}{A} + g\left[Ah_c + A_f h_v\right]\right)}{\partial x} = gA(S_0 - S_f) \quad 6\text{-}16$$

where h_v = vapor pressure head of the liquid

To solve the governing equations, the Godunov scheme is utilized in this research. The Godunov scheme is a finite volume numerical scheme widely used in solving hyperbolic partial differential equations (Toro, 2001; LeVeque, 2002). The spatial domain in this approach is broken down into equal size computational cells with a spatial distance of Δx, and the temporal domain is discretized with a constant time step, Δt. The first-order accuracy of the scheme suits the current application as the flow transition from open channel to pressurized flow may induce significant spurious numerical oscillations that can be better suppressed by a first order accuracy scheme. Applying piecewise constant data reconstruction at the computational cells results in first-order accuracy.

By discretizing the governing equations, unknowns at the current time level can be explicitly calculated based on the data retrieved from the previous timeline using the following equation:

$$A_i^{n+1} = A_i^n - \frac{\Delta t}{\Delta x}\left(F^n_{i+\frac{1}{2}} - F^n_{i-\frac{1}{2}}\right) \quad 6\text{-}17$$

$$Q_i^{n+1} = Q_i^n - \frac{\Delta t}{\Delta x}\left(G^n_{i+\frac{1}{2}} - G^n_{i-\frac{1}{2}}\right) + \Delta t g A \left(S_0 - {S_f}_i^n\right) \quad 6\text{-}18$$

where i is computational cell number, $i + \frac{1}{2}$ and $i - \frac{1}{2}$ are referring to the downstream and upstream boundaries of the i^{th} cell respectively, n and $n + 1$ are referring to the previous and current timelines respectively, and F and G are mass and momentum fluxes respectively.

In the Godunov scheme, the mass and momentum fluxes at cell boundaries are calculated by solving the Riemann solution (Toro, LeVeque). The exact Riemann solution can be obtained through an iterative procedure but as shown by Malekpour and Karney (2015) it can produce significant numerical oscillation during flow transition. Khani et al. (2021) adopted the HLL solver that can automatically increase the numerical viscosity of the scheme during the flow regime transient and showed that the scheme provides a non-oscillatory solution at a wide range of acoustic pipe speeds.

The fluxes in the HLL solver are generally calculated through a procedure summarized in Equation 6-19.

$$
\begin{aligned}
&= \Gamma_L \quad if\ S_L > 0 \\
&= \frac{S_R\Gamma_L - S_L\Gamma_R + S_L S_R(U_R - U_L)}{S_R - S_L} \quad if\ S_L \le 0\ and\ S_R \ge 0 \\
&= \Gamma_R \quad if\ S_R < 0
\end{aligned}
\qquad 6\text{-}19
$$

where S_L and S_R are the left and right shock wave speeds respectively, $U_L = \begin{bmatrix} A_L \\ Q_L \end{bmatrix}$ *and* $U_R = \begin{bmatrix} A_R \\ Q_R \end{bmatrix}$ are dependent variables at the computational cells $i - 1$ and $i + 1$ respectively, and $\Gamma_L = \begin{bmatrix} F_L \\ G_L \end{bmatrix}$ and $\Gamma_R = \begin{bmatrix} F_R \\ G_R \end{bmatrix}$ are the fluxes at the computational cells $i - 1$ and $i + 1$ respectively.

Khani et al. (2020, 2021) showed that the numerical viscosity admitted to the numerical scheme is controlled by the magnitude of the right and left wave velocities. They proposed a simple strategy for calculating the left and right wave speeds in both water hammer and open channel flow regions. The left and right wave speeds are calculated using the following equations.

$$S_L = V_L - \Omega_L \; ; \; S_R = V_R + \Omega_R \tag{6-20}$$

$$\Omega_{K(L,R)} = \sqrt{\frac{g[Y_G A_G - (h_C + |h_s|)_K A_K] A_G}{A_K (A_G - A_K)}} \tag{6-21}$$

where variables with sub-index G are the function of Y_G that needs to be estimated.

As shown by Malekpour and Karney (2015) showed that Equation 6-21 significantly increases wave speeds only when the water depth is close to the pipe crown. By using this equation, the artificial viscosity of the scheme is increased whenever require, i.e., when the flow transient is proximate. Khani et al. (2020) found that the optimal amount of artificial viscosity is admitted to the scheme if Y_G is calculated by the following equation.

$$Y_G = K_a \times MAX\,[d_{i-NS}, d_{i-NS+1}, \dots, d_i, d_{i+1}, \dots d_{NS}] \tag{6-22}$$

where $d = h_c + |h_s|$.

Equation 6-22 makes sure that artificial viscosity is distributed within *NS* computational cells on either side of the cell for which the wave velocity is calculated. Numerical exploration reveals that NS should be selected such that the numerical viscosity spread over a length 3 or 4 times higher than the pipe height. In any way, the *NS* should not be less than 3. Numerical exploration also reveals that in the computational cells carrying free surface flow, K_a can take a value of around 1.4 if a pressurization front exists within NS computational cells on either side of the target computational cell. Otherwise, NS can be considered as 1.001.

6.4.3 CFD Analysis

ANSYS Fluent is utilized to perform CFD analysis in the portion of the pipeline experiencing cavitating flow and column separation. Fluent can simulate two-phase flow by numerous approaches among which the Volume of Fluid (VOF) is widely used for capturing

cavitating flow (ANSYS Inc., 2013). In the VOF method, a single set of Unsteady Random-averaged Navier-Stokes (URANS) equations presented below are solved for the mixture of vapor and liquid with a weighted average density and viscosity of ρ_m and μ_m, respectively.

$$\frac{\partial \rho_m}{\partial t} + \frac{\partial}{\partial x_i}(\rho_m u_i) = 0 \quad \text{6-23}$$

$$\frac{\partial}{\partial t}(\rho_m u_i) + \frac{\partial}{\partial x_j}(\rho_m u_i u_j) = -\frac{\partial P}{\partial x_i} + \frac{\partial}{\partial x_j}\left[\mu_m\left(\frac{\partial u_i}{\partial x_j} + \frac{\partial u_j}{\partial x_i} - \frac{2}{3}\delta_{ij}\frac{\partial u_k}{\partial x_k}\right)\right] + \frac{\partial}{\partial x_j}\left(-\rho_m\overline{u_i' u_j'}\right) + \rho_m g_i \quad \text{6-24}$$

with

$$\rho_m = \alpha_v \rho_v + (1 - \alpha_v)\rho_l$$

$$\mu_m = \alpha_v \mu_v + (1 - \alpha_v)\mu_l$$

where u_i = flow velocity vector, P = pressure, ρ_v = vapor density, ρ_l = liquid density, μ_v = vapor viscosity, μ_l = liquid viscosity, δ_{ij} = Kronecker delta, α_v = vapor void fraction, g_i = gravitational acceleration, x_j = spatial independent vector, and t = temporal independent variable.

The above equations are not in closed form as the time averaging included an extra term, $\rho_m\overline{u_i' u_j'}$ well known as Reynolds Stresses term. A few common methods used for approximating the Reynolds stresses are based on the Boussinesq hypothesis that relates the Reynolds stresses to the mean velocity gradients (ANSYS Inc., 2013). In this research, the $k - \varepsilon$ method is employed to calculate the Reynolds stresses.

Mass transfer between liquid and vapor phases during cavitating flow is calculated by including the mass transfer terms on the right-hand side of the following partial differential

equation utilized for tracking the interface of vapor and liquid.

$$\frac{\partial}{\partial t}(\alpha\rho_v) + \frac{\partial}{\partial x_i}\left(\alpha\rho_v u_{v_i}\right) = R_e - R_c \qquad 6\text{-}25$$

where R_e and R_c are mass transfer source terms connected to the growth and collapse of the vapor bubbles respectively.

In ANSYS Fluent, the Singhal et al., Zwart-Gerber-Belamri, and Schnerr and Sauer models can be used for calculating the source terms in Equation 6-25, the latter of which is employed in this study. The Schnerr and Sauer model calculates the sources terms using the following equations.

when $P_v \geq P$

$$R_e = \frac{\rho_v\rho_l}{\rho_m}\alpha(1-\alpha)\frac{3}{\Re_B}\sqrt{\frac{2}{3}\frac{(P_v-P)}{\rho_l}} \qquad 6\text{-}26$$

when $P_v \leq P$

$$R_c = \frac{\rho_v\rho_l}{\rho_m}\alpha(1-\alpha)\frac{3}{\Re_B}\sqrt{\frac{2}{3}\frac{(P-P_v)}{\rho_l}} \qquad 6\text{-}27$$

where $\Re_B$ = radius of the bubbles and P_v = vapor pressure of the liquid.

The vapor void fraction and radius of the bubbles can be calculated by the following equations.

$$\alpha = \frac{n_b\frac{4}{3}\pi\Re_B^3}{1+n_b\frac{4}{3}\pi\Re_B^3} \qquad 6\text{-}28$$

$$\Re_B = \left(\frac{\alpha}{1-\alpha}\frac{3}{4\pi}\frac{1}{n_b}\right)^{\frac{1}{3}} \qquad 6\text{-}29$$

The above equations show that both vapor void fraction and the radius of the bubbles depend on the number of spherical bubbles per volume of liquid (n_b). Assuming that no bubbles

are created or destroyed, the initial conditions for the nucleation site volume fraction and the equilibrium bubble radius would therefore be sufficient to specify the bubble number density (n_b). It is worth noting that to accurately calculate column separation and resulting waterhammer pressures, the liquid phase needs to be considered compressible. The compressibility of the liquid is included through a User-Defined Function (UDF). The UDF function relates the density of the liquid to its pressure with the aid of the following equation.

$$\rho_l = \rho_{ref}\left(1 + \frac{P - P_{ref}}{K_{eq}}\right) \quad 6\text{-}30$$

where ρ_{ref} = density of the liquid at a reference pressure (P_{ref}) and K_{eq} = equivalent bulk modulus elastic of the liquid that can be calculated based on the real acoustic speed of the pipe by the following equation.

$$K_{eq} = a^2\rho_{ref} \quad 6\text{-}31$$

6.4.4 1D-CFD Coupling

In 1D-CFD analysis, the surface(s) separating the CFD and 1D computational zones are the places where the data are exchanged between the CFD and 1D models. In this study, 1D-CFD modeling is carried out in the context of a simple pipe system in which a vapor cavity is concentrated at a local point. Therefore, a small part of the pipe in which the cavity is expanded and contracted is simulated by CFD and the rest is treated with the aid of MOC and DGCM; the data is exchanged between 1D and 3D computational zones at a single pipe section during the simulation.

There are a handful of approaches presented for exchanging data between 1D and CFD computational regions (Mandair, 2020), but they can be generalized into two categories, partially and fully coupled methods. In the partially coupled method, the data is exchanged in every time

step while in the other one it is done in every iteration made by CFD toward numerical convergence. The former method can provide numerically stable results as long as the shared flow parameters do not change significantly in each time step or when a very small time step is used. Since in the current problem strong waterhammer pressures would be exchanged at the interface, the latter method is utilized.

Figure 6.2

Data exchange between 1D and 3D computational zones

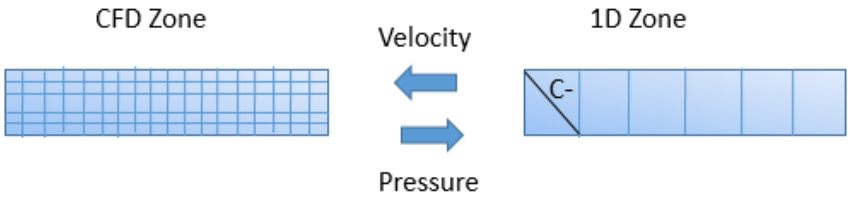

To facilitate explaining the fully coupled method, consider Figure 6.2. The simulation starts from a steady-state flow condition in which both CFD and 1D flow regions agree on both flow velocity and pressure at the interface. In each CFD iteration toward convergence, the total pressure calculated at the interface in the CFD zone is employed to calculate the resulting new flow velocity the 1D using the positive characteristic equation. This method can produce some over- and undershooting around the solution and makes the convergence to be hardly achieved. A relaxation method proposed by Wu et al. (2015) is used to resolve the convergence issue. In this method, the weighted average of the velocities obtained in two subsequent iterations is used to update the velocity at the CFD boundary. As shown in Figure 6.3 the convergence is assumed to be reached when the difference between the velocities (e) becomes less than a predefined value. Note that by reducing the relaxation factor (R_f), a better convergence condition is achieved but at the expense of more iterations.

Figure 6.3

Iteration loop in the 1D-CFD coupling

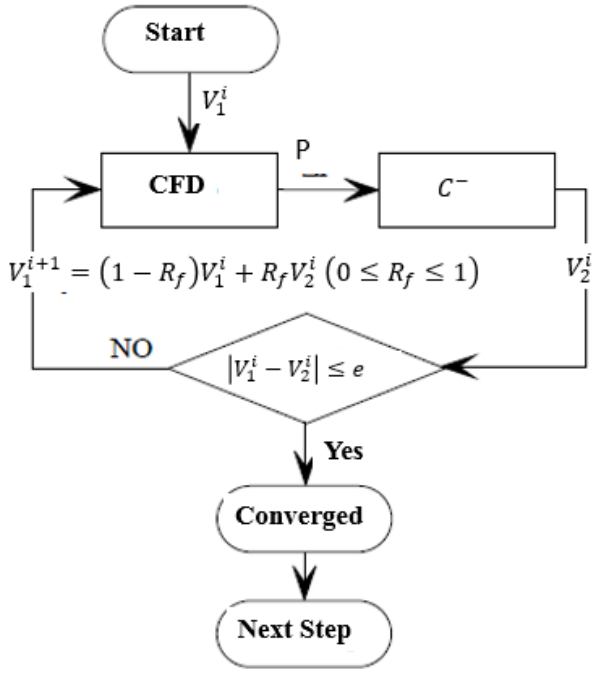

6.5 Numerical Results

The 1D-CFD analysis is performed in the context of a pipe system utilized by Bergant and Simpson (1999) for experimenting with column separation. As shown in Figure 6.4, the test rig consists of a copper pipeline with an internal diameter, length, wave velocity, and upward slope of 22.1 mm, 37.23 m, 1319 m/s, and 5.6%, respectively. The pipe connects two pressurized tanks with constant pressures. Column separation is induced by closing the upstream valve in 0.009s when the system is running in a steady-state condition at a flow velocity of 1.5 m/s. During transient, the pressure head at Tanks 2 is kept constant at 22 m.

Warda et al. (2020) utilized a 3D-CFD analysis for calculating column separation in the above-described system and showed that a local vapor cavity would form at the upstream end of the pipe right after the valve. This local vapor cavity was shown to remain in the upstream 30 cm

of the pipe. Thus, in the 1D-CFD coupling, only the upstream 50 cm of the pipe is considered the CFD zone, and the rest (36.73 m) is analyzed by the DGCM. Numerical explorations show that a time step = 0.0001 s provides a numerical stable condition when the CFD zone is covered with a fine mesh with an average size of 1 mm. The number of the computation cells in the 1D analysis is selected in such a way that: 1) the time steps in both 1D and CFD become identical 2) the Courant number in the 1D zone remains at 1. This results in 278 computational cells with a spatial increment length of 0.1321 m. Note that when the Courant number approaches 1, interpolation error tends to zero and the MOC provides quite accurate results (Ghidaoui and Karney, 1994).

Figure 6.4

The schematic of the experimental apparatus used by Bergant et al. (1994)

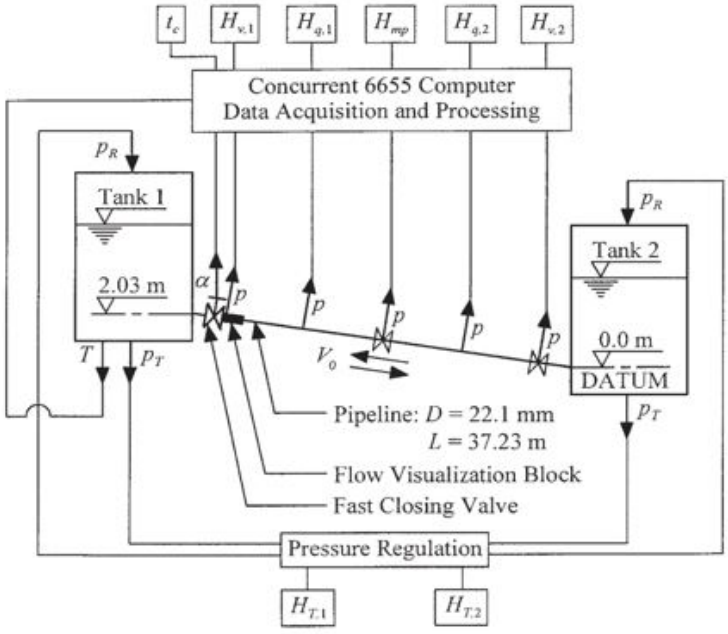

The 1D-CFD analysis is performed for two distinct cases, 2D and 3D CFD analysis. A UDF is developed to linearly reduce the flow velocity at the upstream face of the CFD zone from

1.5 m/s to 0 in 0.009 s. Figures 6.5 and 6.6 compares the pressure time histories obtained from both the DGCM and the 1D-2D coupling method with the experimental results at the valve location and the midpoint of the pipe. As can be seen, the results are in excellent agreement with the experiments. Figure 6.7 also demonstrates the evolution of the vapor cavity in different computational times.

Figure 6.8 compare the pressure time histories obtained from the 3D-1D coupling method with the experimental results at the valve location and the midpoint of the pipe. As can be seen, the numerical results are in good agreement with the experiment. Comparing Figures 6.8 and 6.6 reveals that both the 1D-2D and 1D-3D coupling approaches provide almost identical results. Figure 6.9 also shows the evolution of the vapour cavity in different computational times. Comparing Figures 6.9 and 6.7 reveal that the shapes of the cavity captured by the1D-2D and 1D-3D methods are almost identical.

Although the experimental data confirm the validity of the results captured by 1D-CFD coupling, it is not known if 1D-CFD coupling succeeded in capturing the shape of the vapor cavity. The CFD results obtained from a CFD analysis are utilized to verify this aspect of the model. Warda et al. (2020) captured the evolution of the cavity for the current problem using 3D CFD analysis. Figure 6.12 shows a few snapshots of the cavity shape during its contraction and expansion. Note that Figure 6.12 shows the first 30 cm of the pipe while Figures 6.7 and 6.9 represent the whole CFD domain, 50 cm. Comparing Figures 6.7 and 6.9 with Figure 6.12 reveals that the shape of the cavity in 1D-CFD analysis differs from what is captured by the CFD analysis. The figures demonstrate that in the CFD analysis, the cavity is formed on top of a film of liquid, but in the 1D-CFD analyses, the vapor cavity partially occupied the whole section of the pipe. In the absence of an experimental study, it is not easy to identify which one better

represents reality. Nevertheless, the physics of the flow shows that the results from the CFD analysis can better represent the reality. Due to the gravity effect the pipe obvert receives higher pressure than the bottom, so a vapor cavity starts forming at the top and growing toward the bottom. This explanation may explain why the vapor cavity grows over a film of liquid.

An independent way of justifying the shape of the vapor cavity is to simulate the current problem with the aid of the MTPA. Figure 6.11 shows the cavity evolution calculated by this method. It is seen that like pure CFD results the cavity is expanding and growing over a film of liquid which is another justification that the CFD can represent the cavity evolution better than coupled 1D-CFD model. That the 1D-CFD model distorts the shape of the cavity may be attributed to the issue of considering a uniform velocity at the interface between the CFD and 1D domains. In reality, the velocity distribution is not uniformly distributed on the pipe cross-section, and this may explain the discrepancy between CFD and coupled CFD-1D model. This is of course just a hypothesis that is subject to verification.

Figure 6.5

Pressure time histories calculated by DGCM at; a) valve; b) pipe mid-point

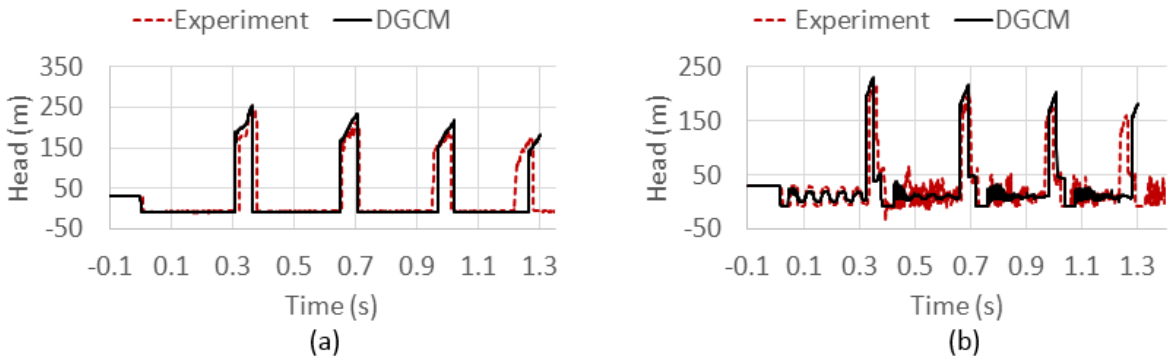

Figure 6.6

Pressure time histories calculated by 1D-2D at; a) valve; b) pipe mid-point

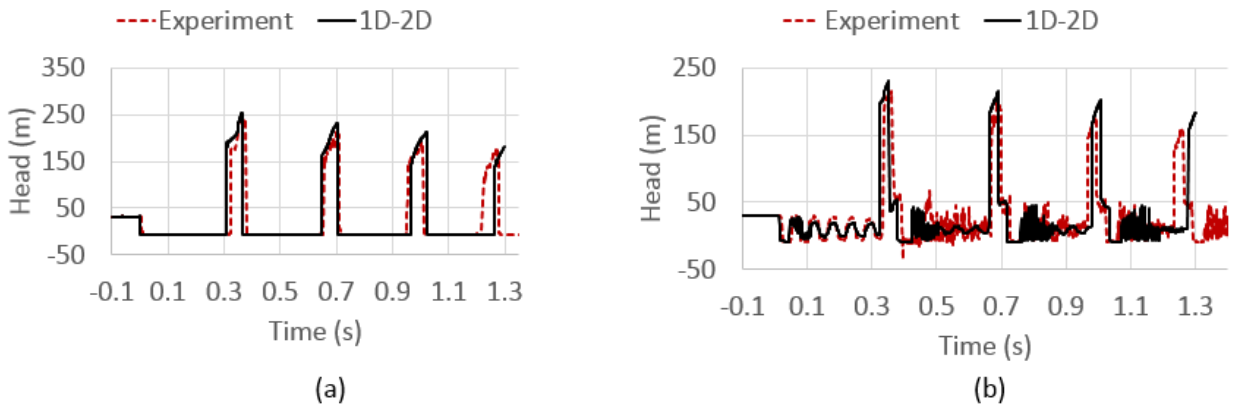

Figure 6.7

Cavity size evolution captured by 1D-2D

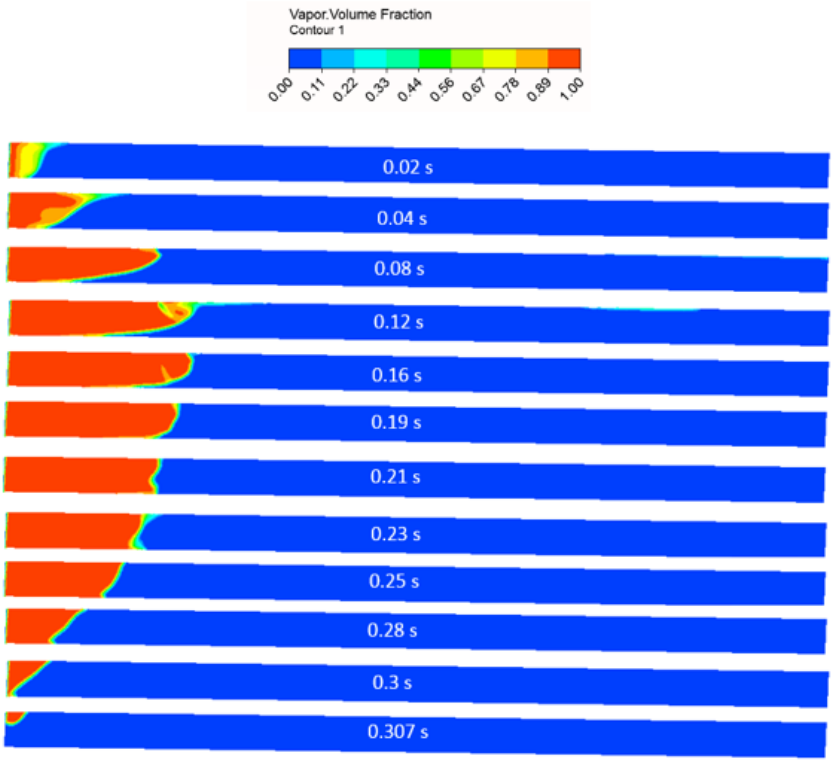

Figure 6.8

Pressure time histories calculated by 1D-3D at; a) valve; b) pipe mid-point

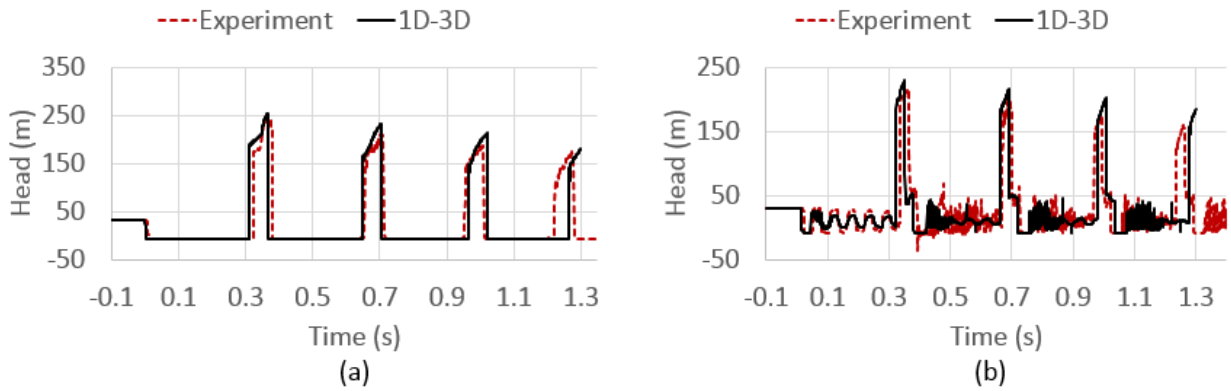

Figure 6.9

Cavity size evolution captured by 1D-3D

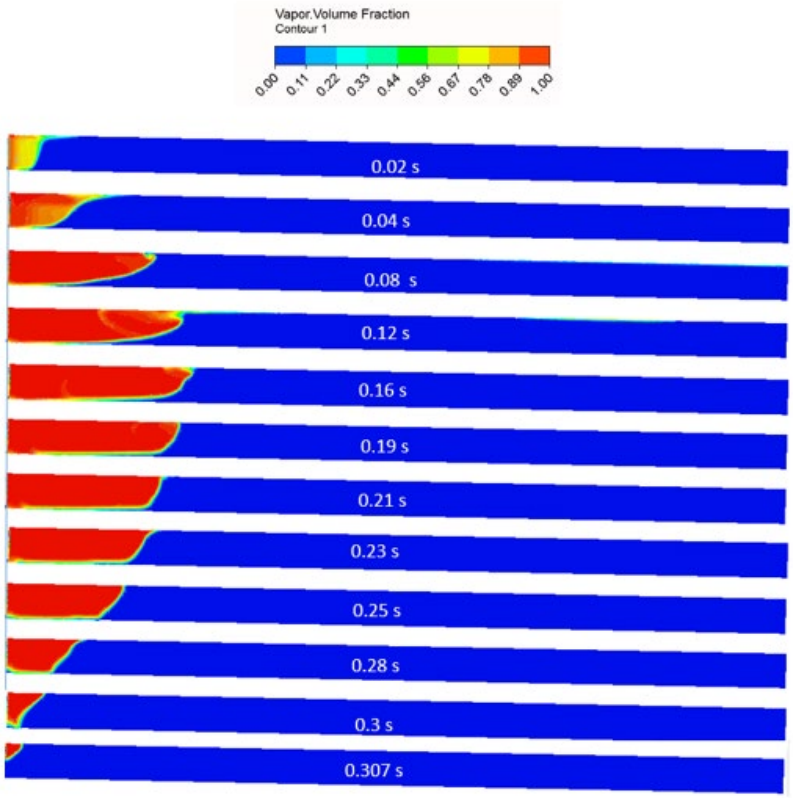

Figure 6.10

Pressure time histories calculated by MTPA at; a) valve; b) pipe mid-point

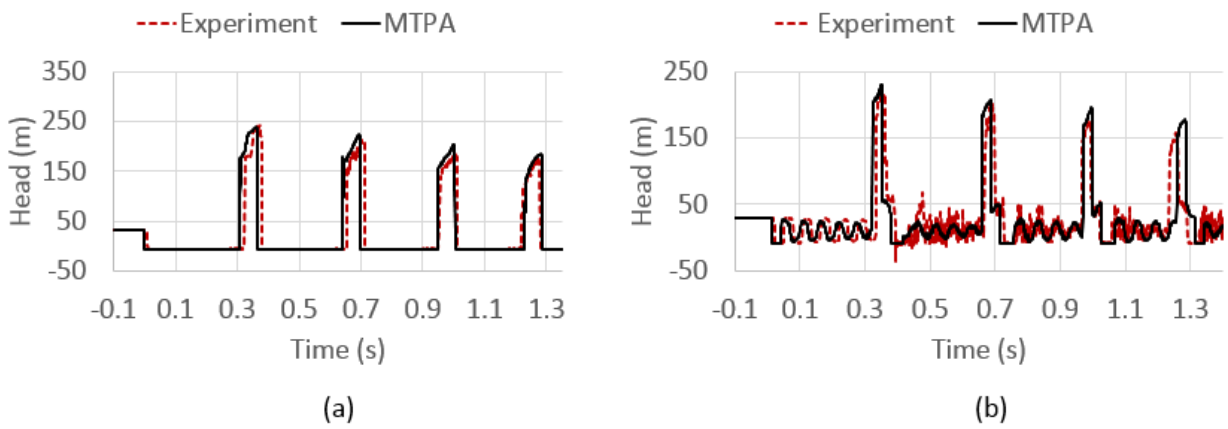

Figure 6.11

Cavity size evolution captured by MTPA

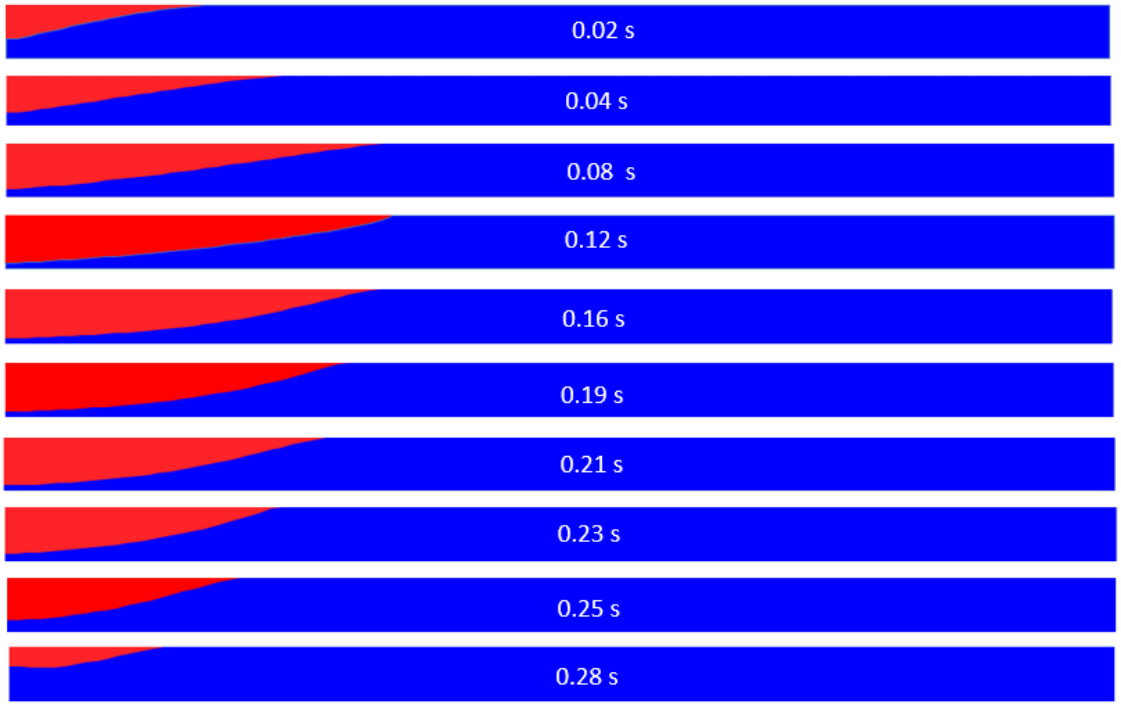

Figure 6.12

Cavity size evolution captured by CFD (Warda et al., 2020)

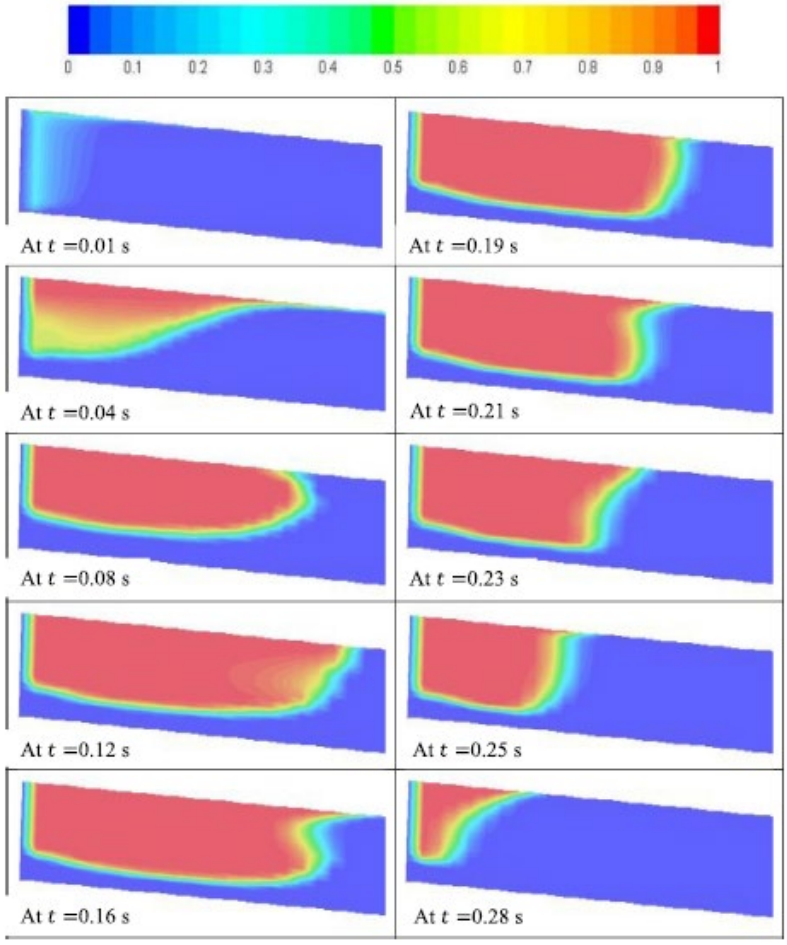

6.6 Summary and Conclusions

ANSYS Fluent is utilized to calculate cavitating flow and column separation, and the Method of Characteristics and the Discrete Gas Cavity Model (DGCM) are employed to conduct 1D transient analysis. The simulations are conducted in the context of a lab-scale pipe system for which experimental data are available. The small portion of the pipe containing the vapor cavity is treated by CFD analysis while the rest of the system is analyzed by the 1D model. The model uses a fully coupled approach in which the data is exchanged in every CFD iteration through the

pipe section separating 1D and CFD zones. A relaxation approach is utilized to ensure the convergence of the CFD analysis in each time step. Both 2D and 3D CFD analyses are independently employed to explore to what extent the 3D effect can affect the solution.

The results show that the proposed model with both 2D and 3D CFD analysis captures the transient responses of the system with almost identical accuracy that are both in very good agreement with the experiment. Since the evolution of the cavity has not been experimented with, the results of a pure CFD analysis published in the literature are employed to evaluate the performance of the proposed model in capturing the shape of the vapor cavity. The comparison shows that although the results are in general agreement, there is still some discrepancy that needs to be explained. The vapor cavity in the pure CFD model is established and grown on top of a film of liquid while in the proposed model the cavity in someplace fills the whole pipe cross-section.

As a further test, the proposed model results are compared to the results obtained from the Modified Two-Component Pressure Approach (MTPA), a novel open channel-based 1D model recently proposed by the author for calculating column separation. The MTPA results also confirm the results from the CFD analysis that the cavity is formed and evolved on top of a film of liquid. What makes the proposed coupled 1D-CFD model distorts the shape of the cavity may be attributed to the way the data exchanges between 1D and CFD model. In each time step, the flow velocity calculated by the 1D model applies to the CFD boundary with a uniform distribution. However, in reality, the velocity distribution at that section of the pipe is not uniform and this may affect the shape of the cavity. Nevertheless, this is just a hypothesis that warrants a detailed investigation.

6.7 References

Adamkowski, A., & Lewandowski, M. (2012). Investigation of hydraulic transients in a pipeline with column separation. Journal of Hydraulic Engineering, 138(11), 935-944.

ANSYS, I. (2013). ANSYS Fluent Theory Guide, Release 15.0.

Autrique, R., & Rodal, a. E. (2013). Laboratory studies of water column separation. IOP Conference Series: Materials Science and Engineering. 52, p. 022022. IOP Publishing.

Baltzer, R. (1967b). A study of column separation accompanying transient flow of liquids in pipes. PhD Thesis. Michigan: University of Michigan.

Baltzer, R. A. (1967a). Column separation accompanying liquid transients in pipes. Journal of Basic Engineering, 837-846.

Bergant, A., & Simpson, A. R. (1994). Range of validty of the discrete vapour cavity model for pipeline water-hammer. University of Adelaide, Department of Civil and Environmental Engineering.

Bergant, A., & Simpson, A. R. (1999). Pipeline column separation flow regimes. Journal of Hydraulic Engineering, 125(8), 835–848.

Bergant, A., Simpson, A. R., & Tijsseling, A. S. (2006). Water hammer with column separation: A historical review. Journal of Fluids and structures, 22, 135-171.

Chaudhry, M. (1987). Applied Hydraulic Transients. New York: Van Nostrana Reinhold Co.

Cunge, J. A., & Wegner, M. (1964). Numerical Integration of Bane de Saint-Venant's Flow Equations by Means of an Implicit Scheme of Finite Differences. Applications in the Case of Alternately Free and Pressurized Flow in a Tunnel. La Houille Blanche, 1, 33-39.

Ghidaoui, M., & Karney, B. W. (1994). Equivalent differential equations in fixed-grid characteristics method. Journal of Hydraulic Engineering, 120(5), 1159–1175.

Kalkwijk, J., Kranenburg, C., Vreugdenhil, C., & De Vries, A. (1972). Cavitation caused by water hammer in horizontal. Delft: Delft Hydraulics Laboratory,Publication No. 97.

Kerger, F., Archambeau, P., Erpicum, S., Dewals, B. J., & Pirotton, M. (2011). An exact Riemann solver and a Godunov scheme for simulating highly transient mixed flows. Journal of Computational and Applied Mathematics, 235, 2030-2040.

Khani, D., Lim, Y. H., & Malekpour, A. (2020). Hydraulic Transient Analysis of Sewer Pipe Systems Using a Non-Oscillatory Two-Component Pressure Approach. Water, 12(10), 2896.

Khani, D., Lim, Y. H., & Malekpour, A. (2021). A Mixed Flow Analysis of Sewer Pipes with Different Shapes Using a Non-Oscillatory Two-Component Pressure Approach (TPA). Modelling, 2(4), 467-481.

Khani, D., Lim, Y. H., & Malekpour, A. (2022a). An Innovative Open Channel Based Model for Calculating Column Separation in Conduit Systems. Submitted to the Journal of Hydraulic Engineering.

Khani, D., Lim, Y. H., & Malekpour, A. (2022b). Investigating the Performance of the Modified Two-Component Pressure Approach in Capturing Column Separation with Large Vapor Cavities. Submitted to the Journal of Hydraulic Research.

LeVeque, R. (2002). Finite volume methods for hyperbolic problems. Cambridge, UK: Cambridge Press.

Maddahian, R., Shaygan, F., & Bucur, D. M. (2021). Developing a 1D-3D model to investigate the effect of entrapped air on pressure surge during the rapid filling of a pipe. IOP Conference Series: Earth and Environmental Science. 774(1), p. 012069. IOP Publishing.

Malekpour, A., & Karney, B. (2015). Spurious Numerical Oscillations in the Preissmann Slot Method: Origin and Suppression. Journal of Hydraulic Engineering, ASCE.

Mandair, S. (2020). 1D and 3D Water-Hammer Models: The energetics of high friction pipe flow and hydropower load rejection. PhD diss., University of Toronto (Canada).

Marsden, N., & Fox, J. (1976). An alternative approach to the problem of column separation in an elevated section of pipeline. Second International Conference on Pressure Surges (pp. 1–13). London: BHRA.

Martin, C. (1983). Experimental investigation of column separation with rapid closure of downstream valve. Fourth International Conference on Pressure Surges (pp. 77–88). Cranfield, UK: BHRA Fluid Engineering.

Provoost, G. A., & Wylie, E. B. (1981). Discrete gas model to represent distributed free gas in liquids. 5th International Symposium on Water Column Separation, 1, pp. 28-30. Obernach, West Germany.

Sanders, B. F., & Bradford, S. F. (2010). Network implementation of the two-component pressure approach for transient flow in storm sewers. Journal of Hydraulic Engineering, 137(2), 158-172.

Siemons, J. (1967). The phenomenon of cavitation in a horizontal pipe-line due to a sudden pump-failure. Journal of Hydraulic research, 5(2), 135-152.

Simpson, A., & Bergant, A. (1994). Numerical comparison of pipe column-separation models. Journal of Hydraulic Engineering, 120(3), 361–377.

Simpson, A., & Wylie, E. (1991). Large water-hammer pressures for column separation in pipelines. Journal of Hydraulic Engineering, 117(10), 1310–1316.

Tang, X., Duan, X., Gao, H., Li, X., & Shi, a. X. (2020). CFD investigations of transient cavitation flows in pipeline based on weakly-compressible model. Water, 12(2), 448.

Toro, E. F. (2001). Shock-capturing methods for free-surface shallow flows. Chichester, New York: John Wiley.

Vasconcelos, G. J., & Marwell, T. B. (2011). Innovative simulation of unsteady low-pressure flows in water mains. Journal of Hydraulic Engineering, 137(11), 1490-1499.

Vasconcelos, J. G., & Wright, S. J. (2007). Comparison between the two-component pressure approach and current transient flow solvers. Journal of Hydraulic Research, 45(2), 178-187.

Vasconcelos, J. G., Wright, S. J., & Roe, P. L. (2006). Improved simulation of flow regime transition in sewers: two-component pressure approach. Journal of Hydraulic Engineering, 132(6), 553-562.

Wang, H., Zhou, L., Liu, D., Karney, B., Wang, P., Xia, L., . . . Xu, C. (2016). CFD Approach for Column Separation in Water Pipelines. Journal of Hydraulic Engineering, 142(10), 04016036.

Warda, H. A., Wahba, E. M., & El-Din, a. M. (2020). Computational Fluid Dynamics (CFD) simulation of liquid column separation in pipe transients. Alexandria Engineering Journal, 59(5), 3451-3462.

Wu, D., Yang, S., Wu, P., & Wang, L. (2015). MOC-CFD coupled approach for the analysis of the fluid dynamic interaction between water hammer and pump. Journal of Hydraulic Engineering, 141(6), 06015003.

Wylie, E. (1984). Simulation of vaporous and gaseous cavitation. ASME Journal of Fluids Engineering, 106, 307-311.

Wylie, E. B., & Streeter, V. L. (1993). Fluid transients in systems. Upper Saddle River, N.J.: Prentice-Hall.

Zhang, X. X., Cheng, Y. G., Xia, L. S., & Yang, J. D. (2014). Dynamic characteristics of a pump-turbine during hydraulic transients of a model pumped-storage system: 3D CFD simulation. IOP Conference Series: Earth and Environmental Science. 22(3), p. 032030. IOP Publishing.

Zhang, X.-x., & Cheng, Y.-g. (2012). Simulation of hydraulic transients in hydropower systems using the 1-D-3-D coupling approach. Journal of Hydrodynamics, 24(4), 595-604.

7 CHAPTER SEVEN

7.1 Summary and Conclusions

While responding to a wet flow event, stormwater pipe systems experience complex transient flow in which both open channel and pressurized flow regimes may coexist. The resulting transient flows may induce significant positive and negative pressure surges that can be intense enough to compromise the integrity of the system. Unfortunately, available off-the-shelf software such as InfoWorks, Mike Urban, etc. is not comprehensive enough to capture all features of the resulting transient flow. When the elastic feature of the flow becomes of significant importance, these models fail to capture the magnitude and track of the resulting water hammer pressures as they produce extensive spurious numerical oscillations that compromise the accuracy of the results and in some cases cause the computer simulation to crash. The existing models are also incapable of capturing water column separation that may occur whenever the negative pressure in the conduits falls to the water vapor pressure. Thus far, several models have been proposed to improve transient flow modeling in sewer pipe systems, but none of them succeeded in addressing the aforementioned issues.

This research proposes an innovative one-dimensional numerical model to address part of the shortcomings associated with the existing state-of-the-art models. The model calculates both cavitating and pressurized flow using a single set of equations that governs unsteady flow in open channel flow. The first order Godunov type finite volume method is utilized to numerically solve the equations. To dissipate potential post-shock oscillations generated following the conduit pressurization, artificial numerical viscosity is admitted to the numerical scheme by applying a

proposed HLL Riemann solver which is utilized for calculating the numerical fluxes at the computational cell interfaces. The proposed HLL solver controls the magnitude of the numerical viscosity through adjusting the left and right wave velocities. A wave velocity calculator is utilized to optimally distribute the numerical viscosity over several computational cells around the computational cell in which the pressurization front is located. The HLL solver admits significant artificial numerical viscosity when the pipe pressurization is imminent and automatically reduces it in other places; in this way, the numerical diffusion and data smearing are minimized.

The numerical results are then validated using the data obtained from the experiment, other numerical models, analytical solutions, the CFD analysis results published in the literature and a 1D-3D coupling model conducted as part of this thesis. Based on the obtained results, the following conclusions are made:

1. The numerical results show that the proposed model completely dissipates the spurious numerical oscillations during flow transition, even at high pipe acoustic speeds over 1000 m/s. The results also imply that the model succeeds in capturing negative pressures during transient flows. This concludes that the proposed HLL solver provides a robust and efficient tool for simulating and analyzing transient mixed flow in systems with any conduit cross-sectional area shapes and a wide range of acoustic wave speeds.
2. The proposed model can accurately calculate column separation while accounting for both waterhammer and open channel flow regimes. The proposed model can also successfully calculate the evolution of large cavities that can extend long-distance across the pipe.

3. The results show that both the DGCM and the proposed model provide identical results in pipe systems with smaller pipe diameters. However, with increasing the pipe diameter, the DGCM comes to compromise the frequency of the resulting pressure spikes induced following water column rejoining. The results show that regardless of the pipe diameter, the DGCM keeps the pressure constant at the vapor pressure on the pipe cross section whereby the water column acceleration and deceleration times remain unaffected. The proposed model resolves the problem by including the effect of the water depth in calculating the total pressure acting on the pipe section. This modification causes the water column acceleration and deceleration times to become longer as the pipe diameter increases.
4. This research concludes that conventional models such as the DGCM fails to correctly capture the physics of the cavitating flow when a large cavity is extended in a pipe with a steep slope. To prove this, the numerical results from the proposed model and the DGCM are compared in the context of a hypothetical problem for which an analytical solution exists. The hypothetical problem is designed to converge to a steady-state condition with cavitating flows established in a good portion of the pipe. The results show that for this case, the DGCM converges to a wrong solution while the MTPA accurately calculates the hydraulics of the problem. The results show that the proposed model with both 2D and 3D CFD analysis captures the transient responses of the system with almost identical accuracy that are both in very good agreement with the experiment. Nonetheless, the vapor cavity in the pure CFD results published in the literature is established and grown on top of a film of liquid while in the proposed 1D-CFD model the

cavity in someplace fills the whole pipe cross-section. It is interesting to see that the cavity shapes captured by the MTPA are in better agreement with the CFD analysis than those obtained from the 1D-3D model. What makes the proposed coupled 1D-CFD model distorts the shape of the cavity may be attributed to the way the data exchanges between 1D and CFD model. In each time step, the flow velocity calculated by the 1D model applies to the CFD boundary with a uniform distribution. However, in reality, the velocity distribution at that section of the pipe is not uniform and this may affect the shape of the cavity. Nevertheless, this is just a hypothesis that warrants a detailed investigation.

5. The proposed model has an obvious superiority over the open-channel-based models proposed by others because they are all based on the shock-fitting algorithm which is very cumbersome to implement while the proposed model enjoys using a shock-capturing algorithm which is very easy to develop even in complex liquid systems. In addition, the proposed model is far more accurate than other shock-fitting-based models and provides comparable results to the DGCM.

Moreover, the proposed model has shown to be a powerful tool for calculating column separation with an obvious superiority over the open-channel-based models proposed before, because they are all based on the shock-fitting algorithm which is very cumbersome to implement while the proposed model enjoys using a shock-capturing algorithm which is easy to develop even in complex liquid pipe systems. Furthermore, the proposed model is shown to provide more precise results than other conventional models such as the DGCM. A particular feature of the proposed model is that it can concurrently account for waterhammer and hydraulic transients, cavitating flow, and free surface flow regimes in any shapes of conduit.

Nonetheless, the proposed model is far from a comprehensive model, and further research is required to add so many other features to the model. First, pipe systems may contain many hydromechanical components, including valves, pumps, turbines, air chambers, and surge tanks, among others. Developing boundary conditions for including the influence of these equipment warrants detailed research. In addition, the proposed model cannot account for air movement and accumulation in the system. Including the air phase in the model is another subject that needs a thorough investigation. Lastly, an investigation is suggested to shed some light on why the vapor cavity shapes captured by 1D-CFD analysis somewhat differ from those calculated by a fully CFD analysis.

APPENDICES

APPENDIX A

NOMENCLATURES

A = flow cross-sectional area

A_f =cross-sectional area of the pipe

a = pipe acoustic speed

B = boundary sub-index

D = hydraulic depth

F = mass flux

G = momentum flux

g = gravitational acceleration

g_i = gravitational acceleration

H = pressure head

H_r = reservoir head

H_{Ld} = piezometric head at the downstream side of the gas pocket at point L

H_{Pd} piezometric head at the downstream side of the gas pocket at point P

H_{Pu} piezometric head at the upstream side of the gas pocket at point P

H_{Ru} = piezometric head at the upstream side of the gas pocket at point R

H_V = gas vapour pressure head

h_c = distance between the free surface and the centroid of the flow cross-sectional area

h_s = pressure head

h_v = vapor pressure head

i = sub-index referring to computational cell number

$\mathrm{K_a}$ = amplifying factor

K_{eq} = equivalent bulk modulus elastic of the liquid

L = left sub-index

n_b = volume of liquid

n_m = Manning coefficient

n = sub-index referring to the pervious timeline

$n+1$ = sub-index referring to the current timeline

P = pressure

P_0^* = reference pressure

P_{ref}= reference pressure

P_v = vapor pressure of the liquid

Q = flow rate

Q_{Ld} = flow rate at the downstream side of the gas pocket at point L

Q_{Pd} = flow rates at the downstream side of the gas pocket at point P

Q_{Pu}= flow rates at the upstream side of the gas pocket at point P

Q_{Ru} = flow rate at the upstream side of the gas pocket at point R

R = right sub-index

$\Re_B$ = radius of the bubbles

R_e = mass transfer source term connected to the growth of vapor bubbles

R_h = hydraulic radius

R_c = mass transfer source term connected to the collapse of vapor bubbles

S = wave speed

S_f = frictional slope

S_0 = pipe slope

S_L = left shock wave speed

S_R = right shock wave speed

t = temporal independent variable

T_s = slot width

$\boldsymbol{U}$ = dependent variables vector

u_i = flow velocity vector

V = flow velocity

x = spatial independent variable

x_j = spatial independent vector

Y = flow depth

Z_{Pd} = pipe elevation downstream side of the gas pocket at point P

Z_{Pu} = pipe elevation upstream side of the gas pocket at point P

Δx = spatial distance increment

Δt = temporal time increment

$\boldsymbol{\Gamma}$ = flux vector

$*$ = star zone sub-index

Ω = hydraulic bore wave speed

Φ = Riemann invariant component

ρ = water density

ρ_l = liquid density

ρ_{ref} = density of the liquid at a reference pressure

ρ_v = vapor density

$\forall_P$= gas pocket volume at point *P*

$\forall_R$ = computational cell volume

α_v = vapor void fraction

α_0 = initial gas void fraction

μ_v = vapor viscosity

μ_l = liquid viscosity

δ_{ij} = Kronecker delta

$\rho_m \overline{u_i' u_j'}$ = Reynolds Stresses